FRICTION AND HEAT TRANSFER REDUCTION IN TURBULENT FLOW OF DILUTE ASBESTOS FIBER SUSPENSIONS IN SMOOTH AND ROUGH TUBES

Thesis by

Adrian L. Moyls

In Partial Fulfillment of the Requirements

for the Degree of

Doctor of Philosophy

California Institute of Technology

Pasadena, California

1976

(Submitted April 1, 1976)

ACKNOWLEDGMENTS

I would like to thank the several people who have contributed in one way or another to this research investigation. First I offer sincere gratitude to my adviser, Professor R. H. Sabersky, whose advice, guidance, and encouragement was ever present. I would also like to thank Dr. J. P. Revel for assisting me in obtaining electron micrographs of the fibers, and Dr. A. T. Cheung for his work with filming the fibers flowing under a light microscope.

My appreciation is also extended to the Turner Brothers Asbestos Company of Rochdale England for their generous donation of fibers. I would like to thank Dr. J. Hoyt of the U. S. Navy for supplying fibers and advice. Also I would like to thank Dr. D. Dipprey of JPL for his cooperation and lending of equipment. I am grateful to the Shell Companies Foundation, and the National Science Foundation for their financial support of this research.

Thanks are due to Mr. F. MacDonald and Mr. D. Laird for their high quality workmanship that they have contributed to the experimental program. I am also grateful to Ms. Barbara Hawk, Cecilia Lin, Joan Sarkissian and Michele Suggs for their assistance in preparing the manuscript.

Finally, I'd like to thank my wonderful wife Angela whose patient understanding and moral support has always enabled me to go on.

ABSTRACT

Friction and heat transfer coefficients were obtained in turbulent flow of dilute asbestos fiber suspensions through a smooth and a rough tube. The 3/8 inch nickel tubes were heated electrically. Suspensions of 50, 300 and 600 ppm asbestos fibers were used at Prandtl numbers of approximately 2, 6 and 11. These were obtained by varying the bulk temperature of the suspension. The surface of the rough tube consisted of a close-packed, granular type of roughness with a height-to-diameter ratio of 0.488. The Reynolds number range studies varied from 10,000 (Pr = 11) to 500,000 (Pr = 2).

Maximum friction reductions of 76% in the smooth tube and 87% in the rough tube were observed, along with even greater reductions in heat transfer rates, namely 86% in the smooth tube and 95% in the rough tube. (Heat transfer coefficients with asbestos fibers can be lower in a rough tube than in a smooth tube.) In the present series of experiments the mechanism by which the fibers interfere with the flow lost its effectiveness at high Reynolds numbers.

The data was analyzed in light of analyses developed previously for Newtonian fluids and extended to dilute fiber suspensions. The results indicate that the turbulent diffusivities are reduced in the wall region and bring about a thicker viscous layer.

The most plausible mechanism which may explain the action of the fibers envisions interference of the fibers with the so-called "bursts" which are known to originate in the viscous layer.

SYMBOLS AND ABBREVIATIONS

A	Slope of logarithmic velocity profile
$\mathring{A}$	Angstroms
A^+	Variable damping parameter in mixing length expression
B	Constant in Eq. (13) for velocity profile
β	Dimensionless difference between centerline velocity and average velocity.
C	Concentration
C_p	Specific heat
C_H	Heat transfer coefficient defined in Eq. (6)
C_F	Friction coefficient defined in Eq. (5)
d	Fiber diameter
D	Pipe diameter
ϵ	Roughness height
ϵ_H	Turbulent heat diffusivity
ϵ_m	Turbulent momentum diffusivity
F	Fiber
H_o	Head loss with water
H_s	Head loss with suspension
k	Proportionality constant in mixing length expression
k_1	Constant
k_2	Constant
ℓ	Mixing length
N	Count of number of gear talk passing sensor in 10 sec.
ν	Kinematic viscosity
P_r	Prandtl number
ppm	Parts per million
$\dot{q}_o$	Local heat flux
R	Aspect ratio
R^+	Dimensionless radius

R_v	Radius of streamwise vortex
Re	Reynold's number
ρ	Density
τ_o, τ_w	Shear stress at wall
τ_{oc_r}	Critical shear stress at onset of drag reduction
T_W	Tube wall temperature
T_L	Mixed fluid temperature
T'	Temperature fluctuation in the radial direction
T^+	Dimensionless temperature defined by Eq. (29)
T_b^+	Dimensionless bulk temperature defined by Eq. (33)
θ	Time between turbulent bursts
$\overline{U}, V$	Tube discharge velocity
U_c^*	Dimensionless velocity at the center of the pipe
U_τ	Friction velocity $= \sqrt{\tau_w/\rho}$
ΔU^*	Dimensionless shift in logarithmic velocity profile
U_V	Local circumferential velocity in outer region of a streamwise vortex
u	Local axial fluid velocity
u^1	Axial velocity fluctuation
u^*, u^+	Dimensionless axial velocity $u^+ = u/u_\tau$
v'	Radial velocity fluctuation
ω	Angular velocity of a streamwise vortex
$\dot{\omega}$	Mass flow rate
y	Distance from wall coordinate
y^*, y^+	Dimensionless distance from wall $y^+ = y\frac{u_\tau}{\nu}$

List of Figures

TABLE OF CONTENTS

Chapter I

INTRODUCTION

Since its discovery by Toms [29] and Mysels [24] the phenomenon of turbulent drag reduction in flows containing various additives has received a great deal of attention. The bulk of the work has dealt with long-chain polymer additives in water and their drag reducing effect in interior and exterior flows. Polymers like polyethylene oxide (polyox) give tremendous reductions in drag (70-80%) even at very low concentrations (10 ppm) when added to pipe flows. However, there are many other substances which will also yield considerable drag reduction but only at much higher concentrations than those necessary for polymers. Some of these are fish slime, DNA molecule solutions, wood pulp fiber, nylon fibers, and asbestos fibers. It is the asbestos fibers that have been receiving attention recently because their performance has been found to be comparable to polymer additives. Asbestos fibers that have been prepared to preserve their high aspect ratio will give large drag reductions (70%) for quite low concentrations (300 ppm). In certain applications they are also somewhat less susceptible to degradation, than polymers.

Most of the work in the field has been concerned with drag reduction, but it is known that the effect of additives on heat transfer rate can be even more pronounced than the effect on drag. It may well be that complex fluids (suspensions, dispersions, slurries, etc.) will be used in industry on an ever increasing scale. It is therefore desirable

to develop a more accurate understanding of the friction and heat transfer characteristics of such fluids and to provide information which may be helpful in the design of future heat exchange equipment. The food industry in particular might eventually benefit from such information, as might the pulp and paper industry.

It was the intention of the present research program to obtain design information on such a fluid and also to obtain further insight into the mechanism by which drag (and heat transfer) reduction occurs. Effects studied include variation with concentration, surface roughness and Prandtl number for flows over a range of Reynolds numbers from 20,000 to 500,000. The experiments were limited to hydrodynamically and thermally fully established pipe flows in a smooth and in a rough pipe. The roughness ratio of the rough tube was 0.0488 (typical roughness dimension/diameter). The three-dimensional, close-packed granular form of the roughness is similar to the close-packed sand-grain surface used by Nikuradse for friction measurements. Water suspensions of asbestos fibers were made to flow through a vertical 3/8 in. diameter tube which was heated by passing alternating current through the tube walls. Friction coefficients were determined from flow rate and pressure drop measurements while heat transfer coefficients were obtained from measurements of heating power, tube wall temperatures and fluid temperature. Although the results are restricted to the conditions of the experiment, with one roughness type and one tube diameter, it is expected that they will be applicable in many flows of practical interest that sufficiently approximate the conditions of the present experiment.

Chapter II

LITERATURE REVIEW

The Toms' effect may be described as follows. If a small amount of a certain solute or suspendible material is added to a turbulent pipe flow, a lower pressure gradient can maintain the same flow rate as was achieved with the pure fluid; or a higher flow rate can be obtained using the same pressure gradient. In this Chapter the characteristics of a number of such flows will be reviewed.

One of the earlier studies of the effect was made by Daily and Bugliarello [5] on flows containing suspensions of wood pulp and synthetic fibers. Their tests, performed in 2 in. and 3/4 in. pipes, show reductions in drag on the order of 25% for 1% suspensions in fully turbulent flow. In the laminar regime the effect is quite different. It appears that the flow consists of a central core or "plug" that is surrounded by a peripheral annulus. In this annulus the flow is laminar and the greatest part of the velocity variation from its zero value at the wall to its maximum value at the centerline takes place. In that case the wall friction may be many times that of a Newtonian fluid. As the velocity is increased the laminar wall shear increases at a much lower rate than for Newtonian fluids. Upon the transition to turbulence the friction drops below that for Newtonian fluids and drag reduction occurs, the maximum difference occurring near the end of the transition region. With further increase in velocity the turbulent wall shear increases at a faster rate than for Newtonian fluids so that the Newtonian value for friction factor C_F is approached at high velocities. The test

results also show that C_F decreases with increasing concentration and they indicate that C_F decreases with increasing aspect ratio (length/diameter) as well as with increasing flexibility of the fibers. The C_F values were lower for the larger pipe. The aspect ratios for the wood fibers were 12, 55 and 58 and for the nylon fibers they were 334 and 369. Typical widths for the wood fibers were 40 microns, and for nylon 20 microns.

Daily and Bugliarello [5] also measured velocity profiles for the fiber flows and it was observed that unlike for pure water, the profiles became sharper instead of blunter as the Reynolds number was increased. The profiles did become blunter, however, as concentration was increased. At any given flow rate they were blunter than Newtonian profiles and accompanied by a reduction in wall shear stress to below that for the corresponding Newtonian fluid. These phenomena were explained by the assumptions that the fibers cluster and interlock to oppose the action of shear stresses and in this manner lead to a blunter profile. At a higher flow rate it was assumed that the equilibrium between the disruptive action of the shear stresses and the interlocking shifts in favor of the shear stresses and the velocity profiles become sharper.

Another study of nylon fiber suspensions flowing in a 2 in. pipe was performed by Kerekes [18]. In this study larger fibers were used, (typically 1 mm in diameter) with aspect ratios from 12 to 73. The study is concerned with his so-called "type II" flows where interparticle collisions are important but contact does not dominate the flow. Upper and lower limits to this type of flow are established as functions of volumetric concentration C and aspect ratio R of the fibers. An

expression for the change in wall friction is proposed that involves only the linear relation of one parameter, the product CR. Experiments were conducted for concentrations varying from 0.5% to 8% and for velocities varying from 4 to 10 feet per second. The author then shows that his results may be expressed by the relation

$$\frac{H_s}{H_o} = k_1 - k_2(CR) \tag{1}$$

where H_s is the head loss in the suspension and H_o is the head loss in water. From these results Kerekes concludes that drag reduction may be based on particle dimensions alone rather than on relationships between particle dimensions and flow parameters. It is suggested that the velocity range covered in this series of experiments may have been too narrow to support such a conclusion. Moreover the model proposed by Kerekes shows no dependence on mean flow velocity. This contradicts the results of Daily which show a return of C_F to Newtonian values at high Reynolds numbers.

Kerekes [18] also measured velocity profiles and characterized them according to his parameter CR, the product of volumetric concentration C and aspect ratio R. He noted that as CR increased up to 1.5 the profiles became sharper, more lamimar-like, and the drag reduction improved to 23%. With a further increase in CR from 1.5 to 1.9 the maximum drag reduction of 33% was obtained. The shape of the profiles changed in the direction of becoming more blunt for CR greater than 1.5. For CR = 1.6 the core was even blunter than for pure water and for CR = 1.9 the core profile was flat halfway to the wall. Kerekes takes this to imply that although the drag reduction

is increasing, the core is becoming more like his "type III' suspension in which interparticle contact dominates the flow. This behavior indidates that the drag reduction mechanism occurs in the wall region since the core is plug-like and velocity gradient occurs in wall regions. If CR is increased to 2.4, drag reduction no longer exists but instead there is a drag increase with the velocity profile remaining flat right to the measuring position closest to the wall.

Vaseleski [31], who conducted experiments with polymers as well as fibers, feels that while polymers reduce drag by affecting the wall region, fibers reduce drag by affecting the core. He arrives at this conclusion because of the observed dependency of the velocity profile on parameters such as the aspect ratio and the concentration. His results indicate that the slope of the logarithmic velocity profile is concentration dependent and increases from 2.45 for pure water to 3.00 for a 200 PPM asbestos suspension. He feels that this indicates a concentration affect in the core region. However, it may be that it is the wall region that is important and that determines the core activity. Fibers may indirectly affect the core by altering the turbulent structure at the wall.

Vaseleski also conducted experiments with asbestos fibers in pipes of 4 different sizes (0.9, 1.9, 2.7, 3.7 in. diameter) and his results show no dependency of the friction factor on pipe size at a given Reynolds number. This contrasts Daily's finding that C_F decreased as diameter increased. He also found that the asbestos dispersion degraded with use. A 200 wppm suspension that showed 54% drag

reduction after 10 hours of pumping was found to give only 15% reduction after 184 hours of pumping. In his studies of nylon fibers he found, as did others, that drag reduction increased with increased fiber aspect ratio and concentration.

Temperature effects on the drag reducing ability of asbestos suspensions were studied by Peyser [26] with a rotating disc apparatus. He found that concentrated suspensions were not affected, but that dilute suspensions lost some of their drag reducing capabilities at higher temperatures. The effect was much smaller for asbestos dispersions than for polymers. His electron micrographs showed individual fibers to be about 200 Å to 300 Å thick. Less than 10% of the material, however, was present as single fibers and most of it was in the form of larger bundles. He was not able to see any difference between the sheared and unsheared samples. This led him to believe that it is the long thin individual fibers that are active in drag reduction, with the differences between before and after shear being masked by the large majority of lesser dispersed entangled fibers.

Another series of tests of various additives was made by Hoyt [15] using rotating discs and a turbulent flow rheometer in which the fluid was forced through a 0.046 in. tube. He tried several kinds of asbestos and glass fibers and found that the long, hair-like fibers of the Turner Brothers asbestos were at least 5 times as effective, on a weight basis, as the next best asbestos fiber. They were however, more subject to degradation. After 25 passes through the 0.046 in. tube, the drag reducing ability of a 500 ppm suspension fell from 65% to 48%. Other suspensions, such as those made with asbestos 5R-10

from the Special Asbestos company, actually improved in drag reducing ability the more they were sheared. Apparently the shearing helps to break up the large fiber bundles into their more effective components. The glass fibers also gave some drag reduction but required high concentrations on the order of a percent or more. In another paper Hoyt [16] compares the drag reducing capabilities of various fish slimes. He finds the slime of high speed fish like barracuda to be very effective in reducing drag. Drag reductions of the order of 60% can be obtained with a 1% slime solution in sea water.

Ellis [11] made an interesting comparison between a 50 ppm Turner Brothers asbestos suspension and a 10 ppm polyox solution. The drag reducing capabilities before and after one hour of pumping by an impeller pump in a separate circulating system were observed in a small (0.115 cm) and in a large (1.43 cm) tube. The fluids were run at $Re = 20,000$ in both tubes. The effectiveness of the asbestos dropped slightly in both tubes. The polymer effectiveness, while remaining unchanged for the small tube, dropped from 54% drag reduction to essentially zero in the large tube after pumping. He presumes that the polyox molecules form matrices or agglomerates which entrap volumes of water and interact with flow instabilities to inhibit their growth. His explanation is that the action of shear reduces the "domain" size of the agglomerates, but that there is no reduced effectiveness as long as this reduced size is large enough to interact with the largest energy dissipating vortices that prevail in the small tube with high wall shear stress. In the large tube with low wall shear stress however, the scale of

turbulence is much larger than the reduced domain size hence the drag reducing effect is lowered. Ellis (10) feels that it is the scale of turbulence, not simply pipe size, which governs the effect. It is presumed that the individual asbestos fibers are large enough to affect the dissipative vortices even in the larger of the two tubes. He believes, however, that the fibers would lose their effectiveness eventually if the scale were to be increased sufficiently, i.e. if a sufficiently large pipe were to be used. This may explain the results of Forrester [12] who found that using the polymer Separan in a 10 in. pipe there was no drag reduction below a Re of 60,000.

A combination of asbestos fibers and polymer was tested in pipe flow by Lee, Vaseleski and Metzner [22]. They found that both substances used together provided for more than just a linearly additive effect. Also, the effect was less dependent on scale (pipe diameter) of the system than polymer alone. (Fibers alone were unaffected by scale over the range tested – up to $Re = 2 \times 10^5$.) A drag reduction level of 95% was obtained. They feel that the mechanisms by which the additives affect the flow is different for polymers than for fibers. They feel that the fibers cause changes in the turbulent momentum transport in the core, and that the polymers modify the flow near the wall.

An interesting explanation is also offered by Radin [27]. He believes that the entangled fiber network causes the fluid in the core to move as a plug with most of the shearing taking place in a thin annulus between the plug and the wall. In a fluid that contains only fibers, he speculates that somehow the velocity profile is forced to be less steep in the turbulence generation region ($5 < y+ < 30$), and that hence the

pressure drop is decreased. (He does not indicate how the velocity profile is made less steep in this region. It is the opinion of the writer, however, that the fibers reduce drag by interfering with the bursting process rather than by flowing as a plug. This process will be discussed in more detail in Chapter IX.) At any rate, when polymers are added to the fiber suspension, Radin believes that polymer effectiveness is enhanced, since polymers are most effective in regions of high velocity gradient as would prevail in the annulus. He points out in addition that degraded polymers which are normally ineffective in large diameter tubes, are still effective when used in conjunction with fibers. (Ellis' [11] experiments show that degraded polymers are still effective in small tubes where high shear stresses and velocity gradients exist.) Hence it appears that the concept of a plug flow may be a valid one, especially at lower Reynolds numbers where the shear stresses are insufficient to tear a plug apart. Whether a plug exists or not however, it is the opinion of the writer that the principal mechanism for both fiber and polymer additives is the same, i.e. both are wall region effects. The polymers are capable of damping one range of small eddies involved in turbulence production, while fibers are capable of damping another range of these same eddies when they have grown larger. This is discussed further in Chapter IX.

The effect of different dispersants was looked at by Radin [27]. He compared Aerosol OT to Surfynol 104 and found them to be equal in performance except that the former gave foaming problems and the latter did not. Surfynol 104 is a defoamant as well as a surfactant.

As was mentioned earlier, by far most of the work done on drag reduction has dealt with the effect of polymers. It would, therefore, be appropriate to review some of the better known characteristics of polymeric flows. If a polymer flow is laminar it behaves like the solvent with a slightly increased shear viscosity. At a sufficiently high flow rate, transition to the turbulent regime occurs. Although Virk[32] did not observe a delay in transition, others like Castro [3] and White [33] have concluded that the polymer causes a shift to higher flow rates before turbulence takes place. This shift depends on the concentration, molecular weight, and degree of degradation of the solution as well as such flow characteristics as Reynolds number and wall shear. As the flow rate is increased the friction is at first the same as for pure solvent and then it drops below the normal as drag reduction begins. Sometimes drag reduction occurs in the transition region so it occurs immediately as turbulent flow is obtained. There is a critical wall shear stress below which, drag reduction does not occur. As flow rate is increased still further the extent of the drag reduction increases until a maximum drag reduction asymptote is reached.

It is well established that the onset of drag reduction is associated with a critical wall shear stress. This critical value depends on the nature of the polymer and of the solvent. Although it is approximately inversely proportional to the molecular weight, molecules with similar weights but with different monomeric structures — different number of links in the backbone — have different onset shear stresses [32]. Good solvents tend to expand the molecules and onset occurs at a lower stress than with a poor solvent. Although the critical stress

appears to be independent of pipe diameter and concentration, it does seem to increase with aging of the solution.

Temperature effect tests show that with Polyox, maximum drag reduction is attained at temperatures below 105°F and that at 140°F definite thermal degradation takes place and a marked decrease in drag reduction occurs.

The comparatively little work done on heat transfer to drag reducing fluids indicates that the reduction in heat transfer rates is even greater than the reduction in drag. Some investigators have found that the heat transfer coefficient with polymers obeys a Colburn type analogy

$$C_H \times P_r^{0.6} C_F/2 \qquad (2)$$

but this relationship is certainly not a universal one (see also Chapter VI).

Very extensive work on friction and heat transfer with Polyox solutions was performed by Debrule. The experiments were performed on the same apparatus as the present ones. Debrule obtained a maximum drag reduction of 73% in smooth tubes and of 83% in rough tubes. The maximum heat transfer reduction was even higher, 84% in smooth tubes and 93% in rough tubes. Similarity rules which were developed for heat transfer to Newtonian fluids were extended to polymer flows in the smooth tube. A velocity profile similar to the one proposed by Deissler was taken as a model to interpret the data. It was found that the results could be explained by assuming that the turbulent diffusivities are reduced in the vicinity of the wall which brings about a thickening of the viscous sublayer. The results of this work will be discussed in later

chapters (Chapters III and VI). Rough pipe data were also obtained by White [34] in an extremely rough threaded pipe. While Polyox reduced the friction considerably it again reduced the Stanton number by an even greater amount.

Among the many attempts to explain the actions of polymers in a theoretical manner, the work by Dimant and Poreh is perhaps the most relevant. Dimant and Poreh [7] have constructed a mixing length model with a variable damping parameter based on Van Driest's expression for the mixing length in Newtonian fluids

$$\ell = ky\left(1-e^{-\frac{y+}{A+}}\right). \tag{3}$$

Dimant and Poreh compared their theoretical work with Debrule's test results in the following way. The value of A^+ in Eq. (3) was selected so as to fit the measured C_F values. The corresponding heat transfer coefficients were then computed on the basis of the theoretical model and compared to the ones measured by Debrule. Very close agreement was achieved for the low concentration (10 ppm). The predicted values for the 50 ppm solution were still quite satisfactory, although they generally exceeded the measured ones by about 10%. A larger discrepancy (about 30%) existed for one particular series of tests (Pr = 6.16), but the difficulty could well be based on an experimental error. Finally, mention should be made of the important model proposed by Katsibas and Gordon [17], which is based on the observation by Kline, et al [19]. Kline and his associates had shown previously that the wall layer was not uniform in the circumferential direction. Instead, longitudinal vortices were observed to form intermittently,

which would grow and eventually dissipate, and in this process transport fluid from the wall layer towards the core. This outward movement in turn was seen to be compensated by a flow of fluid from the outer layer towards the wall. Kline referred to the first part of this phenomenon as "bursts", and to second as "sweeps". Katsibas and Gordon then proposed that the drag reducing additives would modify the flow by interfering with these bursts and sweeps. They further strengthened their hypothesis by citing experimental data which showed a decrease in "burst" frequency with the addition of polymers, and in addition they presented a simple analytical model which related this frequency to the friction coefficient. The approach by Katsibas and Gordon is considered to be most pertinent and will be discussed further in Chapter IX.

Chapter III

EXPERIMENTAL APPARATUS

A diagram of the test facility is given in Fig. 1. A 10 in. diameter hydraulic cylinder forces the fluid through the test section. The cylinder is operated by a variable speed DC electric motor through a linear actuator. This method of fluid displacement was chosen over a pump in order to reduce mechanical degradation of the fibers before they enter the test section. After the suspension passes through the test section it is discharged into a reservoir tank to be used again later or to be thrown out. The solutions are prepared in another reservoir tank that is connected to the cylinder by a flexible hose. By correctly positioning three globe valves and retracting the piston it is possible to draw the suspension from the reservoir into the cylinder.

The test section shown in Fig. 2 is heated electrically by passing alternating current through the wall of the tube. The resistance of the tube is only about 0.002Ω and a large current (on the order of 1000 amps) is required to provide the desired heat transfer rates. The current is supplied by a set of transformers, the primary windings of which are equipped with a variable ratio switch. This allows variation in the secondary windings of from 200 to 1200 amps. Large copper conductors connect the secondary windings of the transformer to the electrodes of the test section which is enclosed in a safety housing. There are three safety devices included in the electric circuit. First the power can be turned on only when the housing door is closed and the motor driving the piston is running. Secondly there is a circuit breaker that

opens the power circuit when the wall temperature of the test section exceeds a critical value. Finally there are two limit switches that stop the piston and shut off the power at the end of its run.

The tubes used in this experiment are the ones designed and used by Dipprey [8] in similar experiments with distilled water. They are described in detail in [8] so a description of the main features only will be given here. The tubes are made of nickel, a material for which the thermal conductivity is well enough established to permit the accurate calculation of inner wall temperature from outside wall measurements. The inside diameter of the tubes is about 3/8 in. The rough tube was constructed by electroplating nickel onto a sand-covered mandrel and then dissolving the mandrel away to leave the pure nickel shell. Samples taken from the tube showed a very uniform nickel grain structure with no evidence of inclusions or voids. The significant dimensions of the two tubes are given in Fig. 3. Values for the inside diameter are based on 12 outside diameter measurements of the original mandrel with corrections for mean sand protrusions. As a check the diameter was also obtained volumetrically using the relation

$$D = \left(\frac{4\Delta V}{\pi \Delta X}\right)^{\frac{1}{2}} \tag{4}$$

where ΔV is the volume contained in length ΔX. The effective tube wall thickness used to get the wall temperature drop was calculated from electrical resistivity measurements of the wall material and compared with the thickness measured on photomicrographs taken from the end samples of each tube. A slight longitudinal taper in the

tube wall was observed on both tubes and is taken into account in the data reduction.

The roughness ratio of the rough tube, $\frac{\epsilon}{D}$, is 0.0488. A one in. long smooth section was formed near the start of the heated section of the rough tube at two circumferential locations. Three equally spaced 0.032 inch holes that connect the center of the smooth region to a small ring manifold constitute the pressure tap at the entrance of the heated section. The downstream pressure tap has the same geometry and is located in a smooth section 1/2 in. from the exit end of the rough tube. Copper blocks that are silver brazed to the nickel tube serve as electrode attachment points and as distributors of the electric current. The exit end of the test section is electrically isolated by a special flange which also incorporates a thermal mixing chamber. The mixing chamber consists of a brass thermal equalizer which is isolated from the other metal parts by a teflon sleeve. The equalizer has drilled holes directing the flow first into an outer chamber and then back into the central passage.

Three wall-thermocouple stations are located on the heated test section, but only the downstream one was used in the present experiment in which fully established conditions were to be studied. At that downstream station three thermocouples are mounted 120 degrees apart. The thermocouple junctions were formed by discharge welding 0.005 in. chromel and alumel wires to the nickel tube leaving a 0.020 in. gap between the end of the wires so that a chromel-nickel and a nickel-alumel junction is formed in series. The insulated leads were wrapped around the tube several times and secured to it with high

temperature cement.

The measurements necessary to determine C_F and C_H consist of the following: flow rate, inlet and outlet temperatures, outside wall temperatures at 2 circumferential locations, pressure drop across the test section, and the electric power. C_F and C_H are calculated by the procedure described in Appendix II. The flow rate is derived from the speed of the gear driving the piston actuator and the gear speed is determined from the rate at which the gear teeth pass a magnetic sensor. The signals from the magnetic pick-up are counted over a 10 second period and read on a digital counter. This method was checked by timing the piston over a measured part of its travel at various flow rates. The pressure drop is measured with a Statham differential transducer that is connected to the test section pressure taps as is illustrated in Fig. 2. The transducer output is recorded continuously on a Hewlett Packard strip chart recorder. All of the thermocouples were chromel-alumel and their outputs were displayed on two Keithley digital voltmeters.

Figure 4 shows a schematic diagram of the temperature-measuring circuits. All wires of inlet, outlet, and wall thermocouples are connected to copper wires in the ice bath, thus allowing all switch interconnections to be made with copper wire. Each cold junction is insulated in a small glass tube filled with oil, and all tubes are placed in an ice bath contained in a Dewar. The outlet immersion thermocouple is connected directly to one of the voltmeters. The two wall thermocouples and the inlet thermocouple are connected to a rotary switch which is, in turn, connected to the other voltmeter. The power

necessary to heat the tube walls is derived from the voltage drop across the test section and the electrical resistance of each tube as a function of temperature. The following is a list of the instrumentation used:

(a) Measurement of Flow Rate

1 Counter Timer – Model 101 A (Monsanto)

(b) Measurement of Pressure Drop

1 Differential Pressure Transducer ±15 psid

Model 4233 – PM 280 TC ±15-350 (Statham)

1 Strip Chart Recorder 7100 B (Hewlett Packard)

(c) Measurement of Temperatures

2 Digital Voltmeters – 171 (Keithley)

(d) Measurement of the Voltage Drop across the Test Section

1 True RMS Voltmeter – 3400 A (Hewlett Packard).

Procedures

1. Suspension Preparation – 210 liters of fresh Turner Brothers asbestos is prepared as follows for a 300 ppm suspension. Quantities in parenthesis refer to amount needed for a 50 ppm suspension.

(a) 1.657 (1.675) Kg of the surfactant aerosol OT is dissolved in about 3 liters of water. This is best accomplished by boiling for one or two hours and then letting the solution sit overnight.

(b) The reservoir is filled about 3/4 full with tap water and the dissolved surfactant added.

(c) 2.97 (.495) liters of the asbestos liquid concentrate (21.2 gm/ℓ.) obtained from the Turner Brothers Asbestos Company

is poured into the reservoir.

(d) The rest of the volume of the reservoir is made up with tap water.

(e) The final suspension is stirred periodically over a 15 minute period to ensure uniform mixing.

(f) The suspension is ready to be drawn into the cylinder and forced through the test section.

The quantities of the Aerosol OT are those required to yield a 0.8% solution of surfactant. Hoyt [15] and others have found the surfactant necessary to disperse the fibers and prevent flocculation. Drag and heat transfer tests performed with surfactant alone yield the same C_F and C_H curves as pure water. The surfactant was obtained from the Fisher Scientific Company.

The preparation procedure differs slightly for the Pr = 10 (T = 41°F) suspensions. The reservoir is wrapped with insulation and filled about half full with asbestos, surfactant, and water. A 100 lb. cake of ice is then broken up and dropped into the suspension. More water is added to bring it up near to volume and the ice mixture is stirred periodically. After a few hours the temperature drops to about 40°F and the small amount of remaining ice is removed. Volume is made up to 210 liters with water, the temperature is checked, and the suspension is ready for use. Before the actual run it is necessary to cool down the cylinder. This can best be done by drawing in the cold suspension and ejecting it again, several times, while the ice is still present in the reservoir.

The Pr = 2(T = 182°F) suspensions are prepared at room

temperature and then heated with a 12 kilowatt General Electric Immersion heater. For reasons similar to those which apply to the cold tests, the cylinder is filled several times near the end of the heating period, before the tests begin.

2. Test Operation – Heat transfer and pressure drop tests were conducted at several different Reynolds numbers for each of the two tubes, each suspension concentration (0, 50, 300 ppm) and for each of three Prandtl numbers (2, 6, and 10 nominally).

(a) The suspension is prepared.

(b) The piston is moved forward to the end of its stroke (minimum cylinder volume).

(c) The exhaust tube downstream (and physically above) of the test section is filled from above with water.

(d) The pressure lines connecting the wall taps to the transducer are opened by setting two three-way valves and the pressure lines are allowed to bleed for a minute to remove trapped air.

(e) These valves are closed and the voltage output from the transducer at zero pressure difference is traced on the strip chard recorder.

(f) The appropriate valves are opened and the piston is drawn back slowly to avoid degradation of the suspension as it flows from the reservoir into the cylinder.

(g) The variable ratio switch of the transformers primary is positioned to provide the output voltage that will in turn

supply the appropriate heat flux to the test section.

(h) When the piston has moved back its full distance (maximum cylinder volume) the appropriate valves are adjusted to allow expulsion of the fluid through the test section.

(i) The piston is moved forward slowly to allow further bleeding of the pressure lines if desired. Readings of the inlet and outlet thermocouples are recorded.

(j) The piston speed is then increased to give the desired Reynolds number by setting the speed selector switch to a given position.

(k) A scale is selected on the chart recorder to correspond to the expected voltage output from the pressure transducer.

(l) The power is turned on and the test section is electrically heated. There is a five second time delay incorporated in this circuit to enable the operator to shut down the test in case of emergency.

(m) The number of teeth of the piston-driving gear that pass a magnetic sensor in 10 seconds is recorded.

(n) The rotary switch is adjusted to read the inlet and the two wall temperatures. The outlet temperature is read from the other voltmeter.

(o) The voltage drop between the two electrodes of the test section was read on the RMS voltmeter.

(p) The motor (and piston) is stopped either manually or automatically via the limit switch.

(q) The valves are set for another refill of the cylinder and recordings are read and readings tabulated.

(r) After a set of runs is completed the pressure lines are bled again and the transducer zero is rechecked as in steps (d) and (e).

3. Calibrations – The calibrations performed in the experimental program are described in Appendix I.

4. Data Reduction – After a series of tests adequate for one curve was completed, the measured data were reduced by computer. A program was written in FORTRAN to take into account all calibrations and small corrections inherent to the reduction. From an input consisting of all instrument readings the program computed Re, Pr, C_F, C_H and other pertinent parameters for each test. The program is presented and explained in Appendix II, along with the procedure to calculate C_F and C_H from the basic measurements.

Chapter IV

FUNDAMENTALS

It is the purpose of this section to briefly review the methods of analysis used by other researchers, most notably Debrule [6], in dealing with drag reducing flows. The following assumptions were generally made:

1) fully turbulent steady pipe flow.
2) hydrodynamically fully established flow in which the mean fluid motions are invarient with axial position.
3) fully established thermal conditions whereby the radial temperature profile referenced to the local wall temperature is independent of axial location.
4) constant fluid properties, density (ρ), viscosity (ν), thermal conductivity (k), specific heat capacity (C_p).
5) surface roughness patterns which are statistically independent of circumferential or axial position.

These conditions were well approximated by Dipprey [8] and Debrule [6] in previous experiments on the same apparatus. Some authors have observed a delay in transition to turbulence with polymers present, so it may well be that fibers do this also. However, as with Debrule, the smallest Reynolds number used was over 10^4 and the thermocouple station was 40 diameters from the pipe entrance, so it is assumed that fully established conditions prevailed since the entrance length for fibers is expected to be similar to polymers and the latter is still of the same order of magnitude as for water. The

condition of constant properties is approximated by keeping the wall to bulk temperature difference low (order of 10°F). Data were not extrapolated to zero heat flux because for the relatively low heat fluxes of the present experiments, the effect of the heat transfer rate on C_F and C_H was virtually negligible and well within the instrument reading error. The effect is largest at low Reynolds numbers. Even at the lowest Re however, the possible error was insignificant compared to the difference between the values for the suspensions and the corresponding values for pure water. Photomicrographs of the tube surface taken by Dipprey showed that condition (5) was met.

The coefficients of friction and heat transfer are defined as follows:

$$\text{friction coefficient} \quad C_F = \frac{\tau_o}{\frac{1}{2}\rho\overline{U}^2} \tag{5}$$

$$\text{heat transfer coefficient} \quad C_H = \frac{\dot{q}_o}{\rho\overline{U}C_p(T_W - T_L)} \tag{6}$$

where

$\overline{U}$ = tube discharge velocity, defined as

$$\overline{U} = \frac{2}{R^2}\int_o^R U(r)\,r\,dr \tag{7}$$

R = pipe radius

τ_o = shear stress at wall

ρ = density

$\dot{q}$ = local heat flux

T_W = tube wall temperature

T_L = mixed fluid temperature, defined by

$$T_L = \frac{2}{R^2 \overline{U}} \int_o^R T(r)\, U(r) r dr \tag{8}$$

C_p = specific heat of fluid.

In order to calculate C_F and C_H, $\overline{U}$ must be calculated. This requires a knowledge of the velocity profile $U(r)$. The time averaged momentum equation for pipe flow gives:

$$\frac{\tau}{\rho} = -\overline{u'v'} + \nu \frac{du}{dy} \ . \tag{9}$$

The shear distribution is linear across the tube so

$$\tau = \tau_o (1 - \frac{y}{R}) \ . \tag{10}$$

Hence

$$\frac{\tau_o}{\rho}(1 - \frac{y}{R}) = \overline{-u'v'} + \nu \frac{du}{dy} \tag{11}$$

With the assumption that the viscous term $\nu \frac{du}{dy}$ governs the flow in the vicinity of the wall while the Reynolds stress term $\overline{-u'v'}$ governs the flow in the core, and the assumption that the shear stress is constant and equal to the wall stress in the wall region, the following velocity relations are obtained.

Near the wall $U^* = y^*$

where

$$U^* = \frac{u}{u_\tau} \ , \quad U_\tau = \sqrt{\frac{\tau_w}{\rho}} \ , \quad y^* = y \frac{U_\tau}{\nu} \ . \tag{12}$$

Away from the wall

$$U^* = A \ell n\, y^* + B + \Delta U^*(C, F) \tag{13}$$

where A and B are constants.

This is the same as the usual logarithmic velocity distribution

obtained for water, except that there is an effective slip velocity, ΔU^* (C,F), added that is a function of the nature and concentration of the fibers

By integrating this expression over the pipe cross section the following relation between Reynolds number and friction coefficient is obtained

$$\sqrt{\frac{2}{C_F}} = A\ell nRe\sqrt{\frac{C_F}{8}} - \beta + B + \Delta U^* \qquad (14)$$

β is the dimensionless difference between centerline velocity and average velocity. This expression may be used to determine ΔU^* with an accuracy which is generally sufficient.

The momentum equation can also be written

$$\frac{\tau_o}{\rho}(1 - \frac{y}{R}) = (\epsilon_m + \nu)\frac{du}{dy} \qquad (15)$$

where $\epsilon_m = \overline{-u'v'}/du/dy$ is the turbulent momentum diffusivity. Similarly if the heat flux is assumed to vary linearly with radial position, the energy equation can be written as

$$-\frac{\mathring{q}_o}{\rho C_p}(1 - \frac{y}{R}) = (\epsilon_H + \frac{\nu}{P_r})\frac{dT}{dy} \qquad (16)$$

where $\epsilon_H = \overline{-T'v'}/dT/dy$ = turbulent heat diffusivity. $\overline{T'v'}$ is a time average of the product of the turbulent fluctuations in velocity radially away from the wall and temperature. If it is assumed that the large changes in temperature and velocity occur very close to the wall, these equations become

$$\frac{\tau_o}{\rho} = (\epsilon_m + \nu)\frac{du}{dy} \qquad (17)$$

$$-\frac{\dot{q}_o}{\rho C_p} = (\epsilon_H + \frac{\nu}{Pr})\frac{dT}{dy} \tag{18}$$

The assumption is made that the distances from the wall at which the velocity equals the average velocity $\overline{U}$ and the temperature equals the mixed temperature T_L, are the same. Use is made of Reynolds analogy, in fact it will be assumed that $\epsilon_H = \epsilon_m$.

Using these expressions Debrule was able to obtain the following relation:

$$\frac{\frac{C_F}{2C_H}\frac{\epsilon_H}{\epsilon_m} - 1}{\left(\frac{\epsilon_H}{\epsilon_m} Pr - 1\right)\sqrt{\frac{C_F}{2}}} = \int_o^{U_c^*} \frac{dU^*}{1 + \frac{\epsilon_H}{\epsilon_m} Pr \frac{\epsilon_m}{\nu}} \tag{19}$$

Here U_c^* is the dimensionless velocity at the center of the pipe. The value of the expression on the left hand side can be evaluated from the data so that the variation of the value of the integral due to the effects of additives can be inferred. He found that for a 50 ppm polyox solution, $Pr = 6.16$, $Re = 100,000$, that the value of the left hand side increased from 7.9 for pure water to 28.1 for the polymer. This was for the assumption that $\epsilon_H/\epsilon_m = 1$. Even if ϵ_H/ϵ_m were not equal to 1.0 but would have values as low as 0.5 and as high as 1.5 the left hand side of Eq. (19) would still result in a very similar change. The only term in the integral that could allow this large change then is ϵ_m/ν. When the wall region is left this term becomes very large and the value of the integral remains essentially constant after a small distance from the wall. Hence it is concluded that the effect of the additive was to change the ϵ_m/ν variation in the wall region. ϵ_m must increase

more slowly as the wall is left in the additive solution – the viscous stresses will remain of importance to a greater distance from the wall and a thickening of the viscous layer will be effected. As a comparison, the value of the left hand side of Eq. (19) was evaluated for a 300 ppm fiber suspension at Pr = 6.16, Re = 100,000, and was found to be 16 which is significantly larger than the value for water which was 7.9. The C_H curve shows the heat transfer reducing mechanism has lost some of its effectiveness at this high Reynolds number. The mechanism is most effective at about Re = 40,000 and here the value of the expression is increased to 26 while the corresponding one for water is slightly less than it was for the Re = 100,000 case, (7.9). Hence it can be concluded that fibers also cause a thickening of the viscous layer.

Also of interest in heat transfer is to compare the effect of Prandtl number and fiber concentration on the relative ability of the flow to transfer heat to its ability to transfer momemtum. The ratio of $2C_H/C_F$ is one possible way to obtain an indication of this relative performance. This is discussed further in Chapter VI.

Chapter V

ASBESTOS FIBER CHARACTERISTICS

The asbestos fibers used in these experiments were obtained from the Turner Brothers' Asbestos Company in Rochdale, England. They were received in a concentrated aqueous suspension and were then diluted to the desired concentrations. The concentrated form contained 2.12% by weight asbestos fibers suspended in a 0.8% Aerosol OT solution. All experiments were run in this 0.8% surfactant solution because it was necessary to disperse the fibers and keep them from flocculating or gathering together in less effective clumps. Drag and heat transfer runs made with surfactant alone yielded the same C_F and C_H curves as pure water.

Chrysotile asbestos is a member of the fibrous mineral family, serpentine. It occurs naturally in veins and has a cylindrical crystal habit with fibrils 200-400 Å in diameter. The orientation of the fibrils is such that the fiber axis is approximately perpendicular to the vein wall and the fiber length is frequently equal to the width of the rock vein. This length refers to macro fiber bundles, each of which contains a large number of parallel fibrils which may be shorter due to defects introduced during growth or by subsequent geological faulting. Thew [28] gives the approximate generic composition as $Mg_3Si_2O_5(OH)_4$. Moffat [23] gives the formula for one kind of asbestos as $Ca_2Mg_5(OH)_2(Si_4O_{11})_2$. The fibrous form of the mineral is brought about by the dimensional mismatch between the $Ca_2Mg_2(OH_2)^{+12}$ sheets and the $(Si_4O_{11})_2^{-12}$ double chains, which

causes the chains to roll into tight tubes. The core and the inter-fiber space are probably filled with a non-crystalline solid of similar chemical composition to the fiber layers.

The fibers obtained from the Turner Brothers Asbestos Company were prepared by gentle stirring of the fiber bundles in the aqueous surfactant to produce dispersed, mainly single fibrils. Great care was taken to minimize fiber damage. A scanning electron micrograph made of a suspension used in our apparatus Fig. (5), shows the fibers to exist both as individual fibrils and as lay fiber ropes containing up to 100 fibrils each. This sample was prepared by filtering a 300 ppm suspension through Whatman No. 5 filter paper and then subsequently washing the fibers with warm water to remove most of the surfactant present. Examination of the individual fibers shows them to have a smooth surface and diameter on the order of 300 Å. They appear to be quite elastic and can bend through a loop of a few fiber diameters without fracturing. An important and obvious characteristic is the fibers' great length when compared to their diameter. In order to see the full length of one of the fibrils in Fig. 5 the width of the picture would have to be increased to about 30 feet. Instead of following this approach, statistical methods [1], [28] have been applied based on the known area of the field of view and the ratio of number of fibrils to fibril ends visible in the field. Some direct length measurements have also been made [28] by fitting several micrographs together into a collage. Thew [28] used both methods in analyzing fresh fiber suspensions and fiber suspensions that had been degraded by being subjected to shear in a rotating disc apparatus. He states that

the statistical method overestimates the size. At any rate, he found the length of the fresh fibers to be of the order of 0.3 mm and the degraded fibers to be 0.1 mm showing that fiber breakage is associated with degradation. A length of 0.3 mm gives an average aspect ratio of 10^4 which is extremely high compared to most other fibers.

The micrograph in Fig. 6 is an enlargement of Fig. 7 and shows the lay fiber rope in the center of the latter figure. The scale in each picture is indicated by the micron bar at the bottom. It must be remembered that because these fibers are the filtrate, they appear like a very closely entangled maze of ropes and nets. In the actual suspension they probably would appear much farther apart. For example, taking into account that the fiber density is about twice that of water, and assuming all the fibers exist as individual fibrils that are equally spaced, an estimate can be made of their separation. In the 300 ppm suspension, looking at the fibers end on, one would see a distance of 144 diameters between them. This distance is actually greater of course because many of the fibers exist in bundles. Still however, one can appreciate that the fibers do exist as a very interconnected and tangled web that is fairly uniformly dispersed throughout the whole fluid. Many single fibrils and small bundles split off from the large fiber ropes at various axial positions, and these can entangle with other ropes and other individual fibers to create an effective three dimensional grid. Hence it is suspected that the drag reduction mechanism employs the fact that; (a) the individual fibers are dispersed throughout the entire fluid very completely so that any

disturbance that occurs cannot grow very long before it encounters a fibril, and (b) once a disturbance starts to interact with one fiber it is very quickly interacting with the entire fiber grid through the entanglement of that fiber with the rest of the grid. Ordinary light microscope observations tend to support this speculation. A slide was made by surrounding a drop of suspension with a horseshoe of vaseline on one glass slide and covering this with another, thinner slide. By pressing on the top slide the fluid could be made to move laminarly. The resolution was insufficient to see the fibrils but the large lay fiber ropes were visible. It was seen that the motion of one rope was closely connected to the motion of another. Furthermore they appeared very elastic and would bend readily. T. V. videotapes of the fluid motion in a channel flow also give the appearance that the fibers form an effective interconnected web that exists throughout the fluid volume. (See Figs. 12, 13). The numbers of Figs. 12 and 13 refer to successive views of the large fiber bundles as they flow across the field of view. The flow is in a duct formed by gluing one glass slide atop another and using thin pieces of glass as spacers. As is depicted in Fig. 12 the bundles rotate as connected bodies when one part of the bundle is retarded by its proximity to the bottom of the slide. The bundle shown in the two views on the lower left hand side of that figure showed a lateral shift when one of its components neared a boundary. Figure 13 shows the same slide with a piece of glass glued to the bottom as an obstruction. When the flow was pulsed back and forth it was seen that dirt particles far from the obstruction showed flow-wise oscillations of large amplitude. Dirt particles near the obstruction however, moved

with very small amplitudes revealing the existence of a fiber web hung up on the obstruction. Although the web fibers were too fine to be seen under the light microscope the uniform motion of the dirt particles showed the web to be quite cohesive. The other two views of Fig. 13 show the motion of large bundles which pass sufficiently close to the web so that a portion of the bundle is entrapped by it. Further support to the grid concept is given by another simple observation. A suspension is stirred in a beaker and the stirring rod is removed. The fluid decreases in rotational speed until it stops and then it counter-rotates in the opposite direction for one or two seconds, stops, rotates forward again and so on in an oscillation of decreasing amplitude until the motion finally stops altogether.

An effort was made to see if any differences could be observed between fresh fibers and fibers that had undergone shear. Micrographs in Figs. 5. 7 and 8 show fibers from a fresh 300 ppm suspension while the micrographs of Figs. 9, 10 and 11 show this same suspension after it was sheared 10 times in the apparatus at a Reynolds number of approximately 1×10^5. Drag reduction was observed to drop from 42% to 6%. Observations are only qualitative but it does appear that: (a) the sheared fibers exist much more as single fibers with fewer and thinner lay fiber ropes; (b) the directional orientation of the sheared fibers is more random than that of the unsheared in which many of a fiber's nearer neighbor lie parallel to it; (c) the sheared sample of Fig. 10 appears like a partially torn-apart piece of cotton batton; (d) the sheared fibers appear generally to lie in a more random and entangled pattern. Presumably the action of the turbulent eddies and stresses causes fiber bundles to be torn apart and tangled up, as well as causing fiber breakage.

Chapter VI

PRESENTATION OF EXPERIMENTAL RESULTS

A. Friction Coefficient and Heat Transfer Coefficient for Water

The first part of the experimental program consisted of obtaining curves of the friction coefficient and heat transfer coefficient versus Reynolds number for ordinary tap water. The two coefficients are defined in the usual way as

$$C_F = \frac{\tau_w}{\frac{1}{2}\rho V^2} \tag{5}$$

$$C_H = \frac{q_w}{\rho C_p V \Delta T_{\text{wall-fluid}}} \quad . \tag{6}$$

These were obtained for each tube at three different Prandtl numbers. (Pr = 2.07 T = 183°F, Pr = 6.15 T = 77°F, and Pr = 10.8 T = 42°F).

The C_F curve for the smooth tube is shown in Fig. 14 and it is seen that it compared well with the curve previously obtained by Debrule [6] which is also shown. As would be expected the C_F curves for the three Prandtl numbers are coincident. The C_H curves are shown in Fig. 15 and it is seen that they are also close to those obtained by Debrule. There were no data taken by Debrule at Pr = 2.07. C_H values for that Prandtl number were computed by the Eagle-Ferguson formula given as

$$\frac{1}{C_H} = A + B(Pr - 1) + C(Pr - 1)^2 \quad . \tag{20}$$

Where A, B and C are given as a function of Re (Ref. [10]). The

comparison of the data with the C_H values predicted by the formula is given in the following table and is considered to be entirely satisfactory.

Re	C_H Data	C_H Formula
50,000	1.8×10^{-3}	1.79×10^{-3}
100,000	1.6×10^{-3}	1.56×10^{-3}
200,000	1.4×10^{-3}	1.37×10^{-3}

The C_F curve for the rough tube was found to be coincident with that obtained from the Moody chart for the same relative roughness, and also to be on the same line as Debrule's. The measured values of C_H for $Pr = 10.8$ also agree well with those obtained by Debrule. The present data for $Pr = 6.15$, however exceed those by Debrule by about 15%. This kind of agreement, however, was considered acceptable for the purposes of this investigation and the test facility was considered to be in proper operating condition. All subsequent C_F and C_H values measured for the suspensions are compared to the C_F and C_H water values that were obtained from the present experiments with pure water.

B. Friction and Heat Transfer Data for the Asbestos Suspension — Smooth Tube.

Two different concentrations of asbestos suspensions were used in the course of the experiment; 50 ppm representing a dilute suspension and 300 ppm representing a concentrated suspension. These distinctions are qualitative and are meant to imply only that with dilute concentrations a change in concentration (like doubling) causes an

almost equally large change in drag reduction, while in the more concentrated suspensions doubling the asbestos has less an effect on the drag reduction. The data for the 50 ppm suspension are shown in Figs. 16 and 17. It is seen that a maximum C_F reduction of 33%, and maximum C_H reduction of 50% are obtained. At very high Re, however, the reduction effect for both C_F and C_H vanishes. Further, it is observed that the C_F curves for the three different Prandtl numbers are not coincident, but that the hotter suspensions reduce drag better at high Reynolds number and the cooler suspensions reduce drag better at the lower Reynolds numbers. The fact that the friction data for these temperatures do not define a single curve on a C_F vs. Re graph should not be surprising. For example, for the hot suspension a high Re is obtained at a substantially lower wall shear stress. Similarly the hot suspension would have to be run at a much higher Re to achieve the same wall shear stress as cold water. If the hot suspension were run at this high Re it would not reduce the shear stress as much as the cold suspension would. These facts clearly indicate that Reynolds number is not the only important parameter in determining drag reduction and that there must be at least one other one, probably a parameter based on shear stress. This concept agrees with the views previously expressed by other authors in connection with polymer solutions (see e.g. Ref. [11]).

The data for the 300 ppm suspension is shown in Figs. 18 and 19. A maximum C_F reduction of 66% and a maximum C_H reduction of 80% are obtained. Trends similar to those of the dilute suspension are again observed; the hotter suspensions show their maximum effectiveness

at higher Reynolds numbers than the colder ones and there is a loss of effectiveness for the highest Reynolds numbers covered by this series of tests. While the dilute suspensions lose their drag reducing ability at about $Re = 2 \times 10^5$ the concentrated suspensions appear to retain some capability up to about $Re = 10^6$. Another important feature that is readily observable from the concentrated suspension is the existence of C_F and C_H minimums, with the C_H minimum occurring much earlier than the C_F minimum. As Re increases from small values, C_F steadily decreases getting farther and farther away from the pure water C_F. At a Re of about 10^5 to 2×10^5 the maximum drag reduction occurs, and as the Re is further increased the C_F curve rises and approaches the one for pure water. The C_H curves exhibit the same general behavior but their minimum occurs at about $Re = 4 \times 10^4$. Also shown in Figs. 18 and 19 are Debrule's curves for a 50 ppm polyox solution. They are seen to give comparable C_F and C_H reduction, but for the given range they show only a very slight bending of the curves upwards back towards the water curves. (This tendency incidentally is more apparent for the 10 ppm Polyox solutions.) A possible design implication of the smooth pipe data, which shows the C_H minimum to occur first, may be to run fiber suspensions at Re higher than those for the C_F minimum if higher heat transfer rates are desired in conjunction with drag reduction.

One run was made at a concentration of 600 ppm and $Pr = 6.15$ shown in Figs. 20 and 21. A maximum C_F reduction of 76% and a maximum C_H reduction of 86% was obtained. The most notable difference was that there was only a slight loss of fiber effectiveness at high

Reynolds number.

C. Friction and Heat Transfer Data for the Asbestos Suspension — Rough Tube

The data for the 50 ppm suspension in the rough tube are shown in Figs. 22 and 23. The best drag and heat transfer reduction occurs at low Reynolds numbers (approximate $Re = 10^4$). A 33% C_F reduction and a 75% C_H reduction was obtained. Again, the hotter suspension is better able to reduce drag at the higher Reynolds numbers, and again the C_F and C_H curves approach those for water at high Reynolds numbers ($Re = 10^5$). Also it is seen that for a typical curve, like the $Pr = 6.15$ line, C_F reduction ceases at about $Re = 6 \times 10^4$ while C_H reduction continues to $Re = 10^5$.

Data for the 300 ppm suspension are shown in Figs. 24 and 25. A maximum C_F reduction of 86% and a maximum C_H reduction of 94% are obtained. A remarkable result that is also apparent in Debrule's data is that for low $Re(\sim 20,000)$ the value for C_H of the suspension is actually lower in the rough tube than in the smooth. The heat transfer mechanism in the rough tube must be drastically affected by the fibers. Debrule proposes that heat is transferred by local flow within a roughness cavity as well as by turbulent exchange between the cavity and the main flow. It seems reasonable that the effect of an additive could be to reduce both modes of heat exchange. As before, the hot suspensions perform better at high Re and the cool ones perform better at low Re. Again this is attributed to the low shear levels prevalent in the hot suspension. Also the C_F and C_H minimums are very distinct, as is the tendency to lose effectiveness at high Reynolds number. A marked

change in the relative positions of the C_F and C_H minimums is observed. Whereas in the smooth tube they occurred about an order of magnitude of Reynolds number apart, in the rough tube they are much closer together. For the $Pr = 6.15$ fluid the C_H minimum occurs first (as in the smooth case) at $Re = 2 \times 10^4$ and the C_F minimum follows at $Re = 3 \times 10^4$. A comparison with Debrule's 10 ppm polyox shows similar results.

A run was also made in the rough tube with a 600 ppm dispersion at $Pr = 6.15$. The results are shown in Figs. 26 and 27. The effectiveness of the fibers is similar to that obtained with the suspension of 300 ppm, at least in the range of Re lower than those where the minimums occur. The concentrated suspension is, however, markedly superior at the higher Reynolds numbers. A maximum C_F reduction of 87% and a maximum C_H reduction of 95% are obtained. The relative positions of the C_F and C_H minimum move even closer together at this higher concentration. The C_H minimum occurs at $Re = 3.5 \times 10^4$ and the C_F minimum occurs at $Re = 4 \times 10^4$.

D. Degradation Tests

In his tests Debrule observed that polyox lost its effectiveness at high Reynolds numbers and attributed it to mechanical degradation of the polymer molecules at the high shear rates. Asbestos fibers are at least an order of magnitude larger than the polymers and it was thought that they would be less susceptible to degradation. The present experiments showed however, that the fiber dispersions also lost effectiveness at high Re. In order to obtain an indication whether or not this loss of effectiveness was caused by actual deterioration of the material it was decided to rerun a 300 ppm suspension in the rough tube after it had

already been passed through it once at a high shear rate. It was thought that, if the loss in effectiveness at high Re was due to degradation of the fibers, then these same fibers should also show a loss of effectiveness when used again at lower Reynolds numbers. As can be seen from Figs. 28 and 29, this is not the case. Although there was a slight drop in maximum drag reduction from 82% to 77% the fibers were still very effective drag reducers and showed only slight degradation effects. Furthermore, a comparison was made between the performance of fibers that were run 1/2 hour after their initial pass and these same fibers that were rested 24 hours after their initial pass. Results of the 1/2 hour test show the suspension to give, at low Re (30,000), drag values that are almost double those of the fresh suspension. At higher Re (60,000) the increase in drag was only about 20% however. After the 24 hour rest, the fibers were regenerated enough to reduce drag at low Re as effectively as the fresh suspension. The rest did not help the flow at high Re where both the 1/2 hour and the 24 hour suspensions showed a small 20% increase in drag over the fresh suspension. Also, surprisingly enough, there appeared to be no regenerative effect in the heat transfer reduction capabilities of the rested suspension at low Reynolds numbers to correspond to the regenerative effect on the drag. It may be more accurate to say that the initial loss in heat transfer reducing effectiveness of fibers (1/2 hour test) was less than the loss in their momentum transfer reducing effectiveness. Hence little improvement in C_H reduction was obtained by resting the fluid. These results were repeated with a different 300 ppm suspension.

E. Tests with another Type of Asbestos

Prior to the Turner Brothers Asbestos (TBA) suspension another kind of asbestos (5R-10) was obtained and drag tests were made with the present apparatus. Comparable drag reductions (50%) were obtained with it, although an order of magnitude higher (2,500 ppm) concentration was required. These fibers existed in larger bundles than the TBA with fewer isolated individual ones. This was evident from Hoyt's [15] microscope pictures as well as from unaided visual observation. Two interesting characteristics were noticed with these fibers when they were used in the present experiment. First it was found that as the same suspension was rerun repeatedly that drag reduction actually improved. Presumably this was caused by the bundles being split up to effectively increase the concentration of high aspect ratio fibers available. After about 25 runs, drag reduction began to fall off, possibly because the bundles were all split up and now there was only fiber breakage occurring. The second interesting characteristic is shown in the shear stress versus Re curve of Fig. 30. In a small Re range centered about Re = 35,000 the output from the pressure transducer oscillated widely. The pressure drop varied by ±20% about its mean value over the course of a run taking about 30 seconds. At other Re the output oscillated only ±1%. Further, when the mean values of these oscillations were plotted versus Re it was seen that the mean shear stress oscillated 10% above and below the values expected if a smooth curve relation were to prevail. Three runs were made at Re = 35,600 and three different means were obtained, one on the expected curve and two below it. The lowest was 37% below the expected curve. These

results were repeatable with the 5R-10 asbestos but there was no corresponding behavior with the Turner Brother's asbestos. This supports the contention that the oscillations were a fluid phenomenon and not just due to some vibrational resonance of the apparatus. The cause of these oscillations was not pursued further. It is mentioned here only, as it may be of interest to a future investigator working with a similar material.

Another test compared the drag reduction of a 200 ppm TBA fiber suspension in the 0.377 in. smooth tube to the reduction obtained by Hoyt [15] in a 0.046 in. tube. At Re = 14,000 Hoyt obtained a 32% drag reduction while the 0.377 in. tube gave 72% drag reduction at this same Reynolds number. Pure water flowing in a 0.046 in. tube at Re = 14,000 gives a shear velocity of 2.16 feet per second. To obtain this same shear velocity with water in a 0.377 in. pipe demands a Reynolds number of 150,000. The drag reduction of the 200 ppm TBA suspension at this Reynolds number in the large tube was found to be 33%. This implies that at least in this case drag reduction correlates better with shear stress rather than with Reynolds number. In general, however, the Re as well as a paramater based on the shear stress will probably be needed to fully describe the flow.

F. Prandtl Number and Concentration Effects.

An inspection of the following boundary layer equations for momentum and heat transfer show that as Prandtl number $\left(\frac{\nu}{\alpha}\right)$ tends toward unity (with the assumption $Pr_t = 1$, i.e. $\epsilon_h = \epsilon_m$) one should expect heat to be transferred more like momentum.

$$\frac{D\overline{U}}{Dt} = \frac{d}{dy}\left[\frac{d\overline{U}}{dy}(\nu + \epsilon_m)\right] \tag{21}$$

$$\frac{D\overline{T}}{Dt} = \frac{d}{dy}\left[\frac{d\overline{T}}{dy}(\alpha + \epsilon_h)\right] \tag{22}$$

The relative improvement of C_H compared to C_F as $Pr = 1$ is approached is seen in Fig. 31 for the smooth and rough tube. In both cases it is apparent that this improvement still persists in the suspensions, albeit to a lesser degree at high concentrations. Also it is seen that the effect of roughness is to decrease the relative ability of the flow to transfer heat. For pure water in the smooth tube the ratio $\frac{2C_H}{C_F}$ approaches 1.0 as the Prandtl number approaches 1.0, which is expected. In the 50 ppm suspension the ratio approached 0.9 while in the 300 ppm suspension in the ratio approaches only 0.5. This shows that somehow the fibers are more adversely affecting the heat transfer rate than they are the momemtum transfer rate and casts doubt on the applicability of the Reynolds analogy assumption that $\epsilon_h = \epsilon_m$. This trend may possibly be explained by the concept that, while a fiber web may effectively damp turbulent eddies, it may still be capable of transmitting shear forces between two fluid layers through strain on the web and tension in the fibers but there is no corresponding mechanism that transfers heat between the two layers. Heat must be transferred by intimate mixing of the layers and the fiber web inhibits this. Also in Fig. 31 the ratio $\frac{2C_H}{C_F}$ is plotted for Debrule's polyox solutions. As there are no measurements below $Pr \approx 4$ it is difficult to estimate the value of $\frac{2C_H}{C_F}$ that would be reached for $Pr = 1$. From the shape of the curves for Polyox however, it seems certainly possible that the

ratio might tend toward unity as Prandtl number approaches 1.0. This would indicate a difference between the behavior of the polyox solution when compared to the fiber suspensions and the existence of a fiber web, as postulated above, might be responsible for this result. In the course of the analysis of the data for the smooth tube the quantity $\frac{2C_H}{C_F}$ was also plotted against the wall shear for various concentrations (Fig.32). This presentation cannot be very general as it is not dimensionless, and in addition the Reynolds number varies as τ_w varies and this variation is different for each of the concentrations. Nevertheless the resulting curves seemed of sufficient interest to be included. The curve for pure water ($C = 0$) is given as a reference, and the data represented by it correspond to those obtained by previous investigators, as mentioned before. The interesting features of the data for the two other concentrations are the fact that the general shape is similar and that the decrease at low values of τ_w simply starts earlier (higher values of τ_w) and goes toward lower ratios of $\frac{2C_H}{C_F}$. It is particularly noteworthy that these three curves are similar to each other and have simple shapes even though the individual curves of C_H and C_F vs. Re (particularly the ones for 300 ppm) have different characteristics.

Figure 33 shows that the effect of increasing fiber concentration is to decrease the relative ability of the flow to transfer heat, for both the smooth and the rough tube.

It is also desirable to get an idea to what extent the Colburn relation

$$C_H Pr^{0.6} = \frac{C_F}{2} \tag{4}$$

might apply to drag reducing flows. This relation implies that for a given Pr, the ratio $\frac{C_F}{2C_H}$ should be constant and independent of Re. Plots of this ratio are given in Fig. 34 for Debrule's 10 ppm and 50 ppm polyox solutions and it is seen that the ratio is fairly constant over the Re range studied with a slight drop as Re is increased. However, both curves are above the $Pr^{0.6}$ level which is the one corresponding to pure water. The 50 ppm solution is well above the line and the ratio is given more closely by $Pr^{.83}$. Again this shows that the heat transfer is more strongly affected than the momentum exchange. The curves for the 50 ppm and 300 ppm fiber suspensions however definitely show that they do not follow the Colburn relation. Although they are closer to the pure water line at high Re they are by no means as constant as the polyox solutions over the Reynolds number range studied. It seems that the Colburn relation is followed poorly for the dilute suspension and not at all for the concentrated suspension. This is a further indication that the transmission of heat and momentum in the suspension is dependent on Re and probably on other parameters.

Chapter VII

COMPARISON WITH OTHER ASBESTOS DATA

It is the purpose of this Section to compare the results of the present experiment with the data of others.

It has been said in a general way that drag reduction is obtained most effectively from fibers that have the highest aspect ratio and smallest diameter. Although our principal interest is in asbestos fibers, the fiber bundles in this case vary considerably in size for any given suspension, and it may be appropriate to recall first the effects of size and shape obtained with the more uniform and the more easily characterized nylon or rayon fibers. Bobkowicz [2] and Radin [27] tested these fibers and found that drag reduction increased with increased aspect ratio at fixed concentrations. They also found that for equal aspect ratios and concentrations, drag reduction increased with decreasing fiber diameter. Radin [27] speculates that this may be due to the larger number of thin fibers present that are necessary to make a given concentration as well as to the increased fiber flexibility. Daily [5] also found that more flexible wood fibers gave better drag reduction than rigid ones. The present experiments indicate a similar trend. It was found that the Turner asbestos suspension ($\ell/d \sim 10^4$) gave nearly twice the drag reduction of a 5R-10 asbestos suspension ($\ell/d \sim 10^3$) and at a concentration which was smaller by an order of magnitude. The improvement of drag reduction with decreased size may also be reflected by the performance of polymers. These latter, if thought of as fibers, are probably about

two orders of magnitude thinner than the Turner asbestos and at a concentration which is about ten times lower than that for the asbestos suspension.

From the available data it may also be said that in general the effect of increasing fiber concentration is to increase drag reduction. This may cease to be true however, if a concentration beyond a certain maximum is used. Radin [27], in commenting on Kerekes [18] nylon fiber data, notes that as concentration increases at a fixed flow rate, drag reduction increases to a maximum. As concentration further increases apparent laminar flow is obtained which is actually a plug flow as described by Daily [5]. Pressure drop then increases rapidly. If the Reynolds number is further increased turbulent flow develops and destroys the plug, and the high concentration suspension will become an excellent drag reducer. He notes that for narrow flow rate ranges, care must be taken to determine what flow regime is present, laminar-type plug flow or turbulent flow. The data of Vaseleski and Metzner [31] illustrate this effect. On their C_F versus Re plot for JM asbestos the first three concentrations (200, 800, 2500 ppm) show increasing degrees of drag reduction with the C_F line shifted below but parallel to the water line. The 5000 ppm line however not only is shifted below the other three but it also falls off about four times as fast indicating that the transition to turbulence is delayed to Reynolds numbers beyond 2×10^5. The concentrations used in the present experiment were insufficient to obtain fully laminar flow, so this characteristic was not investigated. The effect of changes in the concentration on the drag was more pronounced at

dilute (50 ppm) concentrations of Turner asbestos. At high concentrations in both smooth and rough tubes the effect of increasing the concentration was mainly to extend the C_F minimum to higher Reynolds numbers. In the lower Re range there was only slight improvement in drag reduction from the 300 to 600 ppm suspension, but beyond the minimum C_F the 600 ppm was dramatically better (Fig. 26) than the 300 ppm.

It has been found that polymer solutions lose their effectiveness in larger pipes. This does not appear to be the case with fibers. Tests performed by Vaseleski and Metzner [31] on JM asbestos in pipes ranging from 2.4 cm to 9.5 cm showed no change in drag reduction with pipe diameter. Others, like Daily and Bugliarello [5], found a decrease in C_F with increasing pipe diameter. This was for wood pulp flows in 3/4 in. and 2 in. pipes. Ellis [11] using Turner Brothers asbestos also found an improvement in drag reduction in going from a 0.115 cm tube to a 1.43 cm tube.

In the present experiment only one size of tube was used so diameter effects are not known. It was noticed however that much greater drag reduction was obtained in this apparatus than in Hoyt's apparatus which had a tube that was considerably smaller. This was at the same Reynolds number in each case however, and the stresses in the small tube are much higher.

Considering now the effect of degradation, a comparison with the work of others shows similar results in smooth tubes. Ellis [11] observed a drop in drag reduction from 44 to 33 percent in a 0.564 in. tube after his 50 ppm Turner Brothers asbestos suspension was

subjected to shear for one hour by an impeller pump. He ran at a Reynolds number of 20,000. In the present apparatus a 50 ppm suspension was run at Re = 50,000 after it had already passed through the tube once. The wall shear was higher due to the higher Reynolds number and the smaller (.377 in.) tube, so the drag reductions were less. The drag reduction was seen to drop from 30.6% to 22.5% which is proportionally similar to Ellis' results.

Hoyt observed a drop from 65% drag reduction to 64.5% drag reduction in his 0.046 in. tube after one pass at Re = 14,000. This was for a 500 ppm suspension. For pure water, similar stress levels are expected to prevail in the present apparatus at Reynolds number around 150,000. At Re = 140,000 a 50 ppm suspension was observed to drop in drag reduction from 17.4% to 14.7% after one pass. This drop is considered small, like Hoyts', when it is pointed out that the concentration was reduced by a factor of 10. The above results and comparisons serve to emphasize that degradation is a complicated phenomenon that seems to depend on many factors such as shear history, temperature, concentration, fiber type, etc.

Chapter VIII

POREH'S MODEL

A separate section is devoted to the analytical work of Dimant and Poreh [7]. Their analytical predictions have been previously compared to the polymer data of Debrule. The present results will be compared in a similar way, and for this reason the approach of Dimant and Poreh is reviewed briefly.

Dimant and Poreh [7], assumed a mixing length model, and on this basis were able to predict C_H values using measured values of C_F. As mentioned earlier they were able to match quite satisfactorily the data by Debrule for dilute (10 ppm) polyox solutions. Their predictions were somewhat high for the concentrated (50 ppm) solutions.

The model is based on Van Driests' expression for the mixing length in Newtonian fluids

$$\ell = ky\left(1-e^{-\frac{y^+}{A^+}}\right) \tag{3}$$

where

$$A^+ = 26 \qquad k = 0.4 \ .$$

Using this expression, the following relation between dimensionless velocity gradient and shear stress is obtained:

$$\frac{du^+}{dy^+} = \frac{2\tau^+}{1+\sqrt{1+4k^2y^+2\left(1-e^{-\frac{y^+}{A^+}}\right)^2\tau^+}} \tag{23}$$

$$\tau^+ = \frac{\tau}{\tau w} \ .$$

Integrating this gives $u^+ = y^+$ at small values of y^+ and $u^+ = \frac{1}{k}\ell n\, y^+ + B(A^+)$ at large values of y^+. However this expression

fails to describe faithfully the velocity profile in the central region of the pipe, and Poreh modified the u_1^+ profile by adding to it a u_2^+ that is patterened after the law of the wake

$$u^+ = u_1^+ + u_2^+ \tag{24}$$

u_1^+ is the solution to (23) using $\tau^+ = 1 - \frac{y^+}{R^+}$ and u_2^+ is given as

$$u_2^+ = \frac{P}{2k}\left[1-\cos\left(\frac{\pi y^+}{R^+}\right)\right]\left[1-e^{-\frac{2R^+}{A^+}}\right]. \tag{25}$$

The value of P was taken as 0.67 so that the value of the Newtonian friction factor at $Re = 5 \times 10^5$ would satisfy

$$\frac{1}{\sqrt{C_F}} = 4 \log(Re\sqrt{C_F}) - 0.4 \ . \tag{26}$$

Poreh then lets the value of A^+ vary and obtains friction coefficients by numerical integration of u^+. These are displayed in a plot of Prandtl coordinates $1/\sqrt{C_F}$ versus $Re\sqrt{C_F}$ for an A^+ variation from 26 to 350. For drag reducing flows it is only necessary to choose an appropriate value of A^+ that gives the C_F value measured experimentally. This value of A^+ is then used in the computation of C_H.

Eddy viscosity and eddy diffusivity transport equations are used to describe the shear stress and the heat flux.

$$\tau = \rho(\nu+\epsilon)\frac{du}{dy} \tag{15}$$

$$q = -(k+\rho C_p \epsilon_h)\frac{dT}{dy} \ . \tag{16}$$

For constant fluid properties these give

$$\frac{dT^+}{dy^+} = \frac{q^+}{\tau^+} Pr_{eff} \frac{du^+}{dy^+} \tag{27}$$

$$Pr_{eff} = (1+\frac{\epsilon_m}{\nu})/\left(1/Pr + \frac{\epsilon_m}{\nu Pr_t}\right) \tag{28}$$

$$Pr_t = \frac{\epsilon_m}{\epsilon_h} \tag{29}$$

$$T^+ = (T_w - T)C_p \frac{\tau_w}{q_w V^*} \tag{30}$$

$$V^* = \sqrt{\frac{\tau_w}{\rho}} \quad . \tag{31}$$

For the assumptions of $Pr_t = 1$ and constant heat flux, Poreh obtains

$$\frac{dT^+}{dy^+} = \frac{1-(4/Re)\int_o^{y^+} u^+\left(1-\frac{y^+}{R^+}\right)dy^+}{\left(1-\frac{y^+}{R^+}\right)E_o^+} \tag{32}$$

where

$$E_o^+ = \frac{1}{Pr} + \frac{1}{Pr_t}k^2y^+2\left(1-e^{-\frac{y^+}{A^+}}\right)^2\frac{du^+}{dy^+} \quad . \tag{33}$$

The bulk temperature of the fluid can then be found

$$T_b^+ = \frac{\int_o^{R^+} T^+U^+(R^+-y^+)dy^+}{\int_o^{R^+} U^+(R^+-y^+)dy^+} \tag{34}$$

and

$$C_H = \frac{\sqrt{C_F/2}}{T_b^+} \quad . \tag{35}$$

A program was written in Fortran to evaluate C_H. A^+ values for smooth pipe friction factors were found for the dilute and concentrated fiber suspensions. Typical A^+ values were about 50 for the dilute suspension and 200 for the concentrated suspension. C_H values

computed for the various suspensions were plotted versus Re and compared to the measured values on Figs. 35, 36. Poreh made such a comparison with Debrule's data. As a check Debrule's 10 ppm polyox C_H curve was computed and found to be in good agreement with Poreh's results.

The method of Poreh and Dimant was then applied to the present data obtained with asbestos suspensions. For the 50 ppm (dilute) suspension the agreement between measured and predicted values were quite satisfactory, within about 8%. The discrepancies were considerably larger in the comparison with the more concentrated (300 ppm) suspension, particularly for the data at $Pr = 2.2$ and 6.2 where the deviations were of the order of 75%. This type of disagreement, in a comparison which involves measured values of C_F, raises serious doubts about the applicability of this model to suspensions. The principal assumption in Poreh's theory which may be violated by the suspension is probably that involving the Reynolds analogy. The exchange of heat and momentum in a suspension could well be different so that one may no longer set ϵ_m equal to ϵ_H. As mentioned in an earlier section, one may imagine that the individual fibers as well as the grid like structures of the intermingled fibers would reduce the exchange of fluid by turbulent fluctuations. Yet the fiber structure could provide a mechanism to transmit forces. The corresponding transmission of heat by conduction through the fibers is likely to be negligible in comparison. The possibility that Reynolds' analogy does not apply to fiber suspension is, therefore quite plausible. It should be added that Poreh and Dimant did not propose that their theory be used for this application. The

comparison was made, because it was quite successful for polymer solutions, and because even discrepancies would indicate something about the transfer mechanism in the suspension, as they indeed did.

Chapter IX

DISCUSSION OF THE EFFECT OF ASBESTOS FIBER SUSPENSION ON THE FLOW

In the foregoing Chapters the results obtained by many authors were described briefly. These results came from experiments with a great variety of fiber suspensions and polymer solutions. Among the fiber suspensions, nylon, rayon, wood, as well as several types of asbestos were included. The concentrations ranged from 50 ppm to several percent and the operating conditions also varied quite widely, leading to great differences in Re and the wall shear stress. In addition it was shown that the performance of a particular suspension could depend on the process of preparation, on storage time, and on the prior use of the suspension. With these many variables involved direct comparisons with the work of others is difficult. One should expect only a rather general agreement of some of the important features. The data from the various sources all indicate that fiber dispersions can lead to significant reductions in friction and that this reduction is dependent not only on the Reynolds number but probably also on such factors as the ratio of the shear stress to some characteristic of the fiber.

Several concepts were also discussed which had been proposed as explanations for the behavior of the various suspensions. The mechanisms by which the fibers modify the flow include interactions with the turbulence generation, with the dissipation process, and with the discrete, periodic vortices which have been observed in the wall

layer. Some authors feel that the principal modification takes place in the wall layer, others feel that the core flow is affected, and in some instances both regions are believed to be affected. It is also well realized that the mechanism may depend on the properties of the fiber as well as on the concentration.

For the type of fiber dispersion used in the present experiments the mechanism which most plausibly is responsible for the observed effects involves the interaction of the fibers with "bursts" and "sweeps" which have been observed in the wall layer. This phenomen has been investigated with increasing interest in the past ten years and a description of the principal aspects will be given in the following.

Thorough studies by Kline et al [19,20,25] Corino and Brodkey [4], and others [9 ,14,21] have brought to light the importance of these quasi-ordered events. Bursting is an instability phenomenon that has its origins in the wall region of a turbulent shear flow. The basic result of the process is that slow, low momentum wall fluid is hurled out into the mainstream and because of the condition of continuity, fast fluid from the core is swept in towards the wall further downstream. It is believed that these bursts and sweeps are responsible for nearly all of the turbulence production and drag in the flow.

Several investigators [14, 20, 21] have reported on the existence of a streaky flow structure near the wall. In a plane parallel to the wall, the fluid moves downstream in a repeated series of high and low speed streaks moving side by side. It has been fairly well established that these streaks are caused by secondary streamwise vorticity as

illustrated in the sketch of Fig. 37(a). On one side of any given vortex, faster fluid coming from a distance away from the wall is swept towards the wall by the vortex and its neighbor. On the other side relatively slow fluid which has been in contact with the wall is swept up between the vortex and its other neighbor. It is this slow wall fluid that is forced upward between two streamwise vortices that ultimately bursts.

Initially the secondary vorticity that lifts the slow wall fluid is quite low so the low speed streak moves away from the wall quite slowly over a long streamwise extent. Once the streak reaches some critical distance from the wall it starts to move away from the wall much more rapidly. Kline calls this low speed streak "lifting". The relatively rapid outward motion of the low speed fluid into the outer high speed fluid creates a narrow inflexional zone in the instantaneous velocity profile. This high shear zone contains two reversals of slope gradient and an inflection point as illustrated in the sketch of Fig. 37(b). Observations show that this instantaneous inflexional velocity profile leads to the growth of an oscillatory disturbance just downstream of the inflexional zone. The dominant mode of this disturbance is a streamwise vortex motion that grows in strength and size as it proceeds downstream. This rapidly growing and very energetic vortex should not be confused with the comparatively weak secondary streamwise vorticity that causes the formation and lifting of low speed streaks. It is conceivable, indeed likely, that some of the vorticity of this energetic vortex contributes to the large scale secondary vorticity after the burst, however. Kline reports that on the basis of film

observations there is a considerable increase in vortex diameter occurring with a rapid increase in rotational speed. Thus energy is being transferred to the vortex and probably at a rather high rate. The mechanism of this energy exchange has not been investigated. At any rate, this "organized" motion prevails for 3 to 10 cycles of vortex rotation after which a second unstable condition is reached and the fluid bursts, i. e. it is thrown out into the mainstream. The oscillatory growth phase started at $y^+ = 10$ to 30 and grew an order of magnitude to about $y^+ = 400$ in Kline's water channel, which is about half of the boundary layer thickness.

Kline has subsequently shown that the interaction between the bursts and the flow in the logarithmic region produces sweeps of the faster fluid toward the wall. These sweeps in turn, influence the generation of bursts further downstream. He showed this with a combination of wall dye injection, hydrogen bubble lines normal to the wall, and a moveable dye injector located at from $y^+ = 50$ to $y^+ = 200$. Dye from this latter injector was seen to move toward the wall after a burst and these wallward motions of the flow were seen to lead to wall dye lift up as illustrated in Fig. 37(c). The cycle is

(a) lifting of low speed streaks

(b) formation of streamwise vortex

(c) burst of vortex fluid

(d) sweep down of fast core fluid.

The strength of individual bursts varies, as do their positions and frequency of occurrence in the fully developed flow. It is more

realistic to think of a dominant band of length or time scales rather than a single sharply defined value.

Several investigators [14, 20, 21] have found the spacing of the low speed streaks to be given by

$$\lambda = 100 \frac{\nu}{U_\tau} \tag{36}$$

where λ is the mean streak spacing and U_τ is the friction velocity $\left(\sqrt{\frac{\tau_w}{\rho}}\right)$.

Corino and Brodkey [4] performed visualization experiments in a 2 in. pipe to observe the bursting phenomenon and found the process to be similar to that described by Kline et al. They were able to focus on a thin region near the wall where they counted the number of burst events occurring over a fixed time interval. They were able to do this over a Reynolds number range of from 20,000 to 60,000. The same data is also shown as a function of wall shear stress rather then Reynolds number. The Corino Brodkey curve was extrapolated to higher Reynolds numbers and the replotted as N (burst/sec) versus $\tau_w (\text{lbf/ft}^2)$ as is seen in Fig. 39.

Fortunately, some flow visualization has also been done with drag reducing additives. One of the few experiments of this type was performed by Donohue et al [9] by adding polyox to a channel flow. In this flow it was observed that the non-dimensional streak spacing $\left(\lambda^+ = \lambda \frac{u_\tau}{\nu}\right)$ was larger and that the burst frequency was lower than for water. It appeared that the average time between bursts was at the level expected for pure water flow at the reduced wall shear.

As mentioned earlier, Katsibas and Gordon [17] in their important study obtain a relation that gives friction coefficient in pipe flow as the inverse function of the square root of the time between turbulent bursts. This calculation is based on a simple penetration model in which fluid from the outer layer is suddenly brought into contact with the wall and slowed down by shear

$$C_F = \frac{4}{\bar{u}} \sqrt{\frac{\nu}{\pi \theta}} \tag{37}$$

$\bar{u}$ = average bulk velocity

θ = time between turbulent bursts.

They apply this relation to the data obtained by Fortuna and Hanratty [13] on increases in streak spacing with drag reduction, and assume that the scale size increases in the axial direction by the same factor as in the transverse direction. This increase in area/burst is then assumed to be proportional to the increase in θ. Using this value of θ they were able to explain the measured drag reduction values within about 12%. In light of these observations it seems reasonable to postulate that the effect of the additives is to increase the lifetime of a streamwise vortex and to allow it to grow to a larger size.

The correlation between drag and θ indicates that drag reduction might be predicted by studying the effect of the fibers on the time θ . Polymer solutions and asbestos fiber suspensions exhibit high resistance to normal stresses as are encountered in stretching flows. These flows exist in the rapid outflows between pairs of counter-rotating longitudinal eddies (secondary streamwise vorticity responsible for streak lifting) and they exist in the outer regions of the burst

instabilities, i. e. between the rapidly rotating fluid in a streamwise vortex and the relatively "still" fluid that surrounds it. It may well be imagined that polymer chains and fibers interfer with these "bursts" and thereby bring about the observed increase in θ. This concept would also lead to a more plausible explanation on how additives representing a wide range of length scales may interact with the flow near the wall. It also allows a more plausible interpretation of the fact that in many cases additives like polymers and asbestos fibers seem to modify the flow near the wall without noticeably affecting the flow in the turbulent core.

A possible explanation of the observed degradation of suspensions will also be mentioned. One may recall first that the fibers probably exist in an interconnected web. Next one may imagine a fiber which is caught by the vortex. The fluid of the vortex will exert a tension on this fiber and this force will be resisted by: (a) initially, the opposing drag on the "uncaught" portion of the fiber in the "still" fluid as it is pulled through this fluid and by (b) the resistive force of the entire rest of the web to which the fiber is connected, once it becomes "taut". The resistance of the web will restrict the further motion of the fiber relative to the web. As Reynolds number increases however, so does the growth rate of the vortices and the velocity difference between the "still" and "vortecal" pieces of fluid becomes ever larger. This increases the tension on the fiber and eventually it either breaks or is torn from the web. Hence it is postulated that once a characteristic speed U_v of the vortex exceeds a critical value, U_{v_c}, the interference of the fibers with the flow will diminish, and there is a limiting

maximum drag which the fibers can exert on the vortex motion. This kind of mechanism may possibly be responsible for the loss of effectiveness at higher Reynolds numbers and may be the cause of fiber degradation.

To summarize briefly it is felt that fibers cause drag reduction by increasing the time between turbulent bursts. They do this primarily by interfering with the streamwise vortex growth stage of the bursting process. Presumably their high resistance to elongational strain constrains the vortices to grow at slower rates and to achieve larger sizes before they burst.

Chapter X

CONCLUSIONS

The presence of asbestos fibers causes appreciable friction reductions in both smooth and rough tubes. In the present series of experiments the fiber-induced friction reduction was observed to be as high as 76% in a smooth tube and as much as 87% in a rough tube. The comparisons are in respect to pure water at the same Reynolds number. It was also seen that an increase in the concentration lowers the friction coefficient. This effect is more noticeable at low concentrations (50 ppm) than at high concentrations (300 ppm) and it is expected that an asymptotic value will be reached eventually. Accompanying the friction reduction is an even greater reduction in heat transfer coefficient. This coefficient was reduced by as much as 86% in the smooth tube and by a maximum of 95% in the rough tube. For certain flow conditions the reduction in the rough tube can be so drastic as to give a lower heat transfer coefficient than in the smooth tube.

The fibers in a suspension appear to be present as a fairly continuous interconnected web. They exist both as "ropes", with up to 100 fibers in a bundle, and as individual strands. Single fibers partially attached to a bundle were also observed. Individual fibers have diameters of from 200 to 400 angstroms.

The drag reducing mechanism loses its effectiveness at high Reynolds numbers (shear levels) where friction and heat transfer coefficients return to the pure water values. Physical degradation of the fibers – breakage, tangling – appears at most to be a minor

contributor to this loss. It is speculated that the major cause of loss of effectiveness is the occurrence of local extensional strain rates that are greater than some critical value (determined by additive type and concentration). It is postulated that, once the rate exceeds this value, the fibers are torn from their web and that they can then exert only a small constant resistance to the strain. This concept of a yielding web is consistent with the concentration results. Increasing the concentration causes only small reductions in the coefficients at lower Reynolds numbers, but leads to substantially lower coefficients at higher Reynolds numbers. The increased concentration, in other words, extends the effectiveness of the fibers to higher Reynolds numbers. This effect may possibly be explained by imagining that a stronger web is formed in the concentrated dispersion and that this web is more resistant to the high strain rates at high Reynolds numbers. In addition the higher concentrations will, of course, contain a greater number of fibers per unit volume, which may have an effect in itself.

It also appeared that after a suspension has been sheared that some of its lost effectiveness is due to tangling of the fibers rather than fiber breakage. If this suspension is allowed to rest, instead of being resheared right away, it regains some of its effectiveness at the lower Reynolds numbers. Presumably the elastic fibers have some resilience and are capable of straightening or detangling.

As with Debrule's polymer flows, a study of the measured values of C_F and C_H for fiber flows indicates that the turbulent diffusivities are reduced near the wall and the viscous region extends further from the wall than in pure water flows. From the present

study the exact way in which this is accomplished cannot be determined with any degree of certainty. It is proposed, however, that the fibers influence the flow through interaction with the "bursts" and "sweeps" described by Kline et al [19].

Although the characteristics of dilute solutions may be explained fairly satisfactorily in terms of Reynolds analogy, there seems to be definite deviations from this analogy for flows at high concentrations. This is not surprising and one may well imagine mechanisms which would explain such deviations. It is suggested, for example, that while a fiber web can still transmit force between two fluid layers through forces in the web, there is no corresponding method of transferring heat between the two layers. Hence there is a mechanism for momentum transfer to which there is no corresponding heat transfer mechanism, and the Reynold's analogy would therefore not apply.

Finally, it is reemphasized that asbestos suspensions are complicated fluids and there are a multitude of factors that can influence the performance. The origin and method of preparation of the dispersion are important as are the shear history, temperature, effectiveness of the surfactant, and concentration. Moreover, the behavior of the dispersion will probably depend also in some way on the scale of turbulence and level of shear stress in the flow. Further research on all of these factors is warranted and flow visualization experiments are especially recommended for learning more about the drag reducing mechanism.

REFERENCES

1. Atkinson, A. W., Gettins, R. B., Rickards, A. L., "Estimation of Fibrid Lengths in Chrysotile Asbestos Fibers", Nature, Vol. 226, 1970.

2. Bobkowicz, A. J., and Gauvin, W. H., "The Turbulent Flow Characteristics of Model Fiber Solutions", Can. J. of Chem. Engrs., Vol. 44, 1966.

3. Castro, W., and Squire, W., "The Effect of Polymer Additives on Transition in Pipe Flow", Appl. Sci. Res., Vol. 18, 1967.

4. Corino, E. R., and Brodkey, R. S., "A Visual Investigation of the Wall Region in Turbulent Flow", J. Fluid Mech., Vol. 37, Part I, 1969.

5. Daily, J. W. and Bugliarello, G., "Basic Data for Dilute Fiber Suspensions in Uniform Flow with Shear, TAPPI, Vol. 44, No. 7, 1961.

6. Debrule, P., "Friction and Heat Transfer Coefficients in Smooth and Rough Tubes with Dilute Polymer Solutions, Ph. D. Thesis, Calif. Institute of Technology, 1972.

7. Dimant, Y. and Poreh, M., "Momentum and Heat Transfer in Flows with Drag Reduction," Technion, Israel Institute of Tech., Publication No. 23, 1974.

8. Dipprey, D. F., "An Experimental Investigation of Heat and Momentum Transfer in Smooth and Rough Tubes at Various Prandtl Numbers", Ph. D. Thesis, California Institute of Technology, 1961.

9. Donohue, G. L., Tiederman, W. G. and Reischman, M. M., "Flow Visualization of the Near-Wall Region in a Drag Reducing Channel Flow", J. Fluid Mech., Vol. 56, Part 3, 1972.

10. Eagle, A., and Ferguson, R. M., "On the Coefficient of Heat Transfer from the Internal Surface of Tube Walls", Proc. Royal Soc., Vol. 127, 1930.

11. Ellis, H. D., "Effects of Shear Treatment on Drag-Reducing Polymer Solutions and Fiber Suspensions", Nature, Vol. 226, 1970.

12. Forrester, R. H., Larson, R. E., Hayden, J. W. and Wetzel, J. M. "Effects of Polymer Addition on Friction in a 10-inch Diameter Pipe", J. Hydronautics, Vol. 3, No. 1, 1969.

13. Fortuna, G. and Hanratty, T. J., "The Influence of Drag-Reducing Polymers on Turbulence in the Viscous Sublayer", J. Fluid Mech., Vol. 53, 1972.

14. Grass, A. J., "Structural Features of Turbulent Flow over Smooth and Rough Boundaries", J. Fluid Mech., Vol. 50, Part 2, 1971.

15. Hoyt, J., "Turbulent Flow of Drag Reducing Suspensions", Naval Undersea Center, Publication No. 33, 1972.

16. Hoyt, J.W., "Hydrodynamic Drag Reduction due to Fish Slimes", Naval Undersea Center, San Diego, California.

17. Katsibas, P. and Gordon, R. J., "Momentum and Energy Transfer in Turbulent Pipe Flows: The Penetration Model Revisited", AICHE Journal, Vol. 20, No. 1, 1975.

18. Kerekes, R. J. E., "Turbulent Drag Reduction in Pipe Flow of Ideal Fiber Suspensions", Ph. D. Thesis, McGill University Montreal, 1970.

19. Kim, H. T., Kline, S. J. and Reynolds, W. C., "The Production of Turbulence near a Smooth Wall in a Turbulent Boundary Layer", J. Fluid Mech., Vol. 50, Part I, 1971.

20. Kline, S. J., Reynolds, W. C., Schraub, F. A. and Runstadler, P. W., "The Structure of Turbulent Boundary Layers", J. Fluid Mech., Vol. 30, Part 4, 1967.

21. Lee, J. K., Eckelman, L. D., Hanratty, T. J., "Identification of Turbulent Wall Eddies through the Phase Relation of the Components of the Fluctuating Velocity Gradient", J. Fluid Mech., Vol. 66, Part I, 1974.

22. Lee, W. K., Vaseleski, R. C. and Metzner, A. B., "Turbulent Drag Reduction in Polymeric Solutions Containing Suspended Fibers", AICHE Journal, Vol. 20, No. 1, 1974.

23. Moffat, W. G., Pearsall, G. W. and Wulff, J., The Structure and Properties of Materials, Vol. I., John Wiley and Sons, Inc., New York, 1964.

24. Mysels, K. J., Ind. Eng. Chem., Vol. 41, 1949.

25. Offen, G. R. and Kline, S. J., "Combined Dye-Streak and Hydrogen-Bubble Visual Observations of a Turbulent Boundary Layer", J. Fluid Mech., Vol. 62, Part 2, 1974.

26. Peyser, P., "The Drag Reduction of Chrysotile Asbestos Dispersions", J. Appl. Polymer Science, Vol. 17, 1973.

27. Radin, I., Zakin, J. L., and Patterson, G. K., "Drag Reduction in Solid-Fluid Systems", AICHE Journal, Vol. 21, No. 2, 1975.

28. Thew, M. T. and Anand, J.S., "Characterizing Asbestos Fibers Suitable for Drag Reduction", International Conference on Drag Reduction, Sept 4-6, 1974, Paper D2, 1974.

29. Toms, B. A., "Some observations of the flow of linear polymer solutions through straight tubes at large Reynolds numbers" North Holland Publishing Co., Proc. 1st Int. Congress on Rheology, Vo.. II., 1949.

30. Vaseleski, R. C., "Drag Reduction in the Turbulent Flow of Fiber Suspension", M.ChE. Thesis, University of Delaware, 1973.

31. Vaseleski, R. C. and Metzner, A. B., "Drag Reduction in the Turbulent Flow of Fiber Suspensions", AICHE Journal, Vol. 20, No. 2, 1974.

32. Virk, P. S., Merrill, E. W., Mickley, H. S., Smith, K. A. and Mollo-Christensen, E. L., "The Toms Phenomenon: Turbulent Pipe Flow of Dilute Polymer Solutions", J. Fluid Mech., Vol. 30, Part II, 1967.

33. White, W. D., "Drag Reduction Measurements for Three Polymers at 4°C in Viscous Drag Reduction, Plenum Press, New York, 1969, p. 173-182.

34. White, W. D., "Heat Transfer Characteristics of Dilute Polymer Solutions in Fully Rough Pipe Flow", Nature, Vol. 227, 1970.

Appendix I

CALIBRATIONS

A. Pressure Drop Measurements

The differential pressure transducer and strip chart recorder were calibrated against a mercury manometer. Compressed air was simultaneously connected to the high pressure side of the transducer and to one side of the manometer. Voltage outputs were then plotted for the various pressures applied, several points being taken for each scale of the recorder. It was noticed over a period of time that the zero pressure voltage varied by about a tenth of a millivolt and that other pressure voltages would vary by the same amount. Hence it was only necessary to record the zero shift and to correct all readings accordingly. For the corrected readings the same calibration curve could be used. The change in zero during a run was less than 1/100 of a millivolt, and typical pressure drop outputs were several millivolts.

B. Flow Rate Measurements

The flow rate was determined from a count of the number of teeth of the piston-driving gear that passed a sensor in 10 seconds. Upon using the constant 3×10^{-4} developed by Debrule to multiply the teeth number, data were obtained that were consistently low.

The flow rate was checked by timing the piston over a travel of 2 feet. This showed that the multiplicative constant should be 3.075×10^{-4}. The constant was checked several times during the experiment and was found to be invarient. There was no measurable

leakage past the piston. From the flow rate, the average velocity of the flow in the test section could be calculated.

C. Power Measurements

The power required to heat the tube walls was derived from the voltage drop across the test section and the electrical resistance of each tube as a function of temperature. The assumption of a unity power factor seems justified because the tube is a simple resistive load and the present circuit is similar to that of Dipprey's [8] who checked the power factor.

It was necessary to measure the voltage with a true RMS meter because there was a distortion in the sinusoidal wave coming from the transformer and a standard AC voltmeter gave erroneous results. Debrule found the resistance of each tube by passing a known current from a constant current source and measuring the voltage drop across the electrodes on a digital voltmeter which was accurate to 0.1% of the maximum reading. The tube was kept at a given temperature by passing water through it. That temperature was calculated from the inlet, outlet and wall thermocouple outputs. The results of the measurements are given in Table 1 in the form

$$R = C_o + C_1 T + C_2 T^2 \quad . \tag{I.1}$$

D. Temperature Measurements

The outputs from the four thermocouples (inlet, outlet, and two wall) were displayed on two digital voltmeters. The inlet and wall thermocouples were connected via a rotary switch to one voltmeter while the outlet thermocouple was connected directly to the other.

The inlet and outlet couples were calibrated at the Jet Propulsion Laboratory of the California Institute of Technology in a control furnace. Isothermal tests were then performed at low flow rates at various temperatures. From these it was possible to determine the difference in emf between the inlet and the two wall thermocouples as a function of inlet temperature emf. This small emf difference due to differences between couples was then subtracted out in the actual tests. Also subtracted out was the effect of viscous heating. This small effect was obtained by making isothermal runs at various flow rates (or shear stresses) and noting the difference in emf between inlet and outlet couples. The heating was assumed to vary linearly with axial position, so the contribution to wall thermocouple emf due to viscous heating was known.

At the start of a run while at a low flow rate, the voltage output of the inlet and outlet couples are read on the two voltmeters. Ideally they should read nearly the same with the only difference in emf corresponding to that calculated from the Jet Propulsion Laboratory calibrations. Owing to differences in meter response the emf difference is larger than in the ideal case. Hence to get the effect of reading all voltages on one meter, it is necessary to note the emf correction that must be added to the outlet reading to give it the value it would obtain if it were measured with the inlet voltmeter. During the actual heat transfer run, this emf correction is added to the outlet reading to give what it would read on the inlet voltmeter and this corrected reading is used in computations. This correction is assumed to be valid because the rise in water temperature (and hence outlet emf) is generally

quite small so that the same difference between the two meters should prevail.

Appendix II

DATA REDUCTION CALCULATION OF C_F AND C_H

A. Calculation of Friction Coefficient

The friction coefficient C_F can be expressed as

$$C_F = K_2 \frac{\rho \Delta P}{\dot{\omega}^2} \tag{II. 1}$$

where ΔP is the pressure drop in the rough section and K_2 contains various dimensional conversion factors as well as the length and diameter of the rough part of the test section.

The pressure drop ΔP measured by the pressure transducer between the two pressure taps is actually the sum of various pressure drops. It is due to the pressure drop in the rough section ΔP, the pressure drop due to smooth pipe friction in the two .5 inch smooth sections ΔPs (Immediately following the upstream pressure tap and preceding the downstream tap), the difference in dynamic pressure due to a slight difference in diameter at the two measuring stations (q_2-q_1), and the contraction loss $\Delta Pcontr$ and expansion loss ΔPex due to a change in diameter between the smooth sections near the taps and the rough part of the test section (see Fig. 5). Thus

$$\Delta P = \Delta Pmeas - [\Delta Ps + (q_2 - q_1) + \Delta Pcontr + \Delta Pex] \tag{II. 2}$$

therefore

$$C_F = K_2 [\frac{\rho \Delta Pmeas}{\dot{\omega}^2} - \gamma] \tag{II. 3}$$

where

$$\gamma = \frac{\rho}{\dot{\omega}^2} [\Delta Ps + (q_2-q_1) + \Delta Pcontr + \Delta Pex] \ . \tag{II. 4}$$

In the expression for γ, (q_2-q_1) and ΔPex are constants of the

tube while ΔPs is directly proportional to C_F in the smooth tube, and $\Delta Pcontr$ must be determined experimentally in hydraulic tests.

The quantity γ was calculated following Dipprey [8]. The value of $\Delta Pcontr/\omega^2$ was taken to be equal to that used by Dipprey for water. Table I contains the values calculated by Dipprey, of all constants appearing in the data reduction. Future users of these constants must remember that some of the values are only valid for water under certain flow conditions and must be reevaluated if another fluid or test procedure is used.

B. Calculation of Heat Transfer Coefficient

The heat transfer coefficient may be written as

$$C_H = \frac{\dot{q}_{o_x} \pi D^2}{4 C_p \Delta T_{fx} \dot{\omega}} \qquad \text{(II. 5)}$$

where

ΔT_{fx} = wall to mixed-fluid temperature difference at station x.

= Tins wall$_x$ - T_{Lx}

$\dot{q}_{o_x}$ = local heat flux

D = inside diameter of the tube

$\dot{\omega}$ = mass flow rate

In order to express ΔT_{fx} in terms of measured quantities (T outwall - Toutl) and Toutl, ΔT_f is evaluated at station x as follows:

$$\Delta T_f = \text{Tins wall} - T_L \qquad \text{(II. 6)}$$

$$= (\text{Toutl} - T_L) + (\text{Tout wall} - \text{Toutl}) - (\text{Tout wall} - \text{Tins wall}) .$$

$(T_{out\,wall} - T_{outl})$ can be calculated from the thermocouple outputs. In order to calculate C_H from Eqs. (II. 5 and II. 6) it is first necessary to calculate the wall temperature drop $(T_{out\,wall} - T_{ins.\,wall})$ as well as the outlet temperature to local bulk temperature difference $(T_{outl.} - T_{Lx})$ and local heat flux $\dot{q}_{o_x}$.

a) Wall Temperature Drop.

The expression for the local wall temperature drop is developed in Appendix IV-B of Dipprey [8] and is written

$$\Delta T_w = \Delta T_{wp}\left[1 - \frac{1}{6}\left(\frac{t}{R}\right) + \left(\frac{\alpha}{2} + \frac{\beta}{6}\right)\Delta T_{wp}\right] \qquad \text{(II. 7)}$$

where $\dot{q}_o$ = local heat flux normal to the tube wall

t = local tube wall thickness

k = thermal conductivity evaluated at the outer wall temperature

R = tube radius.

$$\alpha = \frac{dk/dT}{k[T_{out\,wall}]}$$

$$\beta = \frac{d\rho_e/dT}{\rho_e[T_{out\,wall}]}$$

ρ_e = electrical resistivity

The quantity $\frac{t}{R}$ appearing in Eq. (II. 7) may be replaced by an average value evaluated for the whole test section. Likewise, the multiplying factor ΔT_{wp} becomes

$$\Delta T_{wp} = \dot{q}_o \frac{\bar{t}}{2k[T_{out\,wall}]} . \qquad \text{(II. 8)}$$

Moreover, $k = k_o[1+\alpha(T-T_o)]$ where k_o is the thermal conductivity evaluated at the reference temperature T_o, and

$$\frac{1}{k[T_{\text{out wall}}]} = \frac{1}{k_o} + \frac{d(1/k)}{dT}\left[T_{\text{out wall}} - T_o\right] . \qquad \text{(II. 9)}$$

Using II. 8 and II. 9 and regrouping terms yields

$$\Delta T_{wx} = k_6 \dot{q}_{o_x} t_x [1 + k_7 T_x][1 - k_8 \dot{q}_{o_x}] . \qquad \text{(II. 10)}$$

The first bracketed term on the right accounts for the variation of thermal conductivity of the wall with temperature. The correction term $(1 - \frac{1}{6}\frac{t}{R})$ in Eq. (II. 7) is absorbed here in k_6 while the second bracketed term represents the other correction term in Eq. (II. 7)

b. Determination of $\dot{q}_{o_x}$ and $(T_{\text{outl}} - T_{L_x})$.

Theoretically, the determination of the local $\dot{q}_o$ and local T_L result in inseparable integral equations. The value of $\dot{q}_o$ depends on the local resistivity of the tube wall ρ_e, which in turn depends on the effective local wall temperature, defined as the temperature in the center of the wall. This effective wall temperature is determined by

1) the local T_L;

2) the heat transfer film conductance of the fluid (h);

3) the thermal conductivity of the wall, evaluated at the local wall temperature.

The pertinent equations (II. 11) are

1) $\dot{q}_{(x)} = \frac{I^2}{2\pi r(x) A(x)} \rho_e[T_{\text{eff}(x)}]$

2) $T_{L(x)} = T_{L(x_o)} + \int_{x_o}^{x} \frac{2\pi r(x)\dot{q}(x)}{\dot{\omega} C_p} dx$ using

$$\dot{\omega} C_p (T_{L_x} - T_{L_{x_o}}) = 2\pi \int_{x_o}^{x} \dot{q}(x) r(x) dx$$

$$3) \quad T_{eff}(x) = T_{ins\,wall}(x) + \frac{\Delta T_w(x)}{2}$$

$$= T_L(x) + \frac{\dot{q}(x)}{h} + \frac{1}{4}\frac{t(x)\dot{q}(x)}{k\left[T_{out\,wall}(x)\right]}$$

(retaining only the first order terms in $\Delta T_w(x)$)

$$4) \quad T_{out\,wall}(x) = T_L(x) + \dot{q}(x)\left[\frac{1}{h} + \frac{1}{2}\frac{t(x)}{k\left[T_{out\,wall}(x)\right]}\right]$$

Moreover

$$\rho(T) = \rho(T_o) + \beta[T - T_o]$$

$$k(T) = k(T_o) + \alpha[T - T_o] \quad .$$

Symbols used in these equations that are not previously defined are:

I = electric current

r = local radius of tube

A = area of a surface passing across the tube in such a way that it is everywhere normal to the current flux lines

$T_L(x_o)$ = bulk temperature at reference station x_o.

Dipprey [8] treated this problem by first putting the above equations into dimensionless form. Then he evaluated the maximum excursion of the various dimensionless coefficients in terms of the parameters of his experiments and expanded the various functional forms in Taylor's series. He was thus able to produce linearized separated expressions for $\dot{q}_o(x)$ and $T_L(x)$, retaining only first order corrections to account for the various interactions, and dropping out the negligible terms. Debrule made a careful examination of the assumptions introduced in the linearization and concluded that Dipprey's results remained valid under his flow conditions. Since the

flow conditions of the present experiment remain the same as Debrule's, it is assumed that Dipprey's results are still valid.

The resulting expressions have the form

$$\frac{W_{Ts}}{\pi D L \dot{q}_{o_x}} = M_x\left[1+B_x\left(\frac{Q_x}{M_x^2}\right)+ \Gamma_x \frac{N_x}{M_x}\right] \qquad \text{(II. 12. 1)}$$

$$\frac{T_{outl}-T_{Lx}}{T_{outl}-T_{in}} = M_{xx}\left[1-\frac{B_x \frac{X}{L}}{2(1+\Gamma_x)} - \frac{\Gamma_x S_x}{(1+\Gamma_x)}\right] \qquad \text{(II. 12. 2)}$$

where the subscript x refers to a particular local thermocouple station, W_{Ts} is the power released in the test section, and L and D are the length and diameter of the heated test section. M_x, N_x, Z_x, M_{xx} and S_x represent various definite integrals depending only on the variation of wall thickness with longitudinal station and on the position of the thermocouple station. Defining $\left(\frac{R}{L}\right)_x$ as the electrical resistance per unit length of pipe at station x and r_{ix} as the inside tube radius at station x,

$$M_x = \frac{1}{L\left(\frac{R}{L}\right)_x}\int_o^L \frac{R}{L}(\xi)d\xi \quad \text{with} \quad \frac{R}{L} = \left(\frac{R}{L}_o\right)(1 - bx) \ , \ b \simeq 4.75 \times 10^{-3} \text{ohm/inch}$$

$$N_x = \frac{r_{ix}}{L\left(\frac{R}{L}\right)_x^2}\int_o^L \frac{\left(\frac{R}{L}\right)^2[\xi]\,d\xi}{r_i[\xi]} - M_x$$

$$Q_x = \frac{(R/L)^2_{ref}}{(R/L)_x^2}\left[Qref + \frac{Mref}{L}\int_x^{xref} \frac{\left(\frac{R}{L}\right)[\xi]}{\frac{R}{L}_{ref}}d\xi\right]$$

with

$$Qref = \frac{1}{L^2\left(\frac{R}{L}\right)^2_{ref}}\int_o^L \frac{R}{L}[\xi]\int_{xref}^x \frac{R}{L}(\xi')d\xi'd\xi$$

$$M_{xx} = \frac{L}{L-x} \frac{\int_x^L \frac{R}{L}[\xi]d\xi}{\int_o^L \frac{R}{L}[\xi]d\xi}$$

$$S_x = \frac{(xN_L)x}{(xM_L)x} - \frac{N_x}{M_x}$$

where $(xN_L)_x$ and $(xM_L)_x$ are defined as N_x and M_x respectively, but this time the integrals are evaluated from x to L.

Finally, B_x and Γ_x appearing in Eq. (II. 12) are defined as:

$$B_x = \frac{\frac{d\rho_e}{dT}[T_{outl} - T_{in}]}{\rho[T_{eff}(x)]}$$

$$= \frac{\beta}{\rho_o + \beta[T_{eff} - T_o]}[T_{outl} - T_{in}] \qquad \text{(II. 13)}$$

$$\Gamma_x \simeq B_x(\frac{D}{4L})(\frac{1}{\overline{C_H}}) \ .$$

Thus B_x is determined from the resistivity of the wall material, a rough estimate of the wall temperature and the measurement of the temperature rise of the fluid passing through the test section $(T_{outl} - T_{in})$.

The factor Γ_x contains the first order correction for the effect of the error caused by estimating the local effective wall temperature to be equal to the local mixed fluid temperature. A crude preliminary estimate of $\overline{C_H}$ in terms of the conditions of the test gives adequate accuracy.

Using the definition of Γ_x, Eq. (II. 12. 1) may be written

$$\frac{W_{Ts}}{\dot{q}(x)} = a_x[1+B_x b_x]$$

or

$$\dot{q}(x) = \frac{W_{Ts}}{a_x(1+b_x B_x)}$$

$$\simeq a'_x W_{Ts}[1-b_x B_x] \quad . \qquad \text{(II. 14)}$$

Likewise, Eq. (II. 12. 2) becomes

$$T_{outl}-T_{L_x} = (T_{outl}-T_{in})M_{xx}\left[1-\frac{B_x}{1+\Gamma_x}\left(\frac{x/L}{2}+\frac{\Gamma_x}{B_x}S_x\right)\right]$$

or, after expanding $(1+\Gamma_x)^{-1}$ in Taylor's series

$$T_{outl}-T_{L_x} \simeq (T_{outl}-T_{in})M_{xx}[1-C_x B_x+d_x B_x^2] \quad . \qquad \text{(II. 15)}$$

It is now possible to calculate C_H from the flow rate $(\dot{w})$, the power released in the test section (W_{Ts}), the wall-to-outlet temperature difference and the outlet to inlet temperature difference.

C. Computer Program

A standard program was written in FORTRAN to reduce the data from both tubes. The values of the constants K_i used in this paragraph, as well as γ, a'_x, b_x, c_x, d_x, t_x, M_{xx} are given in Table I for both tubes.

The input consisted of:

1) V0 = the inlet thermocouple output in millivolts

2) V1 = the outlet thermocouple output in millivolts

3) V2 = one wall thermocouple output in millivolts

4) V3 = the other wall thermocouple output in millivolts

5) V5 = the outlet thermocouple output in millivolts before the test section is heated

6) N = the number of gear teeth passing the magnetic pick in 10 seconds

7) VPRES = the output from the pressure transducer in millivolts

8) VPOW = the voltage drop across the test section in volts

9) SC = operating scale (millivolts) of the strip chart recorder.

The following calibration curves are stored in memory:

1) Calibration of the inlet thermocouple T0 = f(V0)

2) Calibration of the outlet thermocouple T1 = f(V1)

3) Calibration of one wall thermocouple T2 = f(V2)

4) Calibration of the other wall thermocouple T3 = f(V3)

5) Isothermal emf difference between the two wall and the inlet thermocouple DT2 = f(V2), DT3 = f(V3)

6) Friction heat between inlet and outlet FROI = f(VPRES)

7) Friction heat between inlet and wall FRWI = f(VPRES)

8) Calibration of pressure transducer P = f(VPRES)

9) ρ, C_p, μ, P_r = f(T).

The sequence of operations performed by the machine is:

1) Calculation of Temperatures

SHIFT = V5-V0

V1 = V1-SHIFT corrects for the difference between voltmeters

T0 = T0(V0)

T1 = T1(V1)

T2 = T2(V2)

T3 = T3(V3)

DT2 = DT2(V2)

FROI = FROI(VPRES)

FRWI = FRWI(VPRES)

T1 = T1-FROI

T2 = T2-FRWI-DT2

T3 = T3-FRWI-DT3

2) Calculation of C_F

TAV = T0 + (T1-T0)/2

$\rho = \rho(TAV)$

$\dot{\omega} = K_1 N \rho$

$\Delta P = \Delta P(VPRES)$

$$C_F = K_2\left[\frac{\rho \Delta P}{\dot{\omega}^2} - \gamma\right]$$

3) Calculation of C_H

Calculation of the average temperature in the center of the wall:

$$T_{av\,eff} = T_{out\,wall} - (T_{out} - T_{in})K_3 - \overline{\Delta T}_w/2$$

K_3 is a constant depending on the position of the thermocouple station. $\overline{\Delta T}_w$ is the average wall temperature drop which Debrule estimated from calibration tests as a function of V and T_{in}. Evaluation of $\overline{\Delta T}_w$ in the present experiment put its value between 0.3 at low Re and 0.7 at high Re. Elimination of $\overline{\Delta T}_w$ altogether from the expression for $T_{av\,eff}$ makes less than 1% difference, so for the purpose of

data reduction a constant value of . 5 was assigned to ΔT_w.

$RTS = C0 + C1\ T_{av\,eff} + C_2 T_{av\,eff}^2$ evaluates resistance of test section

$WAT = K_4(VPOW)^2/RTS$ evalutes power released in test section

$C_p = C_p(T_{av})$

$C = W C_p(T1-T0)$ evaluates calorimetrically measured rate of heat addition to the fluid

$\% \delta W = 100(C-WAT)/WAT$ % discrepancy between C and W

$BSX = (T1-T0)/(K5+T2)$ approximation of Eq. (II. 13)

$QX = A'_x(WAT)(1+b_x BSX)$ Eq. (II.14)

$\Delta T_{wx} = DTWX = K_6(QX)(t(x))(1+k_7 T2)(1-k_8 QX)$ Eq. (II. 10)

$T_x = TO + k_9(T1-T0)$ T_x = first order approximation for the local bulk fluid temperature

$\mu x = \mu(Tx)$

$C_p x = C_p(Tx)$

$Re_x = K10\ \frac{\dot{\omega}}{\mu_x}$

$Pr_x = Pr(T_x)$

$T_{outl} - T_{L_x} = S_x = (T1-T0)M_{xx}[1-C_x BSX + d_x(BSX)^2]$ Eq. (II. 15)

$\Delta TFX = DTFX = S_x + (T2-T1) - \Delta T_{wx}$

$C_{H_x} = K_{11}\ \frac{\dot{q}x}{C_p \Delta TFX \dot{\omega}}$.

The output consisted of

T0	inlet
T1	outlet
T2	wall
T3	wall
Re_x	Reynolds number
ΔP	pressure drop
τ_ω	wall shear stress'
C_F	friction coefficient
WAT	power dissipated
$\dot{\omega}$	mass flow rate
Pr_x	Prandtl number
C_H	heat transfer coefficient.

The program also plotted

$\log_{10} C_F$ vs $\log_{10}$ Re

$\log_{10} C_H$ vs $\log_{10}$ Re

τ_ω vs Re

D. Table of Constants used in Computer Program (Table I)

$K1 = 3.075 \times 10^{-4}$

$K4 = .9482 \times 10^{-3}$

$K5 = 211$

Constant		E-3 Tube (Smooth)	A-4 Tube (Rough)
C0	$R_{TS} = C_0 + C_1 T + C_2 T^2$	.001695	.001660
C1		5.649×10^{-6}	6.95×10^{-6}
C2		5.22×10^{-9}	0
K2		2.77×10^{-5}	3.87×10^{-5}
K3		.370	.368
K6		408.	380.5
K7		7.54×10^{-4}	7.07×10^{-4}
K8		.005	.004
K9		.871	.809
K10		40.5	38.3
K11		.1117	.1250
γ		-1.34	9.2
a'_x		.0485	.0444
b_x		.344	.337
c_x		.41	.399
d_x		1.65	.55
t_x		.02007	.01874
M_{xx}		.130	.128

Appendix III
Error Analysis

A. Friction Coefficient

The expression for the friction coefficient may be expressed

$$C_F = \frac{\pi^2 D^5}{32 L_R}\left[\frac{\Delta P_{TS}}{K^2 N^2 \rho_{av}} - \gamma\right] \qquad \text{(III. 1)}$$

a) Error in D

According to Dipprey, who used the same tubes, the diameter uncertainties are as follows

Smooth Tube ±0.3% $(1.003)^5 = 1.015$

Rough Tube ±1.3% $(1.013)^5 = 1.067$

b) Error in L

The percentage error in length is assumed negligible compared to other errors in C_F determination

c) Error in N

N was measured over 10 seconds from about 200 (low Re) to 1200 (high Re). The uncertainity in N is ±1, so that uncertainty ranges from

N ±0.5% to N ±0.1%

N^2 ± 1% to N^2 ±0.2%

d) Error in ρ_{av}

ρ error was assumed negligible

e) Error in K

The factor K is defined from the equation

$$\dot{\omega} = K N \rho_{av}$$

and was checked by timing the piston travel over 2 feet.

Error in timing 0.1%

Diameter of cylinder = 10 ± .040 inches ⇒ .4% D^2⇒ .8%

$$\dot{\omega} = KN\rho = V\frac{\pi D^2}{4}\rho$$

$$(1.001)(1.008) \doteq 1 + .001 + .008 \doteq 1.009$$

Error on K is .9%; K^2 1.8%.

f) Error in ΔP

The pressure transducers calibration was checked and found to be repeatable within 0.5%. This error combined with the error introduced by a periodic oscillation in the transducer response to give a total error of 2%.

g) Error in γ

Assumed to be 0 for the smooth tube and .7% for the rough tube.

Errors in D and K are systematic errors while those in ΔP_{TS} and N are random and should cancel out if the data is repeated enough times. Combining just the systematic errors in the most detrimental way in Eq. (III.1), the maximum excursions become:

Smooth tube: C_F ± 3.4%

Rough tube: C_F ± 8.6%

If the systematic errors are combined with the random errors for any one data point in Eq. (III.1), then the maximum excursions become:

Smooth tube: C_F ±6.5% low flow rates, ±5.5% high flow rates

Rough tube: C_F ±11.7% low flow rates, ±10.8% high flow rates.

It should be emphasized that these represent the maximum error excursions. If errors are assumed to be normally distributed the total error in C_F is more like ±3%.

In addition to these errors there is the problem of duplication of the suspensions. One dispersion may differ from another for several reasons. The method of preparation and stirring may vary, the time it is allowed to sit before it is used may vary, temperature histories may vary, and amount of exposure to shear may vary. It was found that in testing several suspensions, that were prepared in the same manner, C_F results could be duplicated within about 10% in both tubes.

Hence an overall estimate of the error in C_F is

$$C_F \pm 13\% \ .$$

This error is small compared to the enormous drag reduction obtained.

B. Heat Transfer Coefficient

The expression for the heat transfer coefficient is

$$C_H = \frac{q_w}{\rho C_p V \Delta T_f} \qquad \text{(III. 2)}$$

a) Error in ρ, C_p is assumed negligible

b) Error in q_w

$$q_w \propto \frac{\text{Voltage}^2}{R_{TS}} \ .$$

Debrule estimated that R_{TS} was determined with an accuracy of 1% and says that a check of these values against those due to Dipprey

supports this estimation. The error in V, including the normal reading error and the possible error in the voltmeter itself is of the order of 1.5%.

$$\frac{(1.015)(1.015)}{.99} \Rightarrow q_w \pm 4\% \quad .$$

c) Error in V

The velocity is directly proportional to the mass flow rate

$$\dot{\omega} = KN\rho \quad .$$

From Appendix IIIA, $K \pm .9\%$ $N \pm .5\% \Rightarrow V \pm 1.4\%$

d) Error in ΔT_f

$$\Delta T_f = T_{ins\ wall} - T_L$$

$$= (T_{outl} - T_L) + (T_{out\ wall} - T_{outl}) - (T_{out\ wall} - T_{ins\ wall}).$$

The first and last terms on the right hand side of the above equation are much smaller than $(T_{out\ wall} - T_{outl})$ so it is expected that essentially all the error in ΔT_f will be from this term.

Using isothermal tests it was found that the difference in temperatures as indicated by the thermocouples and as indicated by a mercury thermometer placed in the exhaust stream was less than 0.5%.

During the actual heat transfer tests it was noted that there could be as much as a 6% discrepancy between the two wall thermocouples in the rough tube. Presumably this could be caused by the two couples being attached to the pipe above different parts of roughness elements, as well as local variations in wall thickness and flow conditions. The error in the smooth tube was 1.5%. The readings of the two wall thermocouples are averaged, so their discrepancy is cut in half. Also, during a run it was noticed that the emf outputs on the

digital voltmeters could vary by 3%. This error can be counted as random however, and if the data is repeated enough times it should cancel out.

If just the systematic errors are combined in the most detrimental way in Eq. (III. 2) then the maximum excursions become

Smooth tube: $C_H \pm 5.8\%$

Rough tube: $C_H \pm 8.3\%$.

For one data point in the rough tube, the possible error (random and systematic) in $T_{outwall}$ is $\pm .5 \pm 3 \pm 3 = \pm 6.5\%$; for the rough tube, the possible error in T_{outl} is $\pm .5 \pm 3 = \pm 3.5$. Error in ΔT_f is then $[T_{outwall} \pm 6.5\%) - (T_{outl} \pm 3.5\%)]$ or $\Delta T_f \pm 10\%$. The corresponding smooth tube case gives $\Delta T_f \pm 7.7\%$. Combining these errors in the most detrimental way in the expression for C_H gives

for the rough tube $C_H \pm 17.2\%$

for the smooth tube $C_H \pm 14.3\%$.

Again, these represent maximum excursions and if the errors are normally distributed the accuracy is better given by

$$C_H \pm 8\% \ .$$

In addition to this error there is the problem of repeatability between separately prepared suspensions. It was found that C_H curves could be repeated to within about 10%. This gives an overall margin as

$$C_H \pm 18\% \ .$$

This error is small compared with the enormous amount of heat transfer reduction obtained.

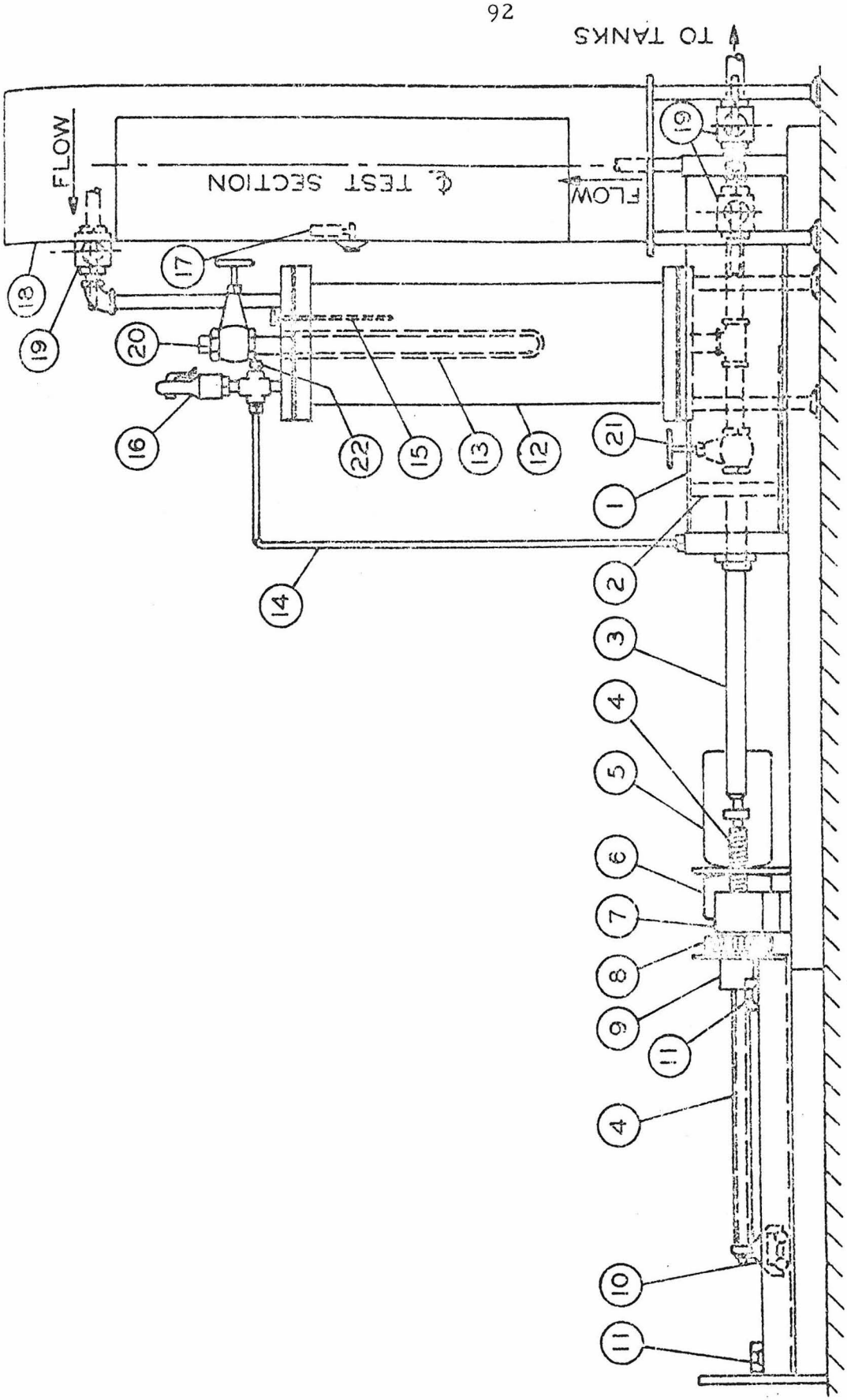

Figure 1. Simplified test facility schematic.

Legend for Figure 1

(1) Cylinder, 10 in. diameter

(2) Piston

(3) Piston rod

(4) Ballscrew

(5) D-C motor, variable speed

(6) Speed reducer

(7) Pillow block with two bearings

(8) Gears

(9) Drive nut

(10) Anti-rotation device

(11) Limit switches

(12) Reservoir

(13) Heating rods

(14) Pressure equalizing line

(15) Immersion thermometer

(16) Safety valve

(17) Safety switch

(18) Test section housing

(19) Globe valves

(20) Filler valve

(21) Drain

(22) Connection to pressure regulator and N_2 bottle

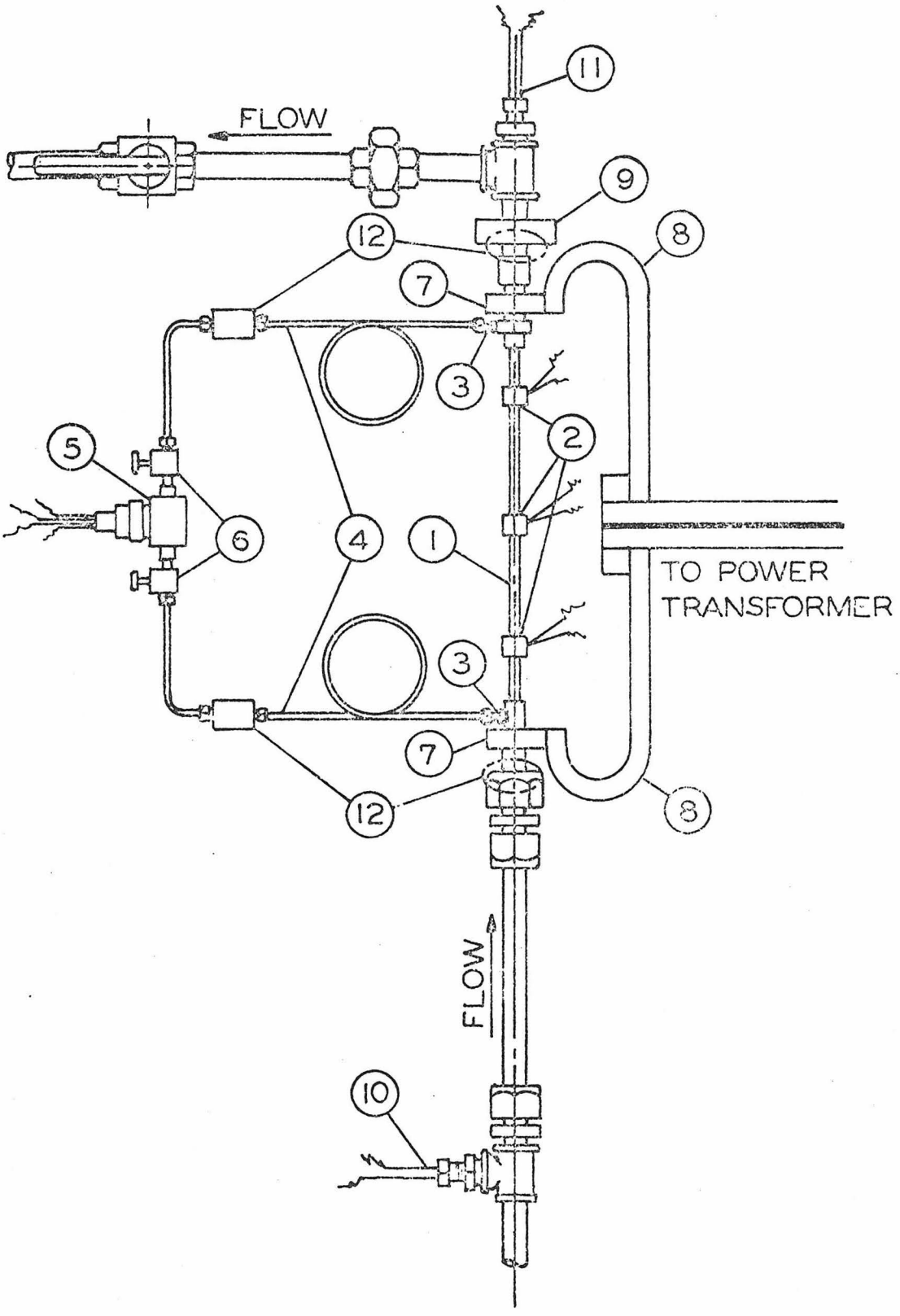

Figure 2. Test section schematic.

Legend for Figure 2

(1) Nickel T.S.

(2) Thermocouples stations (3)

(3) Pressure tap

(4) Pressure lines

(5) Differential pressure transducer

(6) Three-way valves

(7) Copper electrodes

(8) Copper buses

(9) Mixing chamber

(10) Inlet immersion thermocouple

(11) Outlet immersion thermocouple

(12) Teflon electric insulation

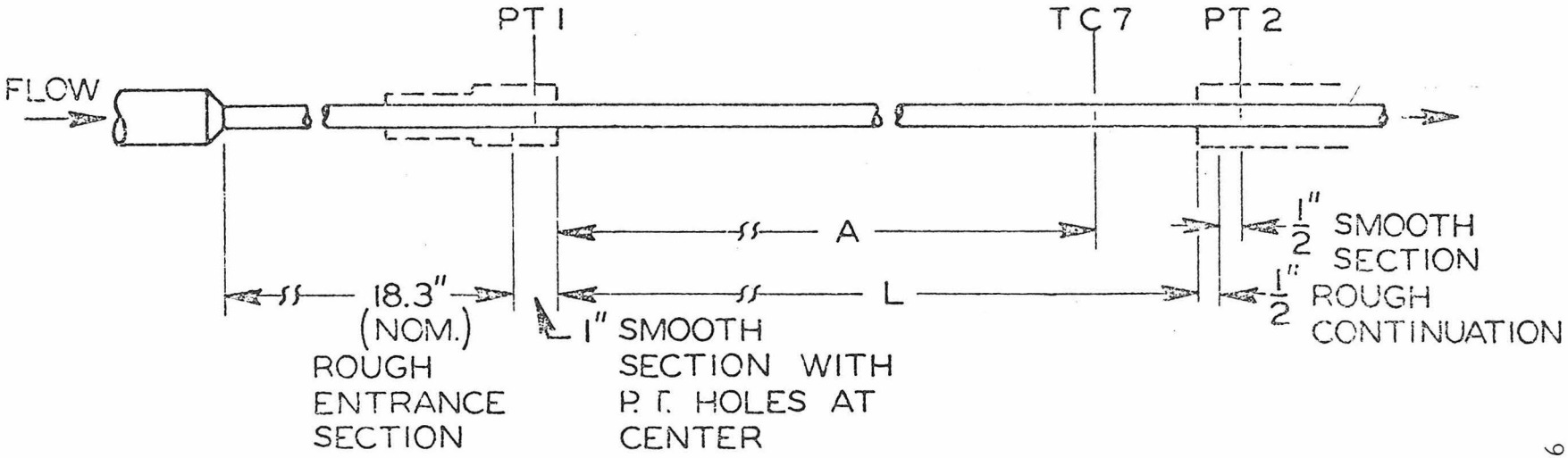

TUBE	D	L	A	t	ϵ	ϵ_s/D
E-3	0.377	17.40	15.14	0.0201	—	—
A-4	0.399	17.41	15.12	0.0187	0.0195	0.0488

ALL DIMENSIONS IN INCHES
PT = PRESSURE TAP
t = WALL THICKNESS AT T.C. STATION
TC = THERMOCOUPLE

Figure 3. Tube dimensions.

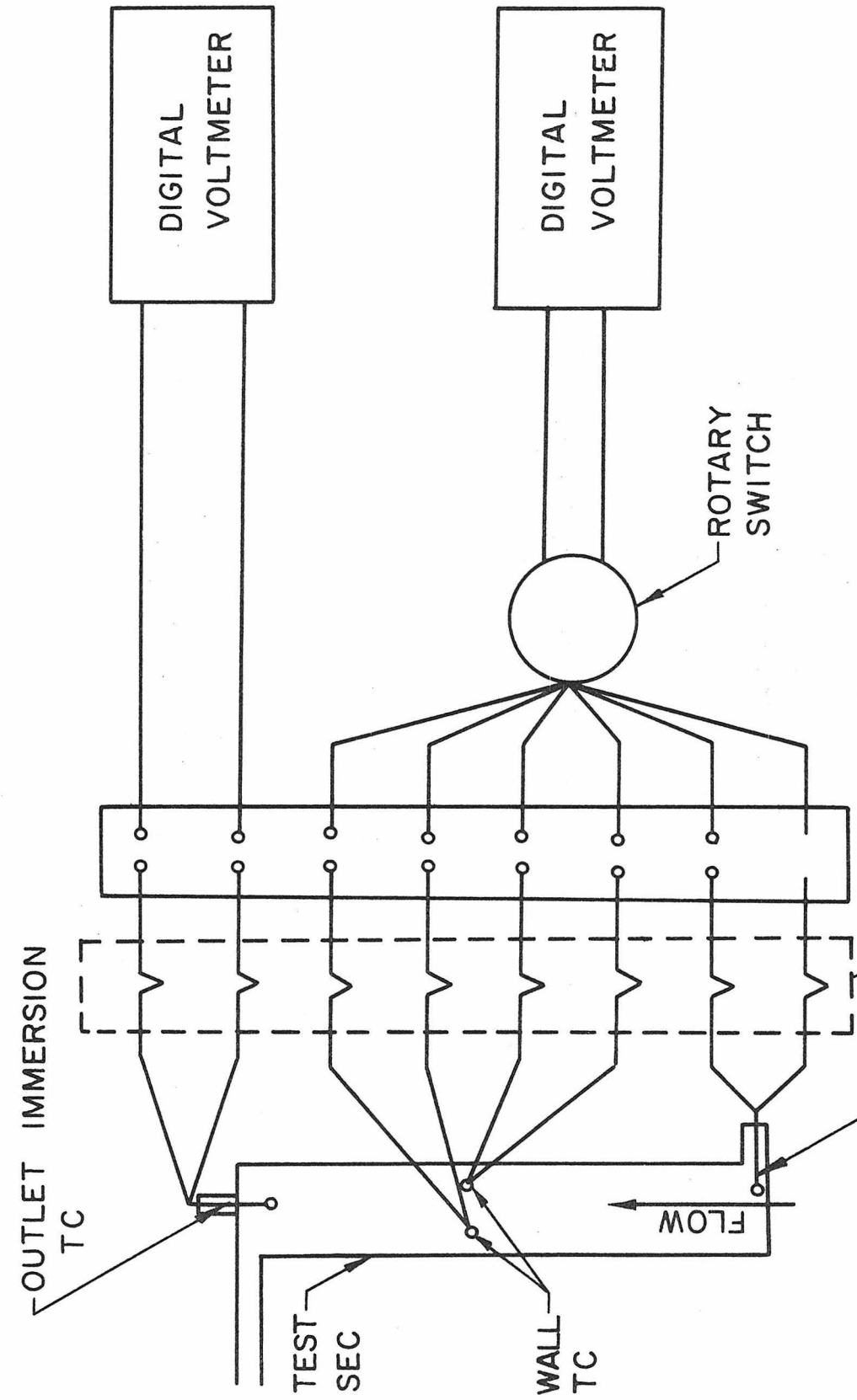

Figure 4. Schematic of circuit for measurement of temperatures.

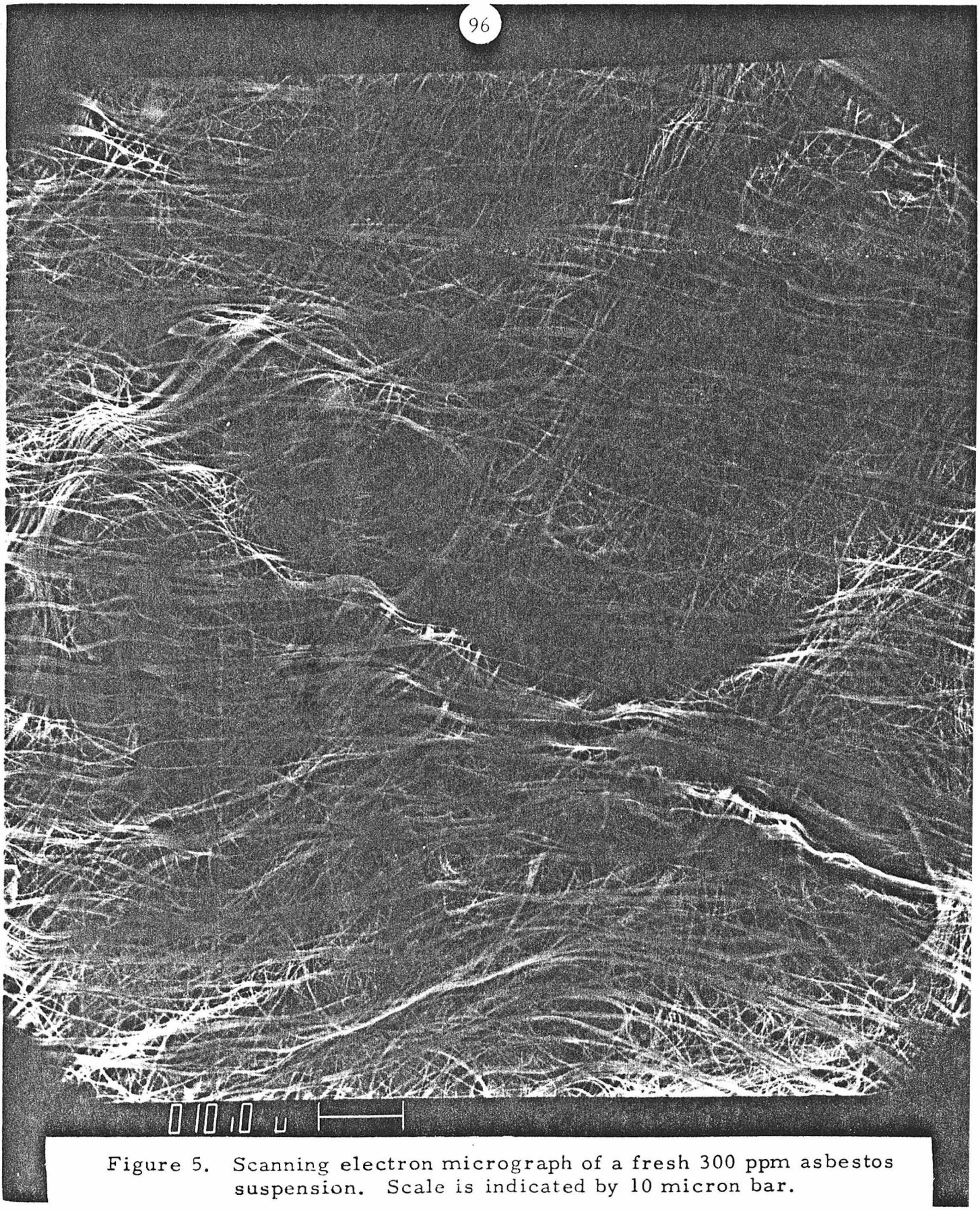

Figure 5. Scanning electron micrograph of a fresh 300 ppm asbestos suspension. Scale is indicated by 10 micron bar.

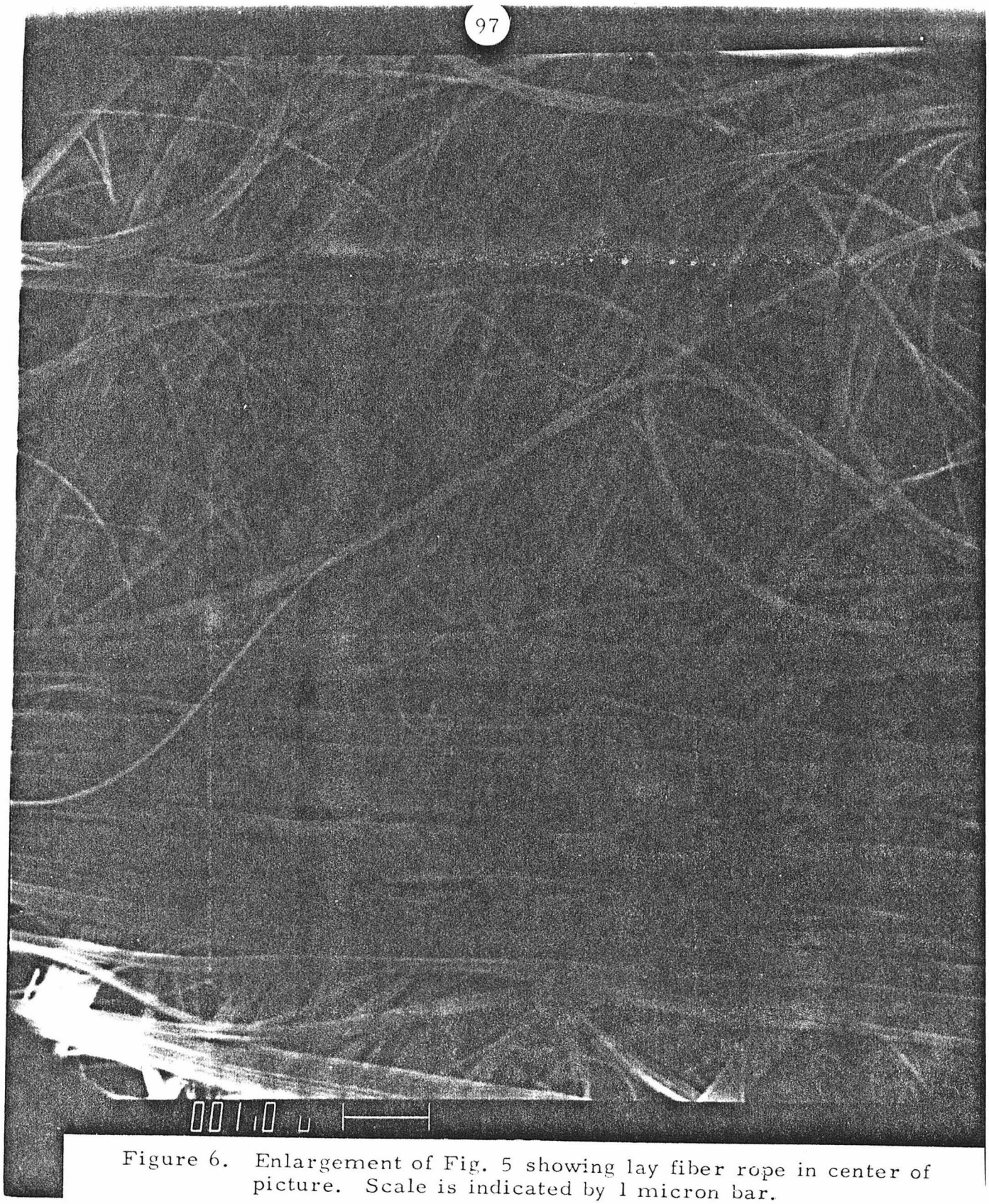

Figure 6. Enlargement of Fig. 5 showing lay fiber rope in center of picture. Scale is indicated by 1 micron bar.

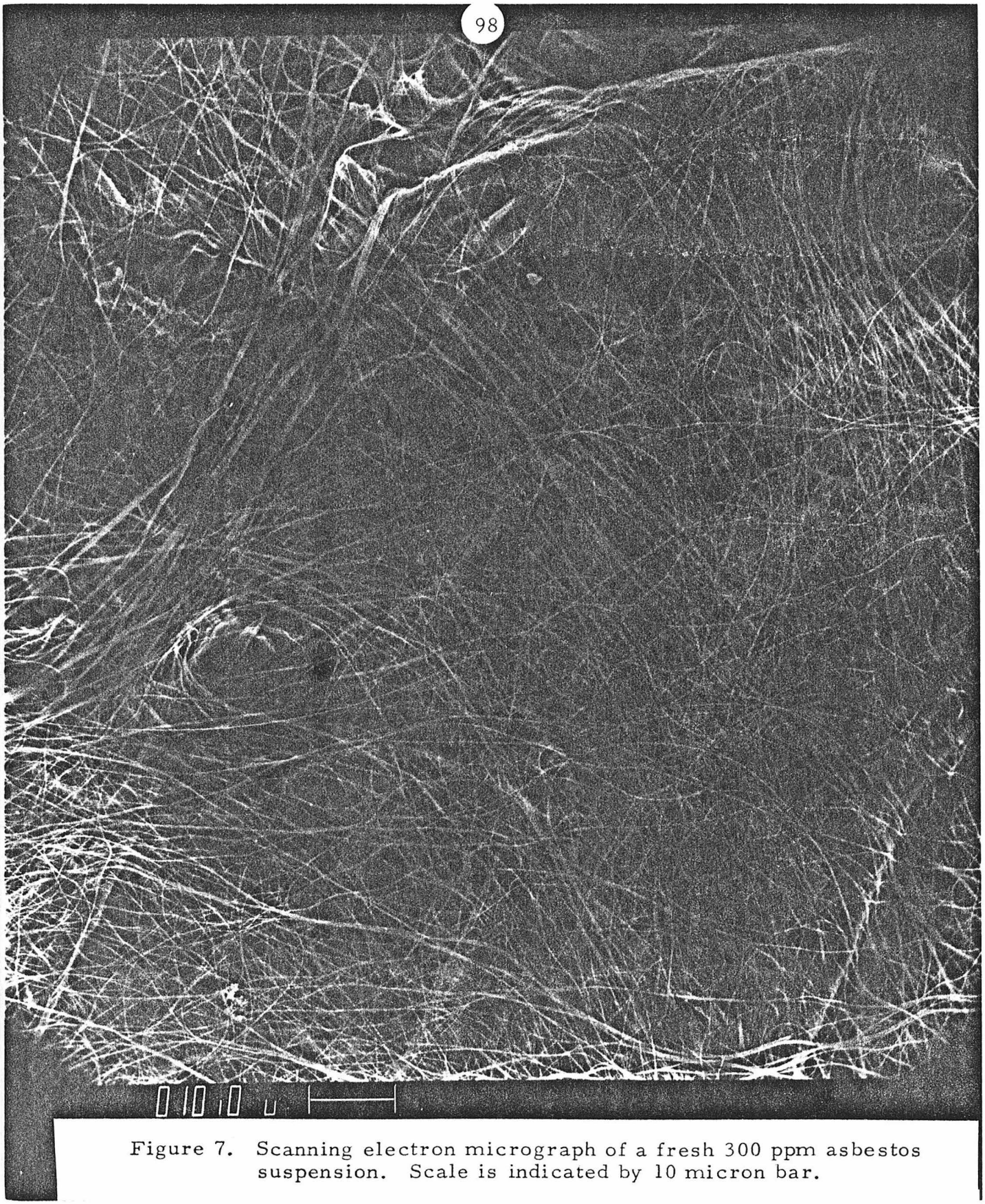

Figure 7. Scanning electron micrograph of a fresh 300 ppm asbestos suspension. Scale is indicated by 10 micron bar.

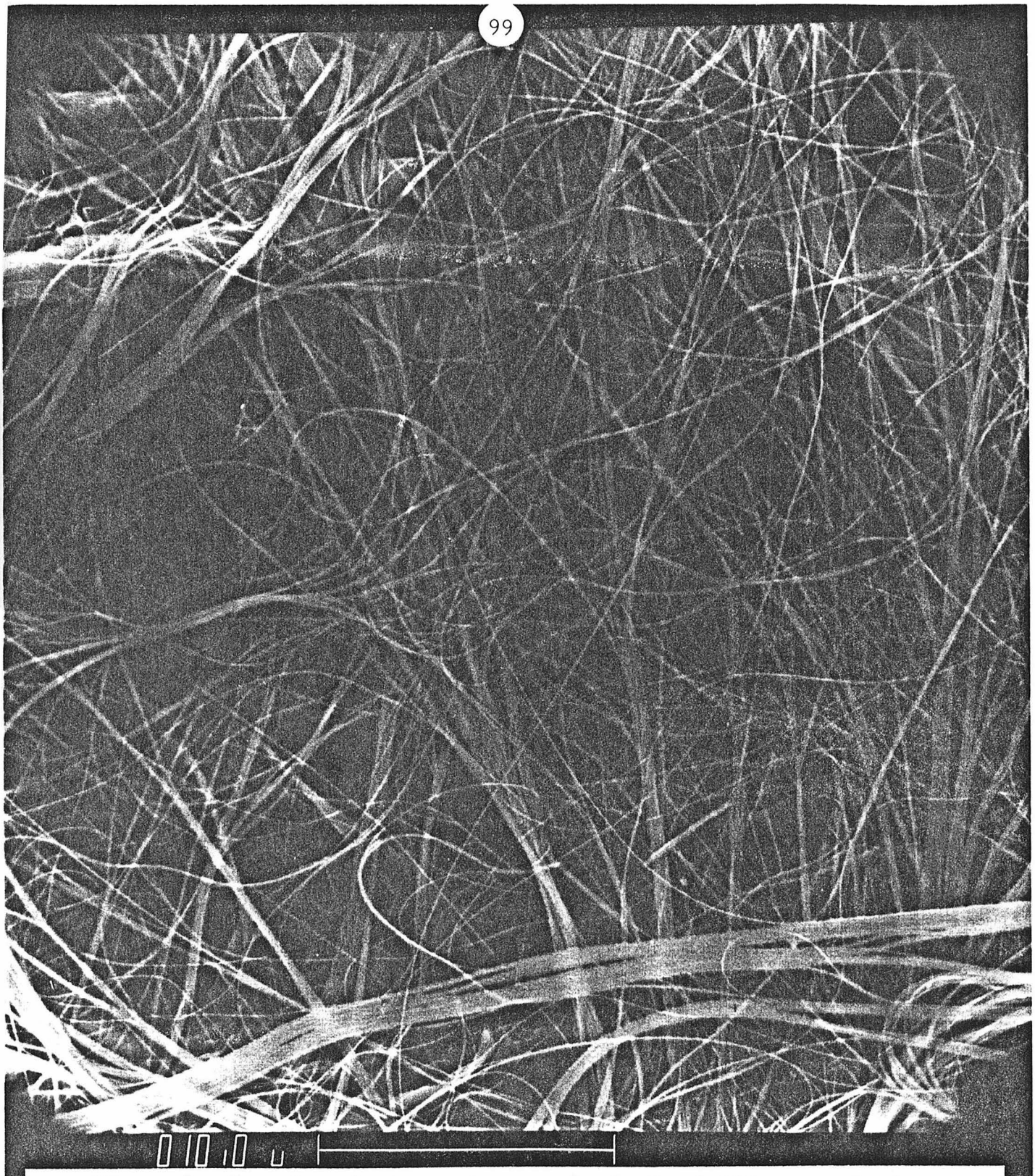

Figure 8. Scanning electron micrograph of a fresh 300 ppm asbestos suspension. Scale is indicated by 10 micron bar.

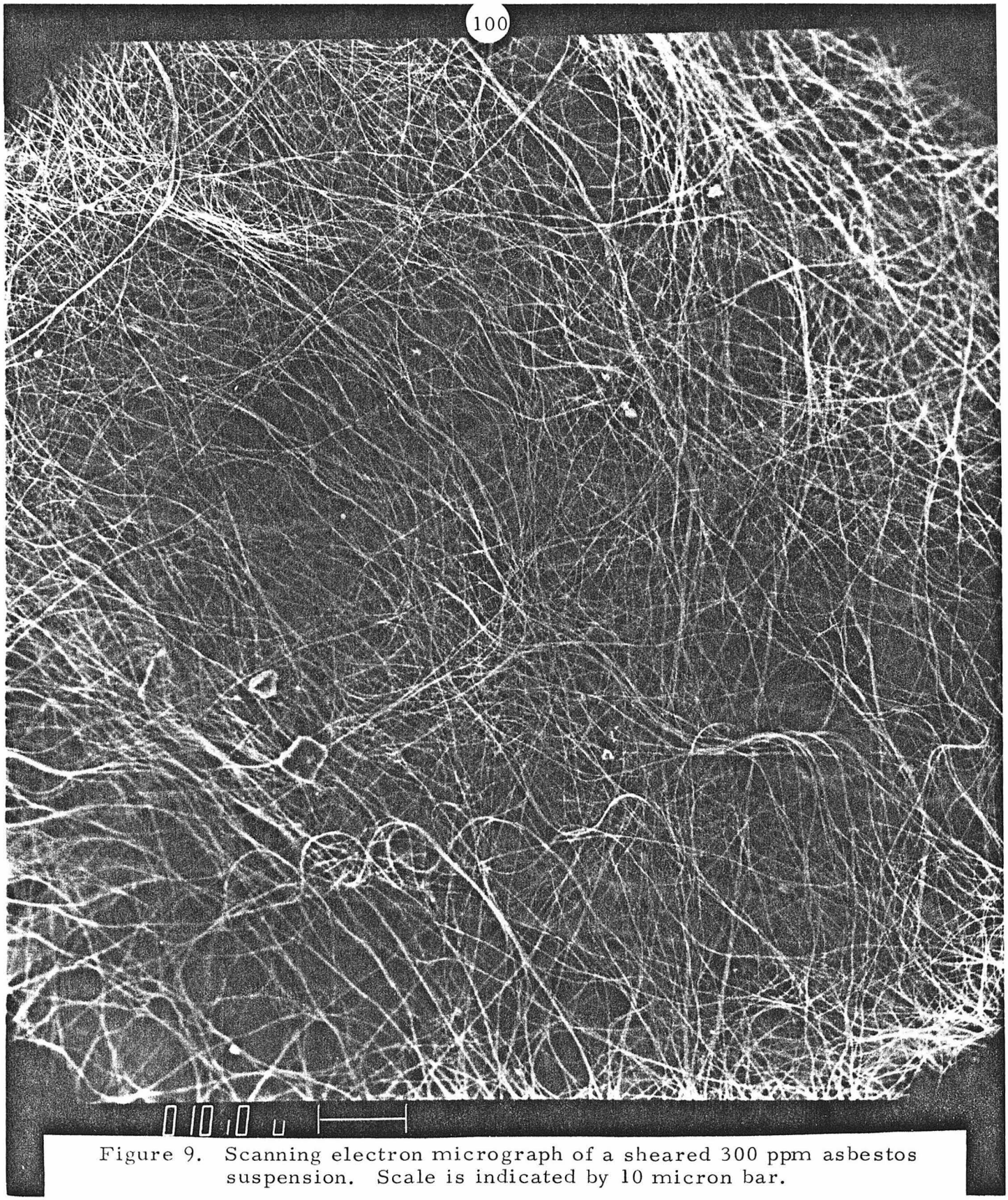

Figure 9. Scanning electron micrograph of a sheared 300 ppm asbestos suspension. Scale is indicated by 10 micron bar.

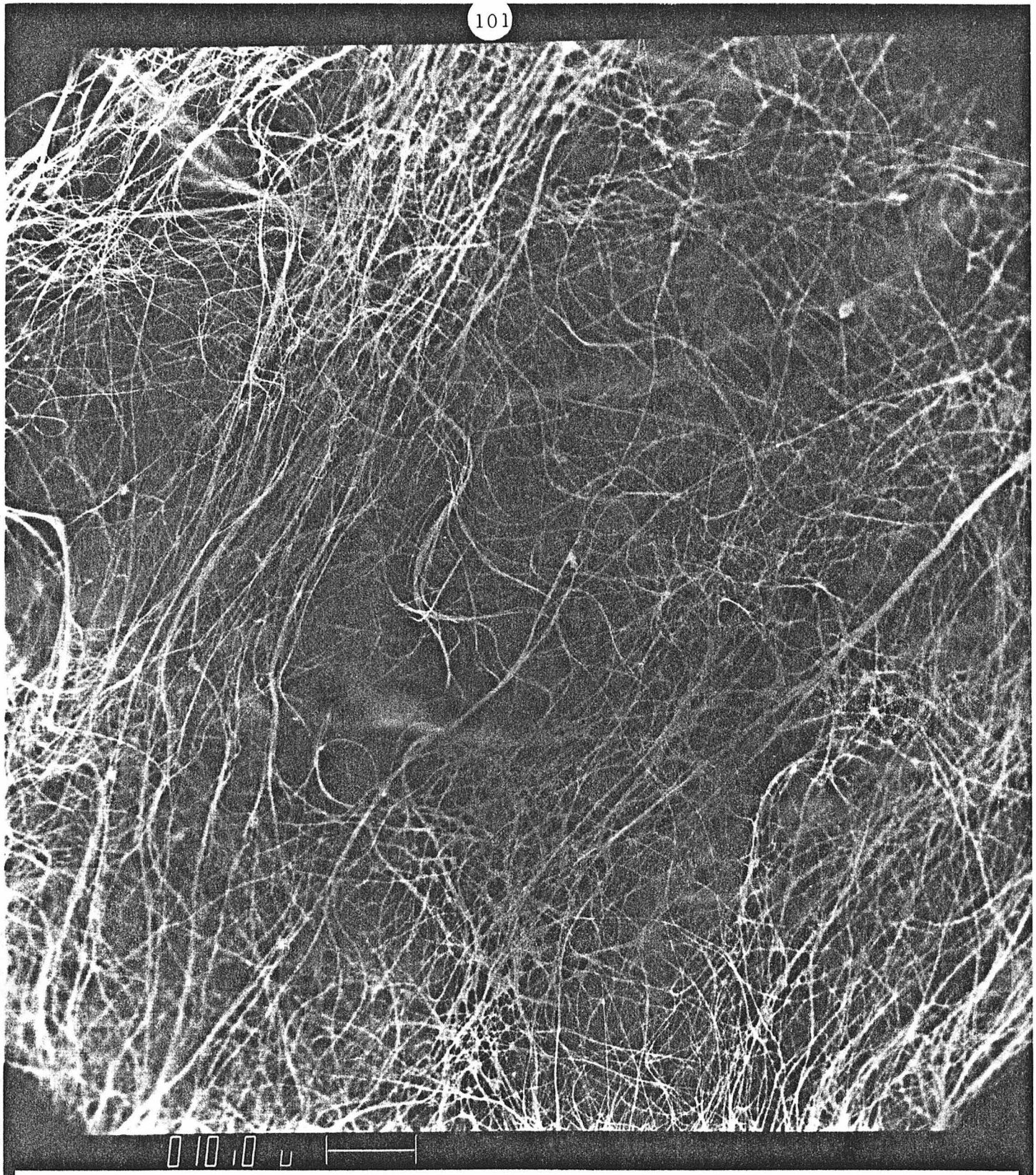

Figure 10. Scanning electron micrograph of a sheared 300 ppm asbestos suspension. Scale is indicated by 10 micron bar.

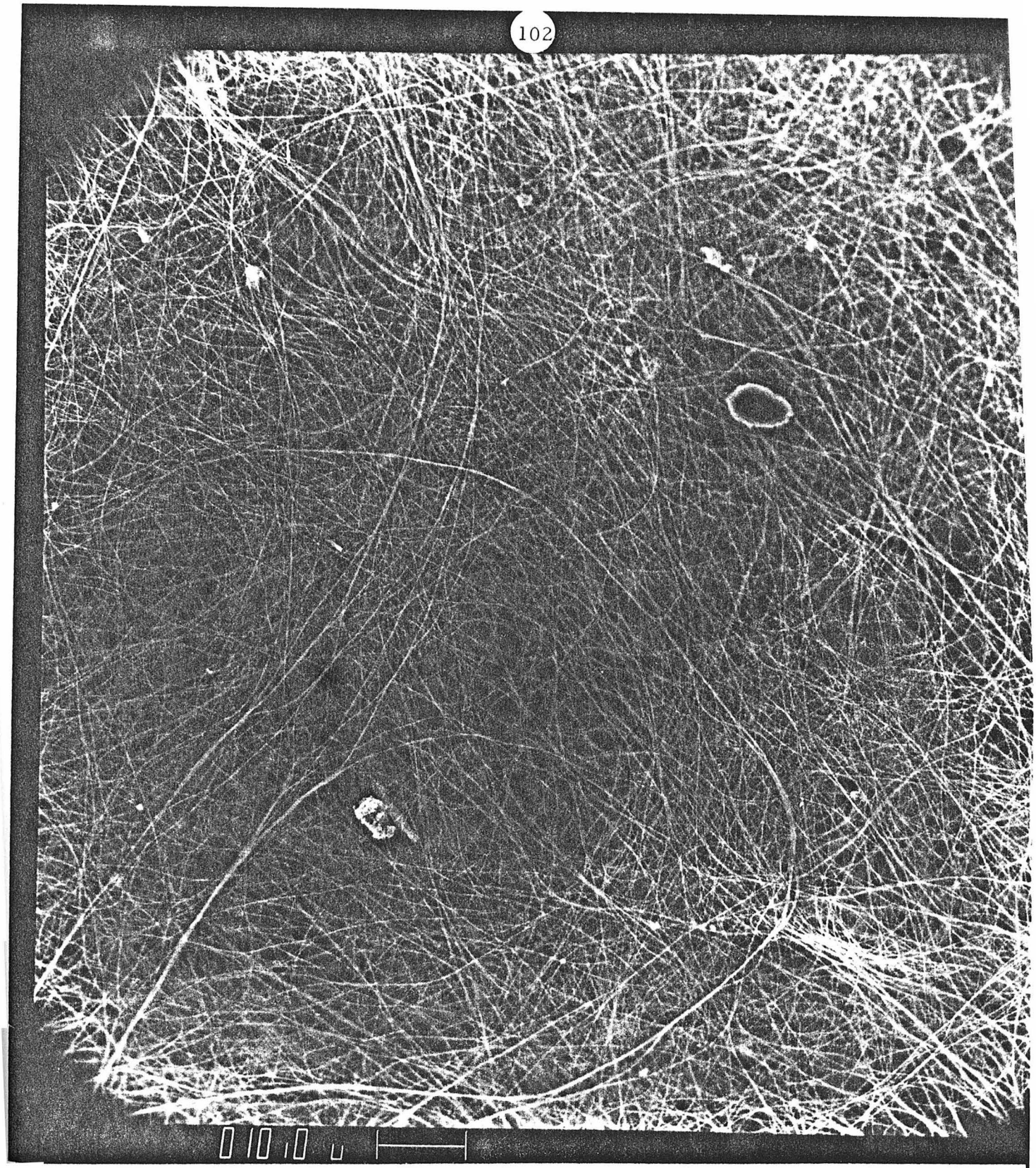

Figure 11. Scanning electron micrograph of a sheared 300 ppm asbestos suspension. Scale is indicated by 10 micron bar.

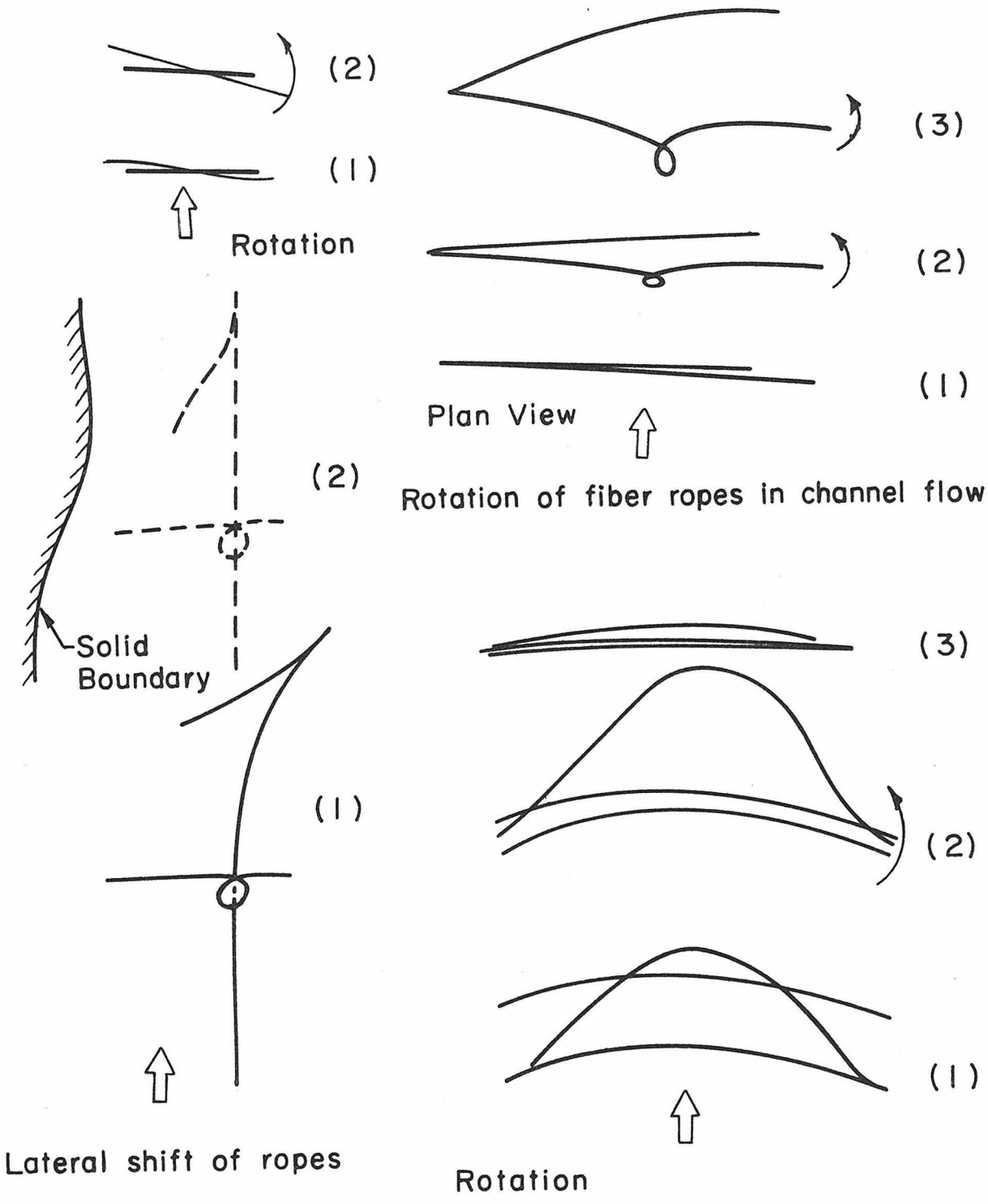

Figure 12. Sketch made from videotape of fiber suspension flowing under a light microscope. Magnification approximately 400X.

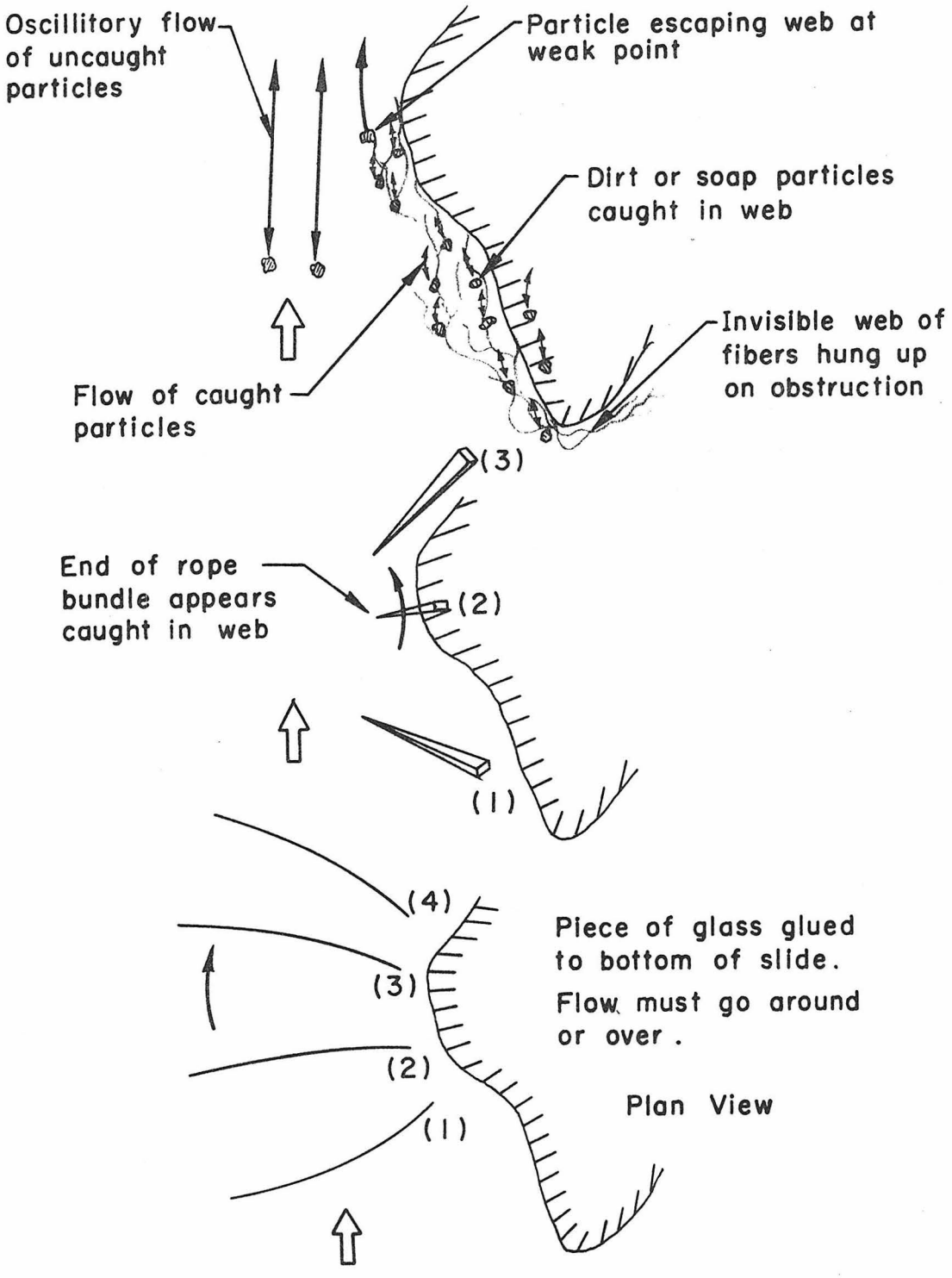

Figure 13. Sketch made from videotape of fiber suspension flowing under a light microscope. Magnification approximately 400X.

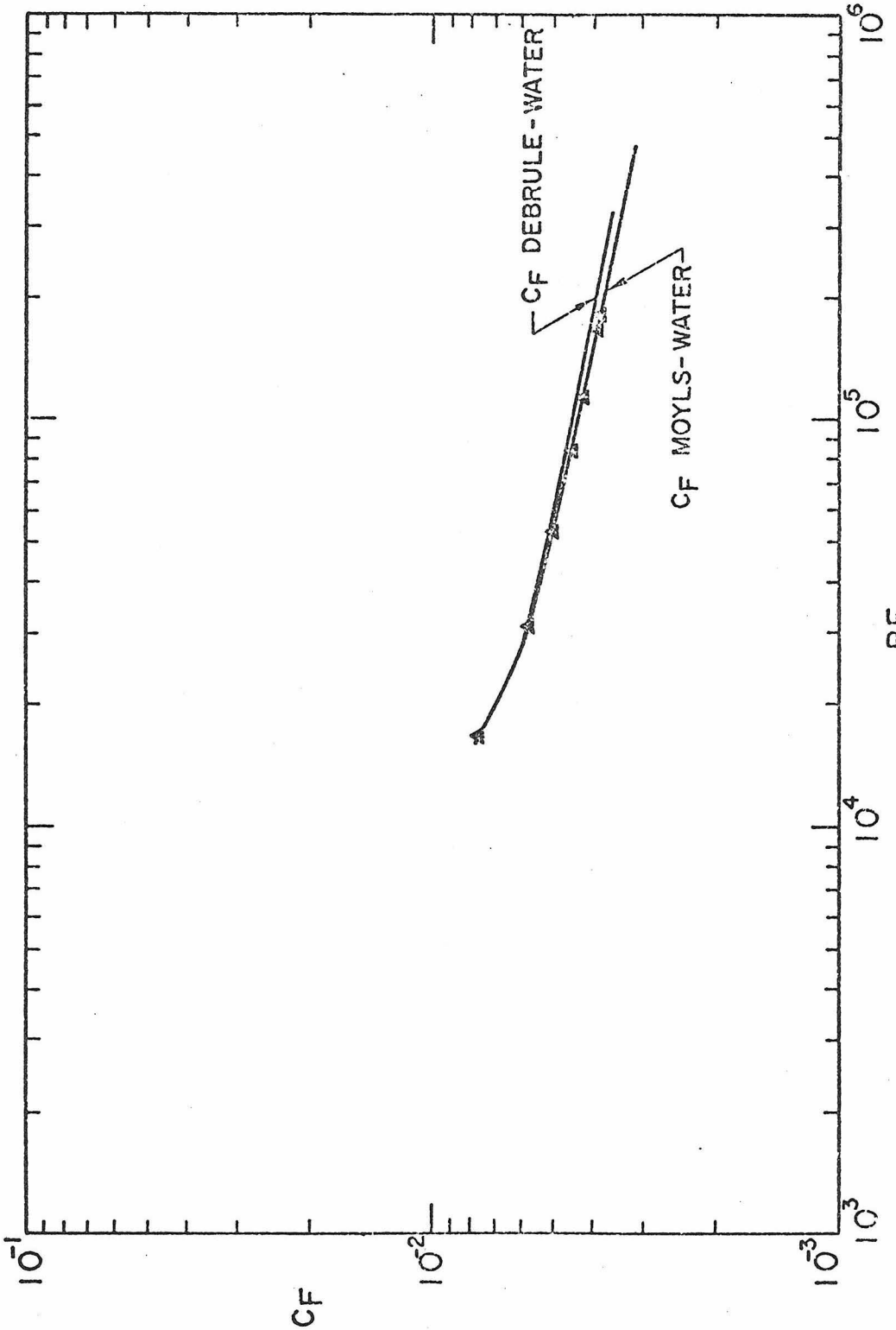

Figure 14 - Water, friction coefficient vs. Reynolds number for smooth tube.

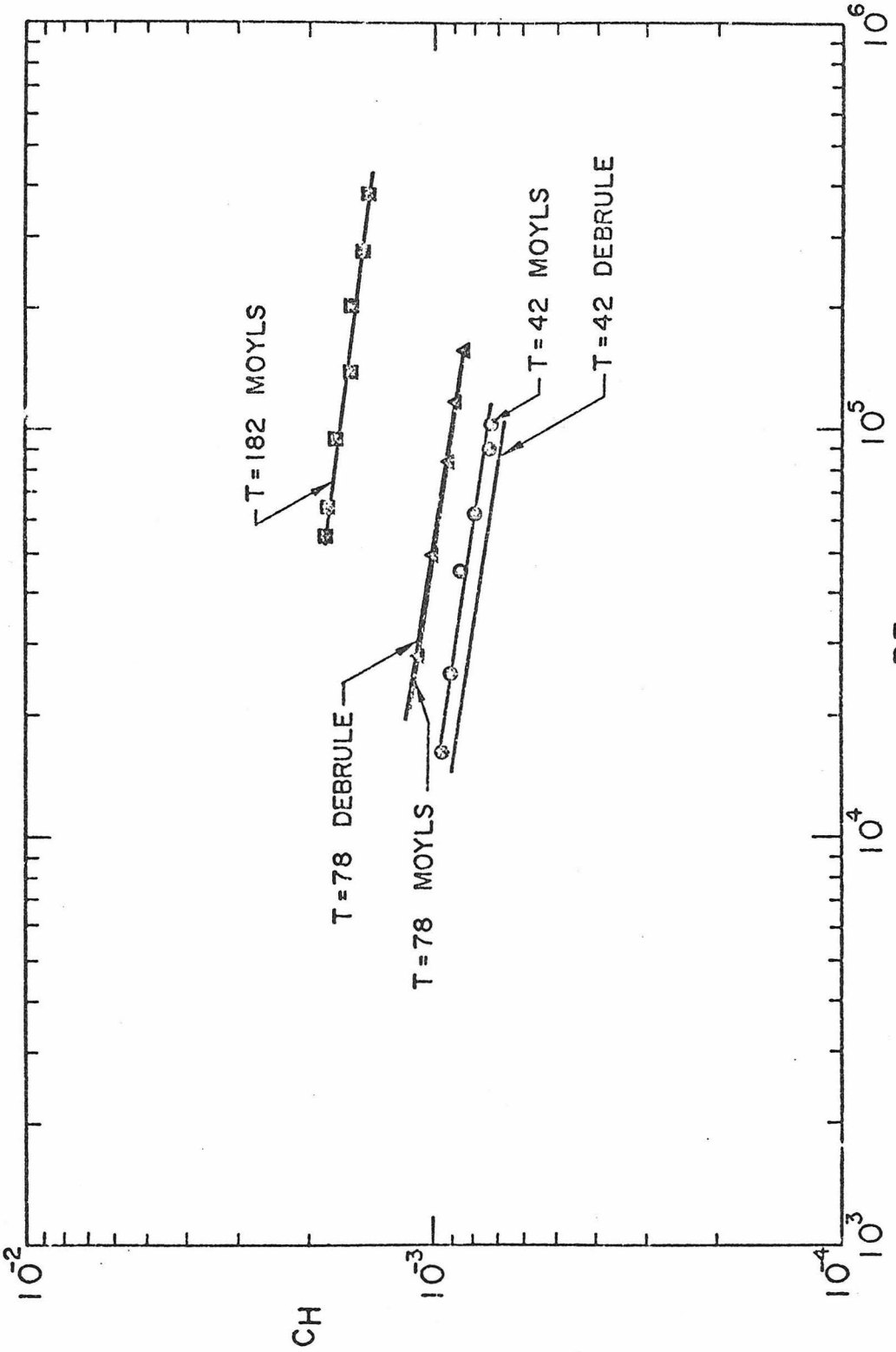

Figure 15. Water, heat transfer coefficient vs. Reynolds number for smooth tube. T = 42°F, 78°F, 182°F corresponds to Pr = 10.8, 6.16, 2.07 respectively.

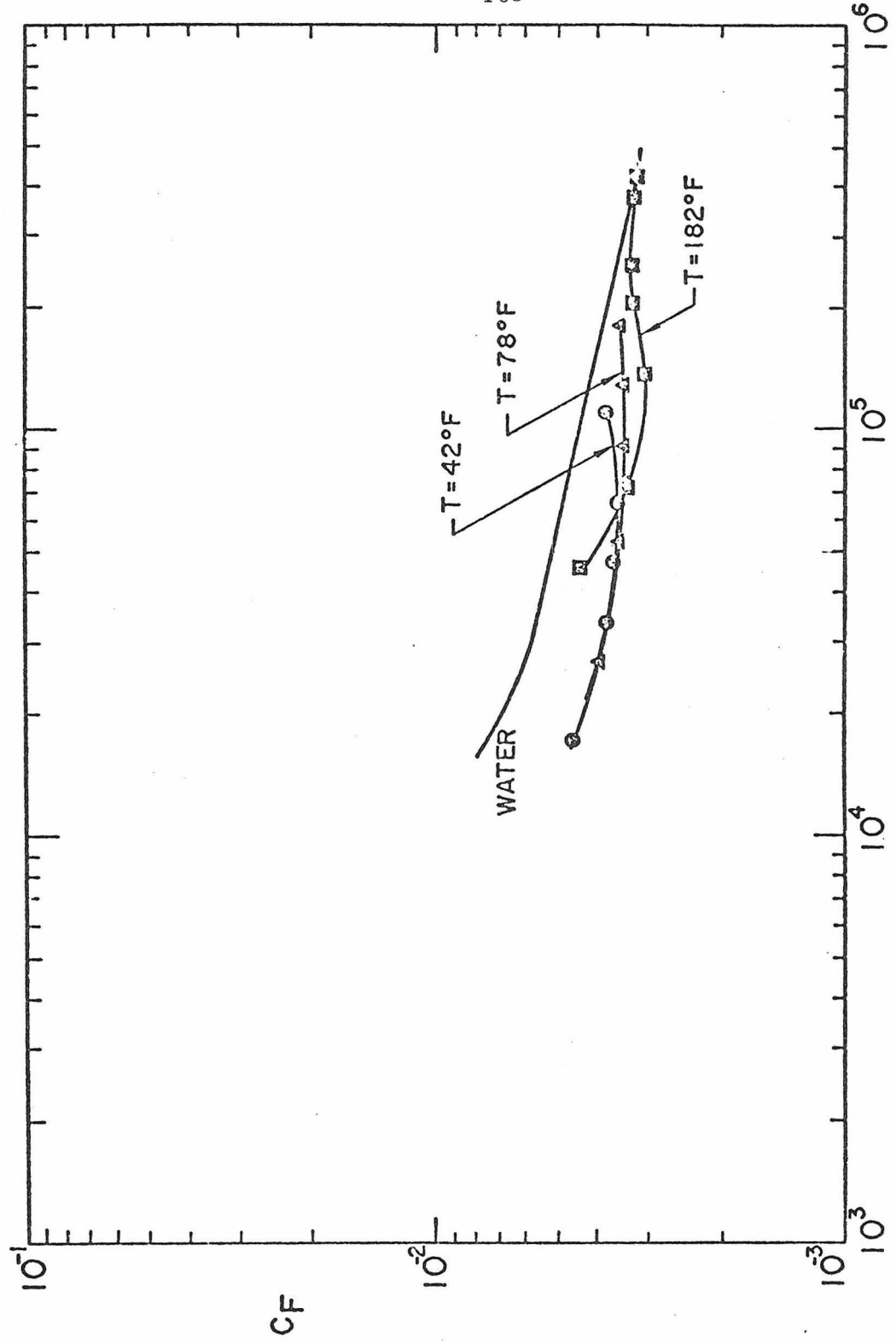

Figure 16. Asbestos 50 ppm, friction coefficient vs. Reynolds number for smooth tube. T = 42°F, 78°F, 182°F corresponds to Pr = 10.3, 6.16, 2.07 respectively.

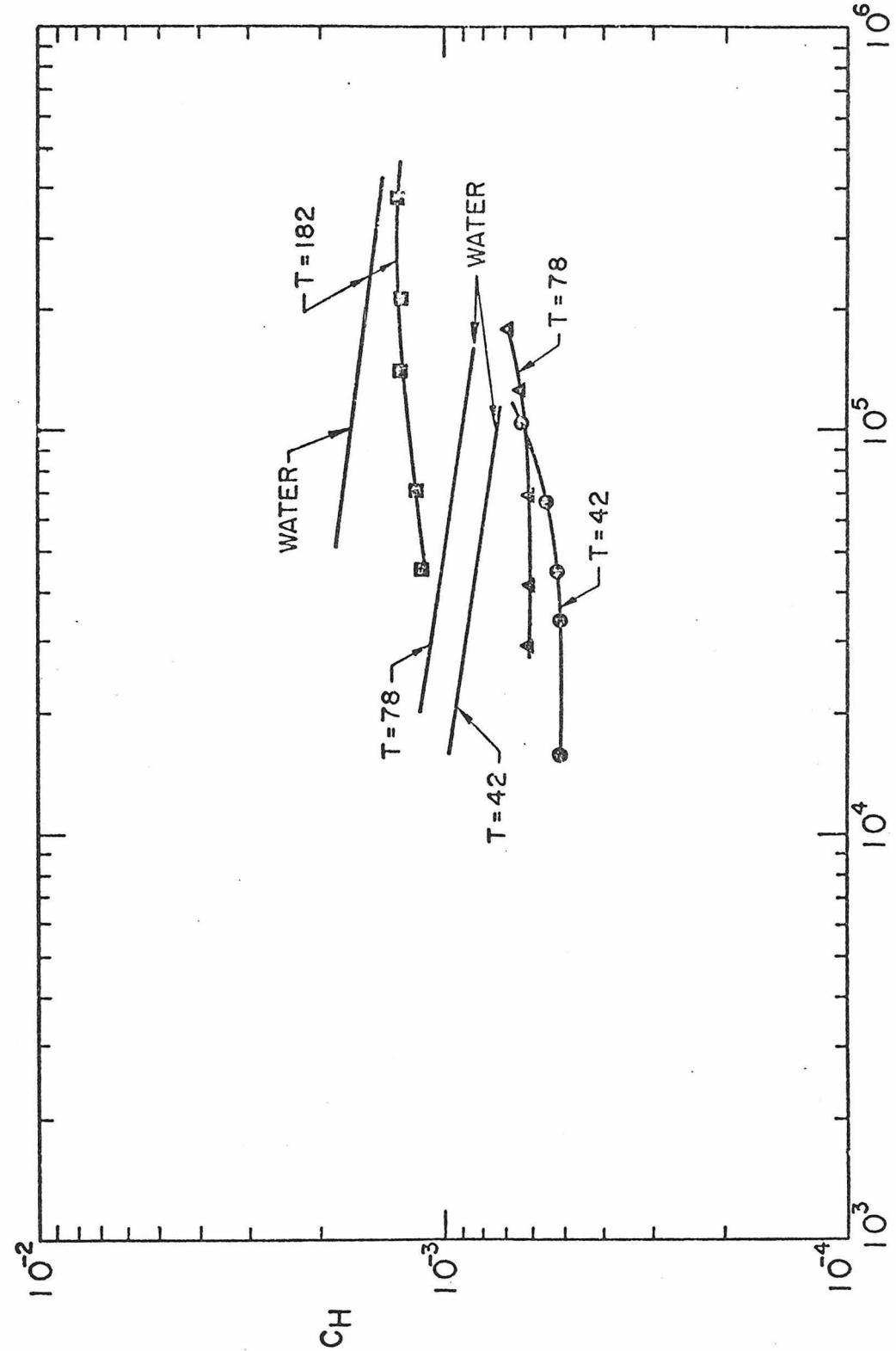

Figure 17. Asbestos 50 ppm, heat transfer coefficient vs. Reynolds number for smooth tube. T = 42°F, 78°F, 182°F corresponds to Pr = 10.8, 6.16, 2.07 respectively.

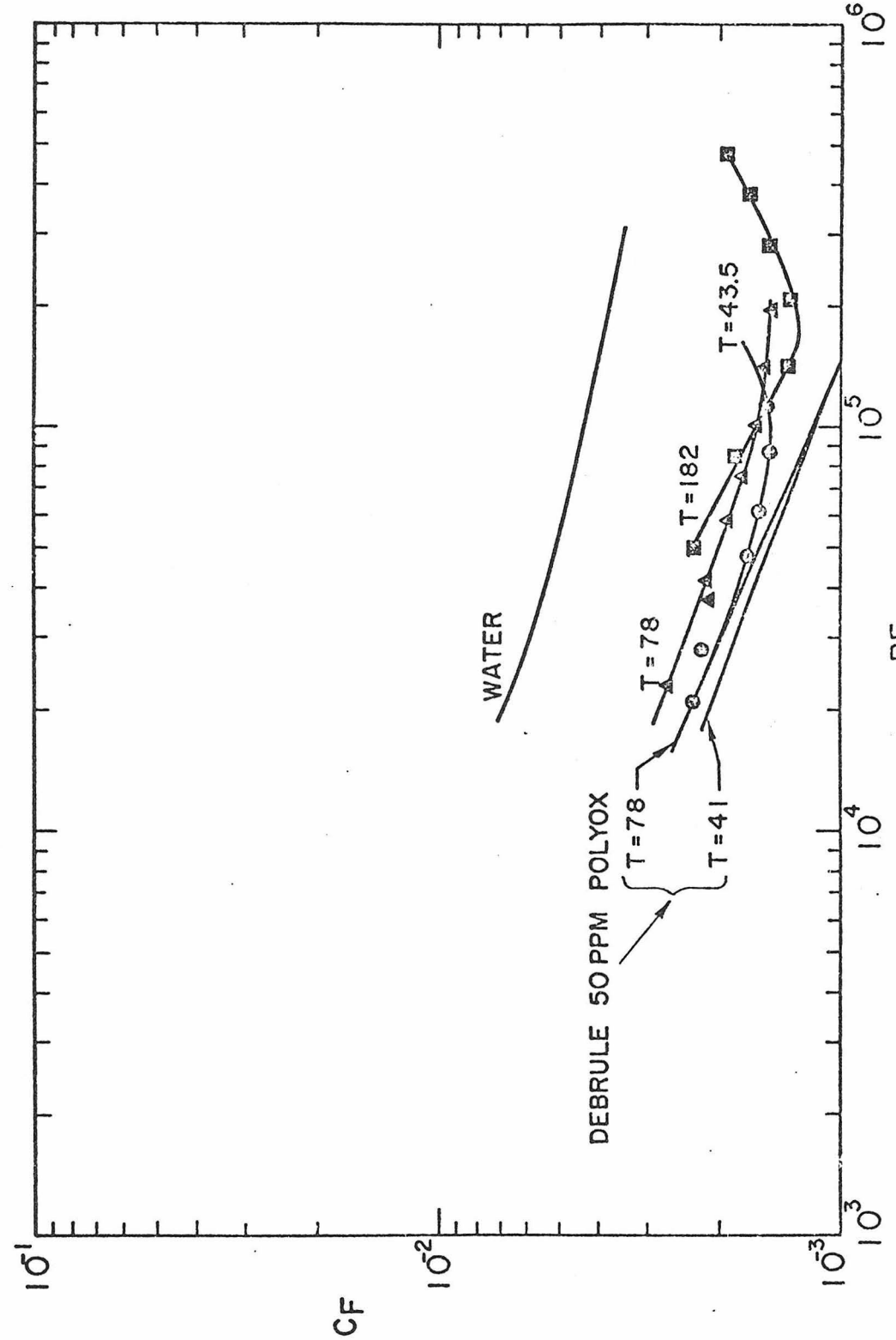

Figure 18. Asbestos 300 ppm, friction coefficient vs. Reynolds number for smooth tube. T = 43.5 F, 78 F, 182 F corresponds to Pr = 10.7, 6.16, 2.07 respectively.

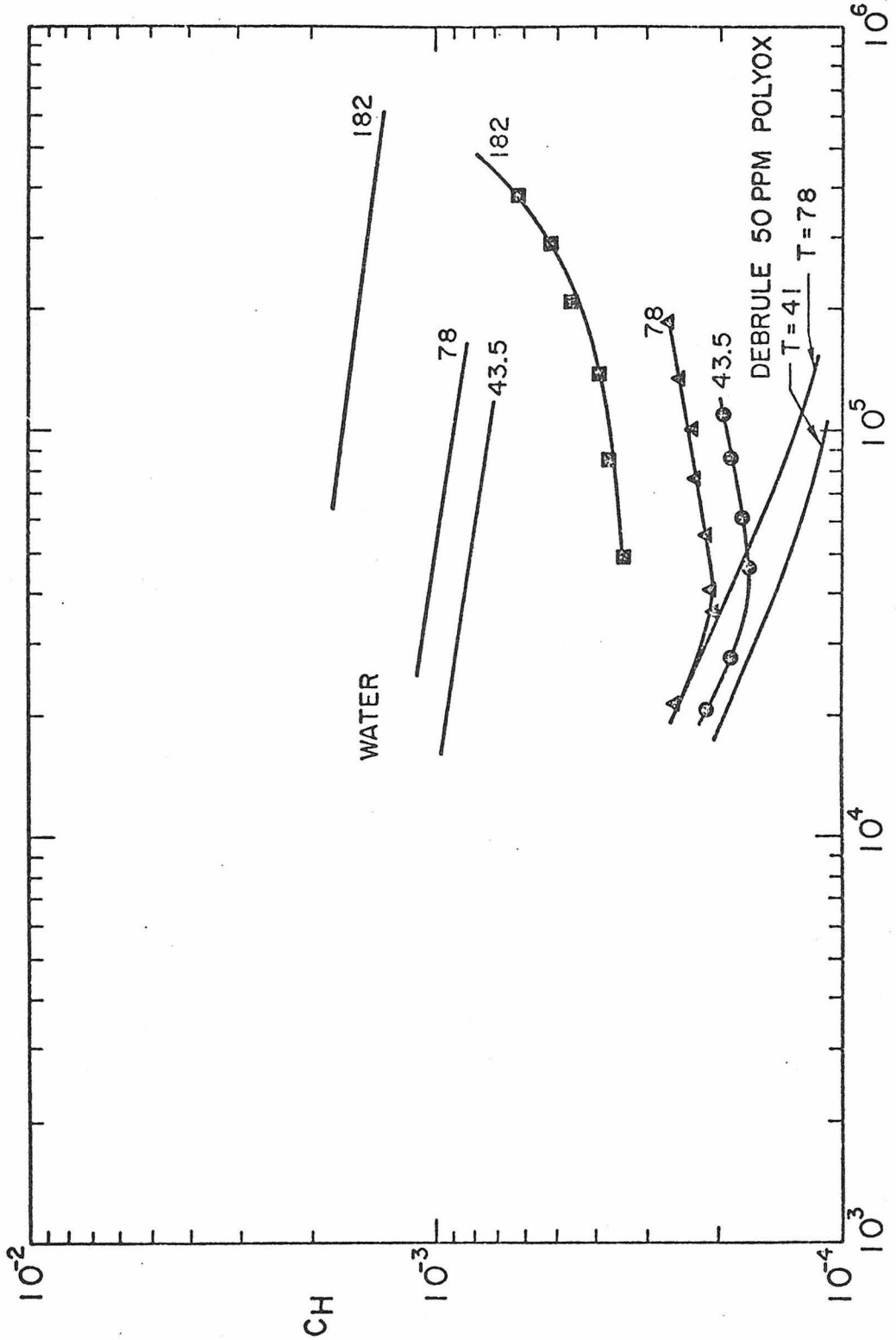

Figure 19. Asbestos 300 ppm, heat transfer coefficient vs. Reynolds number for smooth tube. T = 43.5 F, 78 F, 182 F corresponds to Pr = 10.7, 6.16, 2.07 respectively.

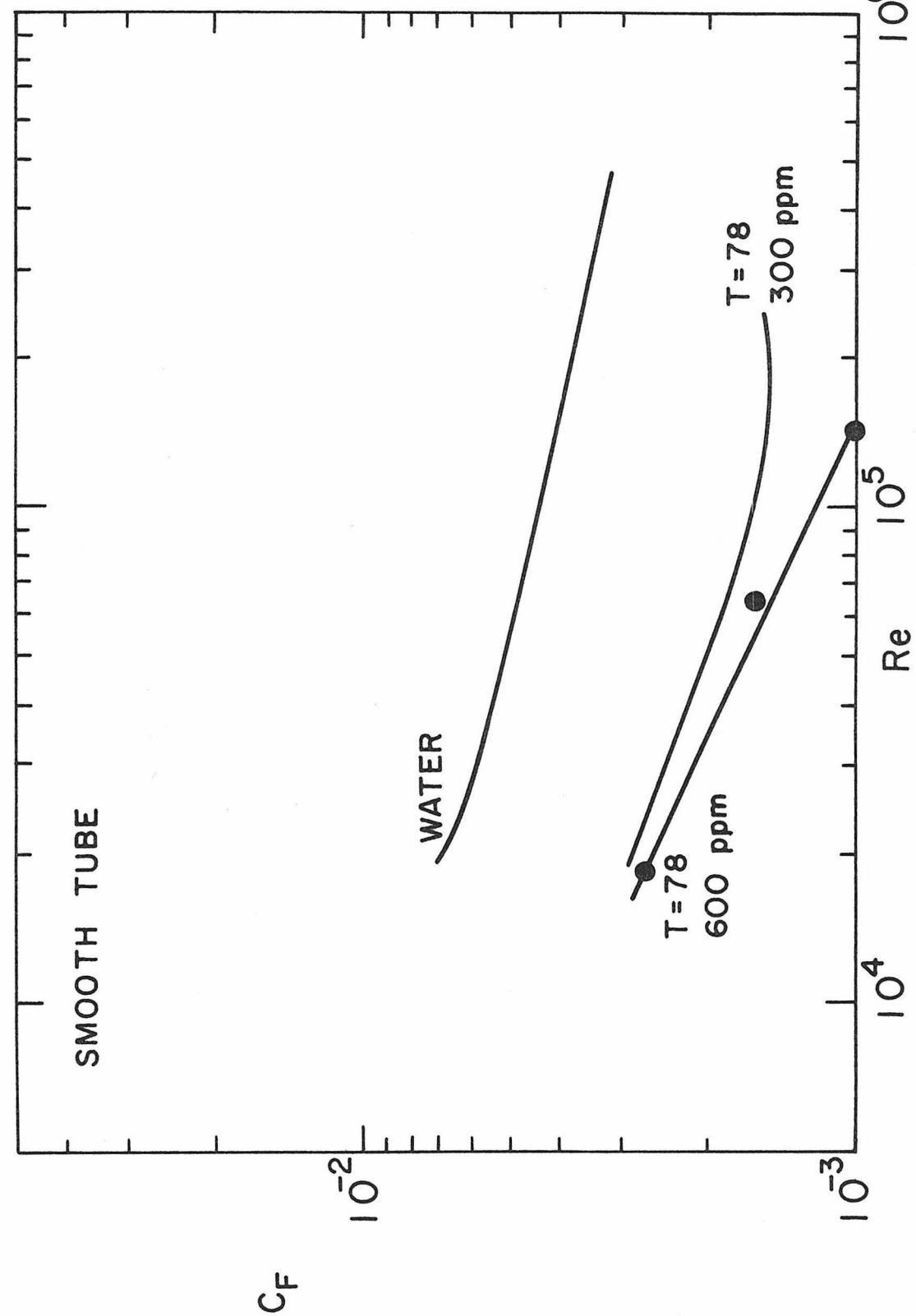

Figure 20. Asbestos 300 ppm, 600 ppm friction coefficient vs. Reynolds number for smooth tube. T = 78° F corresponds to Pr = 6.16.

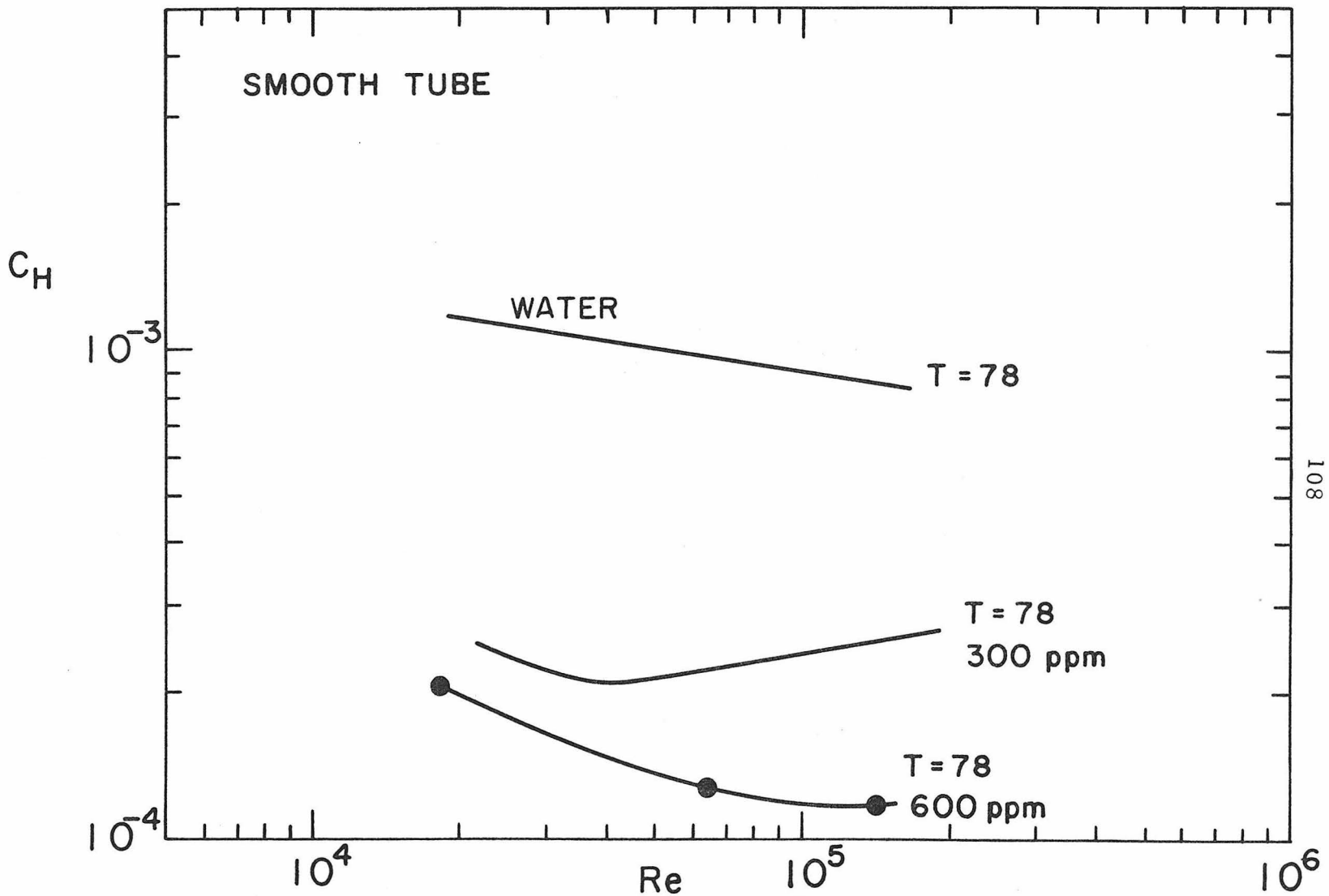

Figure 21. Asbestos 300 ppm, 600 ppm heat transfer coefficient vs. Reynolds number for smooth tube. T = 78° F corresponds to Pr = 6. 16.

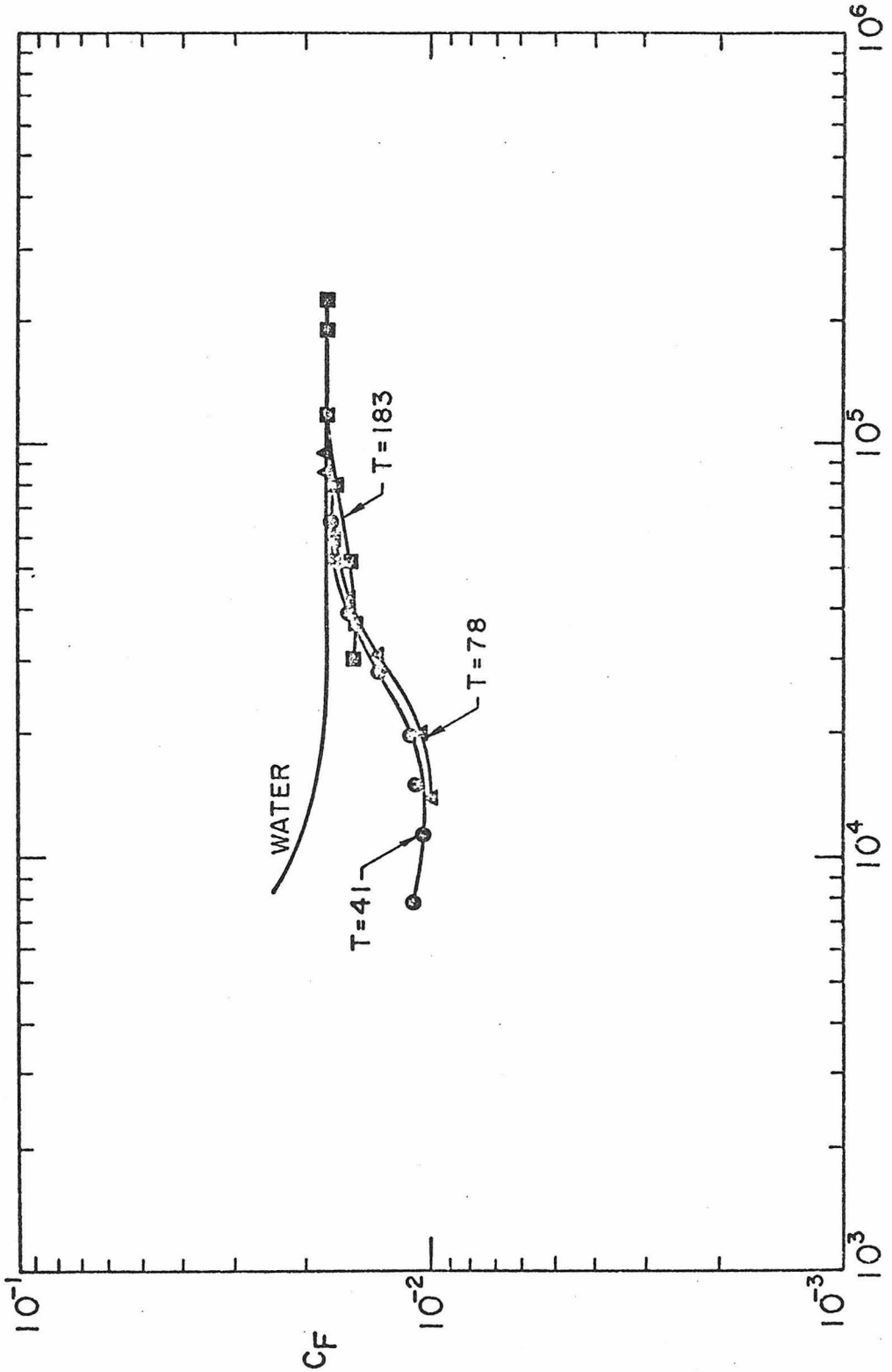

Figure 22. Asbestos 50 ppm, friction coefficient vs. Reynolds number for rough tube. T = 41°F, 78°F, 183°F corresponds to Pr = 10.8, 6.16, 2.07 respectively.

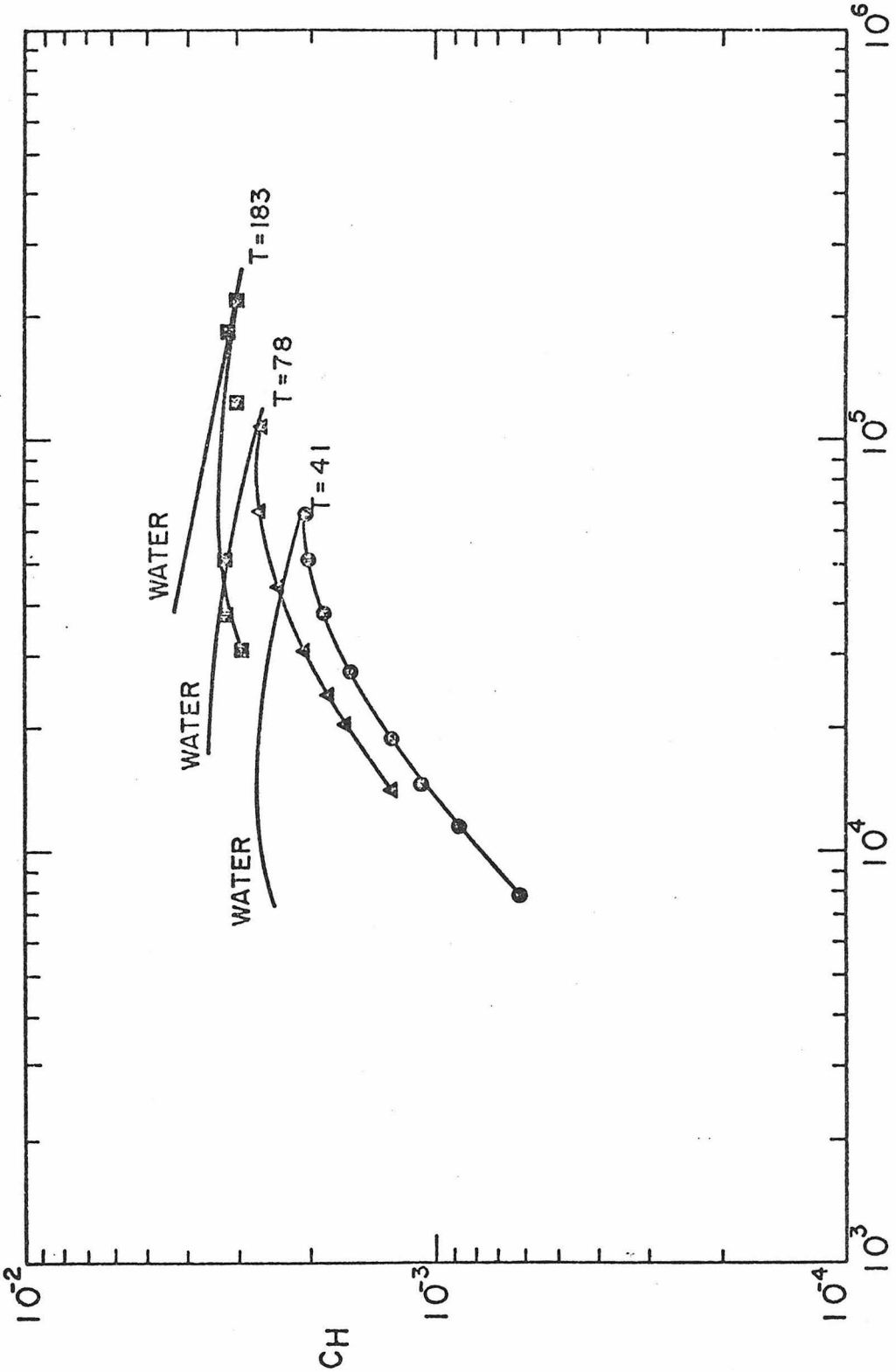

Figure 23. Asbestos 50 ppm, heat transfer coefficient vs. Reynolds number for rough tube. T = 41°F, 73°F, 183°F corresponds to Pr = 10.8, 6.16, 2.07 respectively.

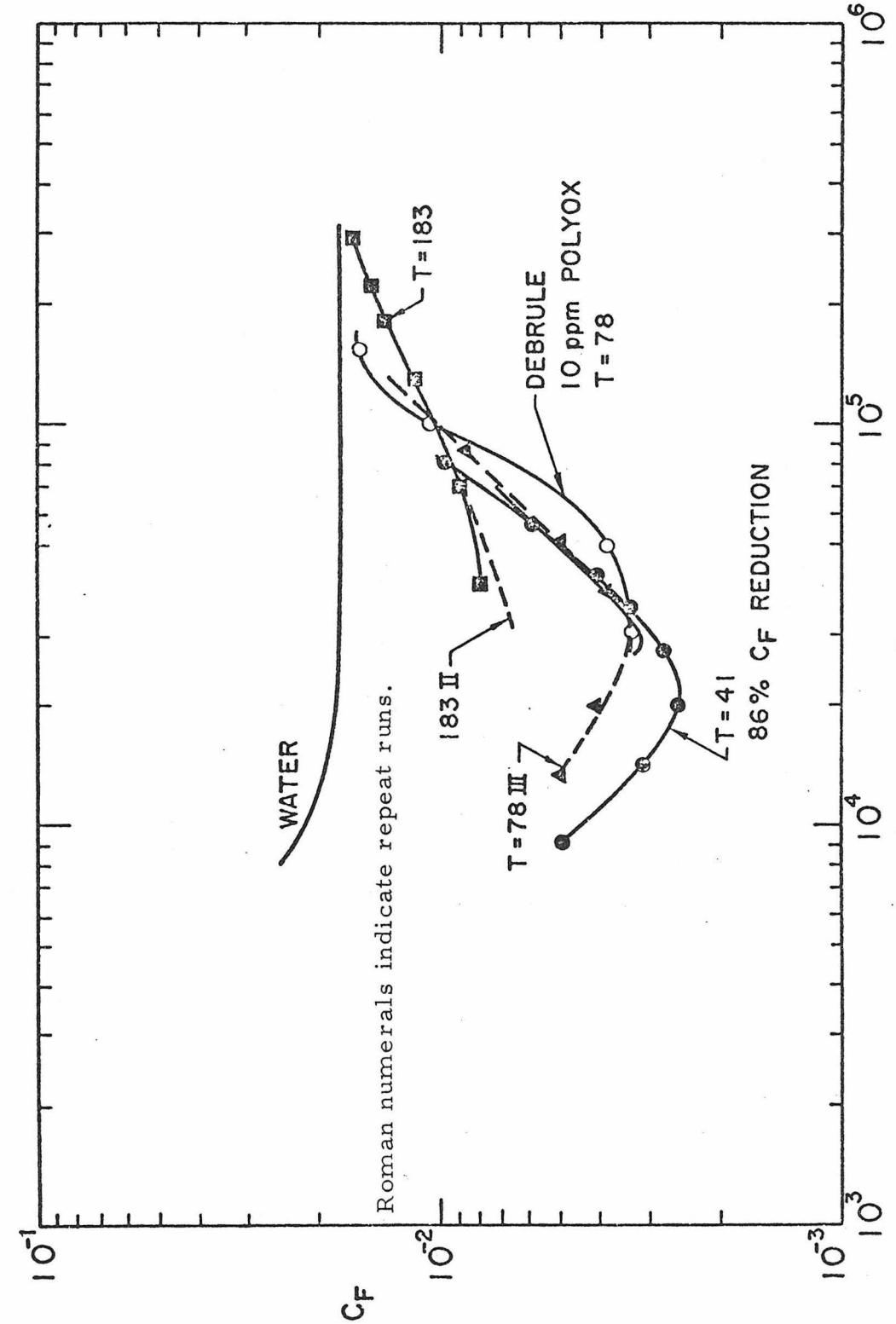

Figure 24. Asbestos 300 ppm, friction coefficient vs. Reynolds number for rough tube. T = 41°F, 78°F, 183°F corresponds to Pr = 10.8, 6.16, 2.07 respectively.

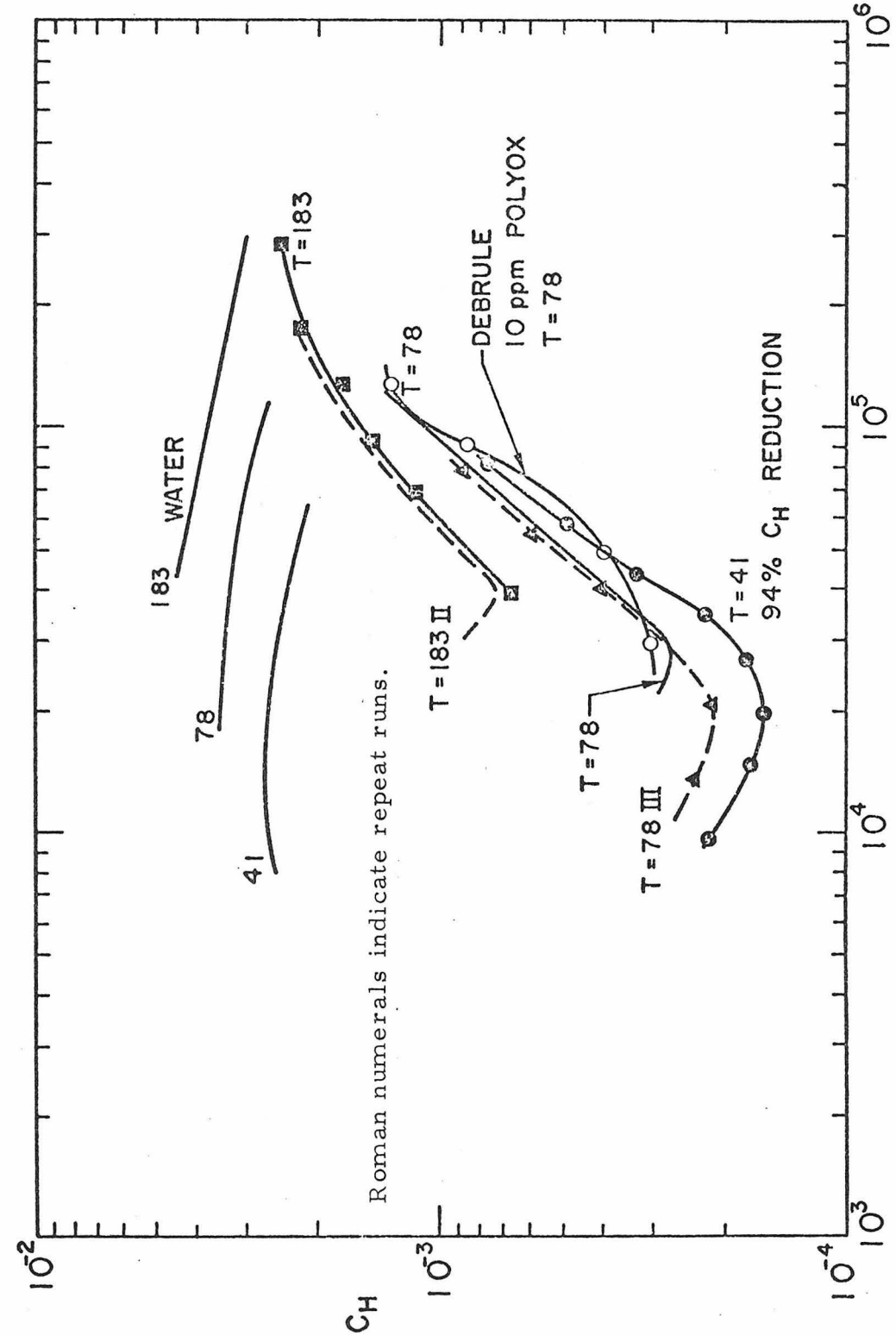

Figure 25. Asbestos 300 ppm, heat transfer coefficient vs. Reynolds number for rough tube. T = 41°F, 78°F, 183°F corresponds to Pr = 10.8, 6.16, 2.07 respectively.

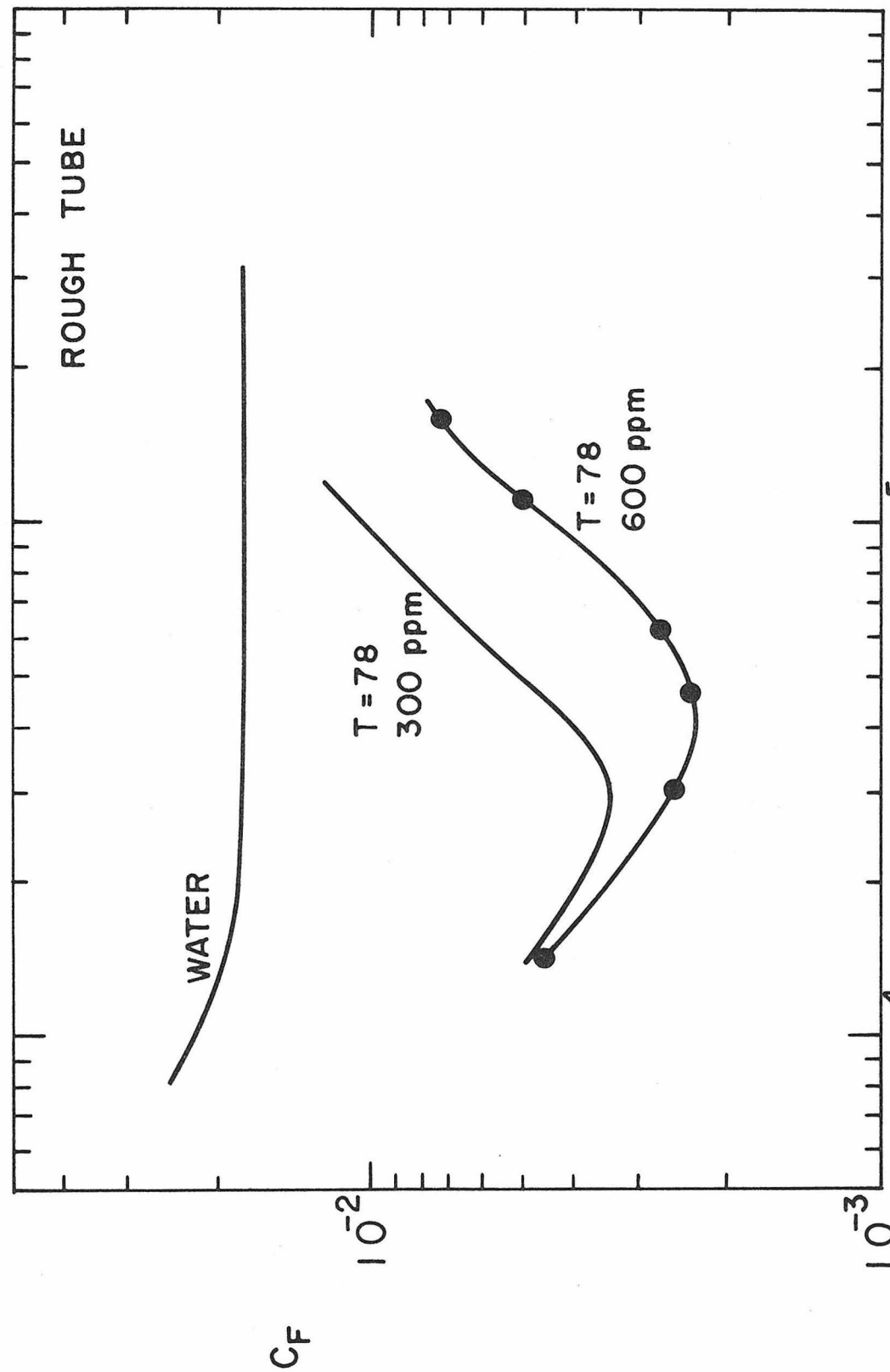

Figure 26. Asbestos 300 ppm, 600 ppm, friction coefficient vs. Reynolds number for rough tube. T = 78°F corresponds to Pr = 6.16.

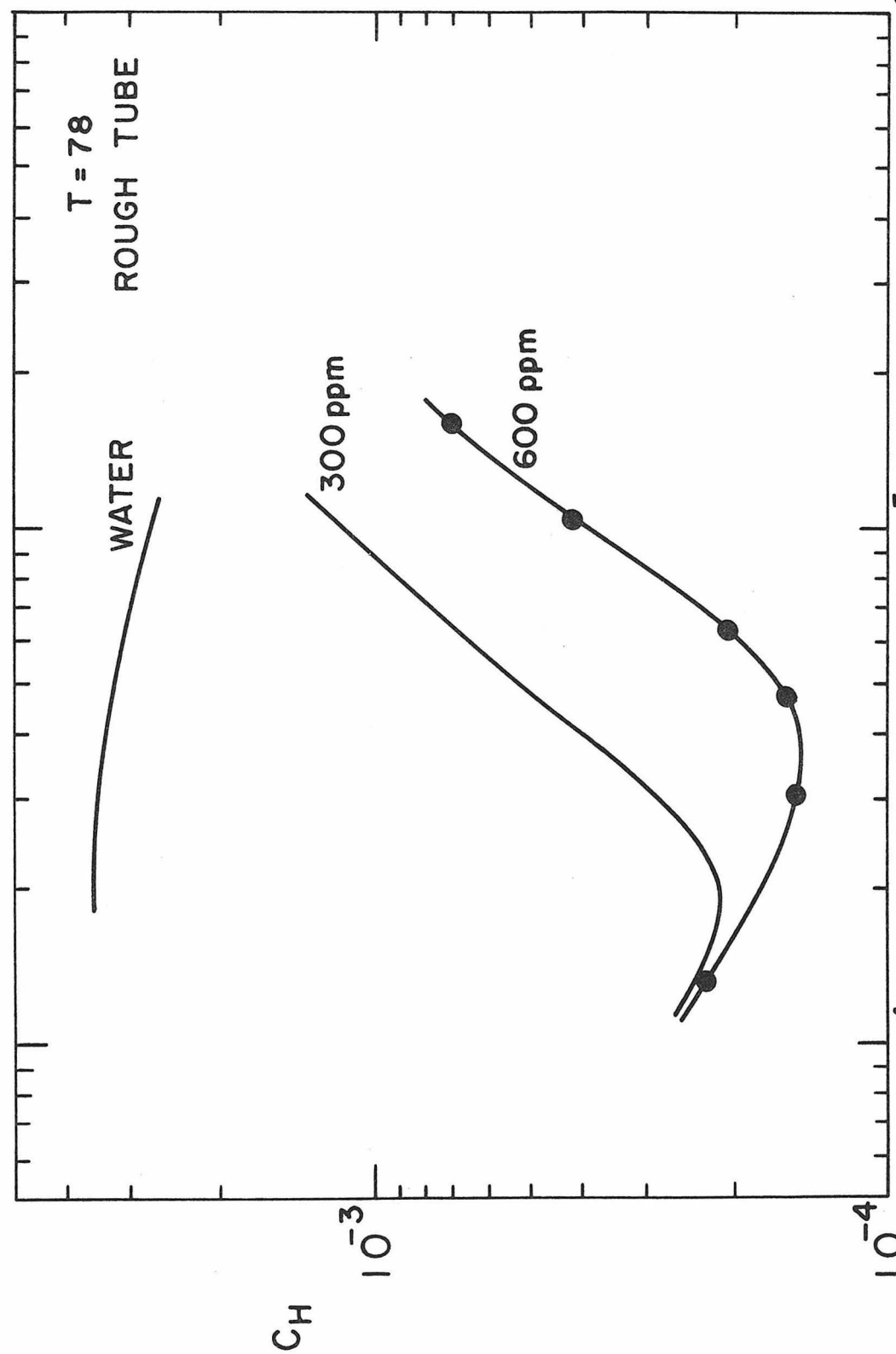

Figure 27. Asbestos 300 ppm, 600 ppm, friction coefficient vs. Reynolds number for rough tube. T = 78° F corresponds to Pr = 6.16.

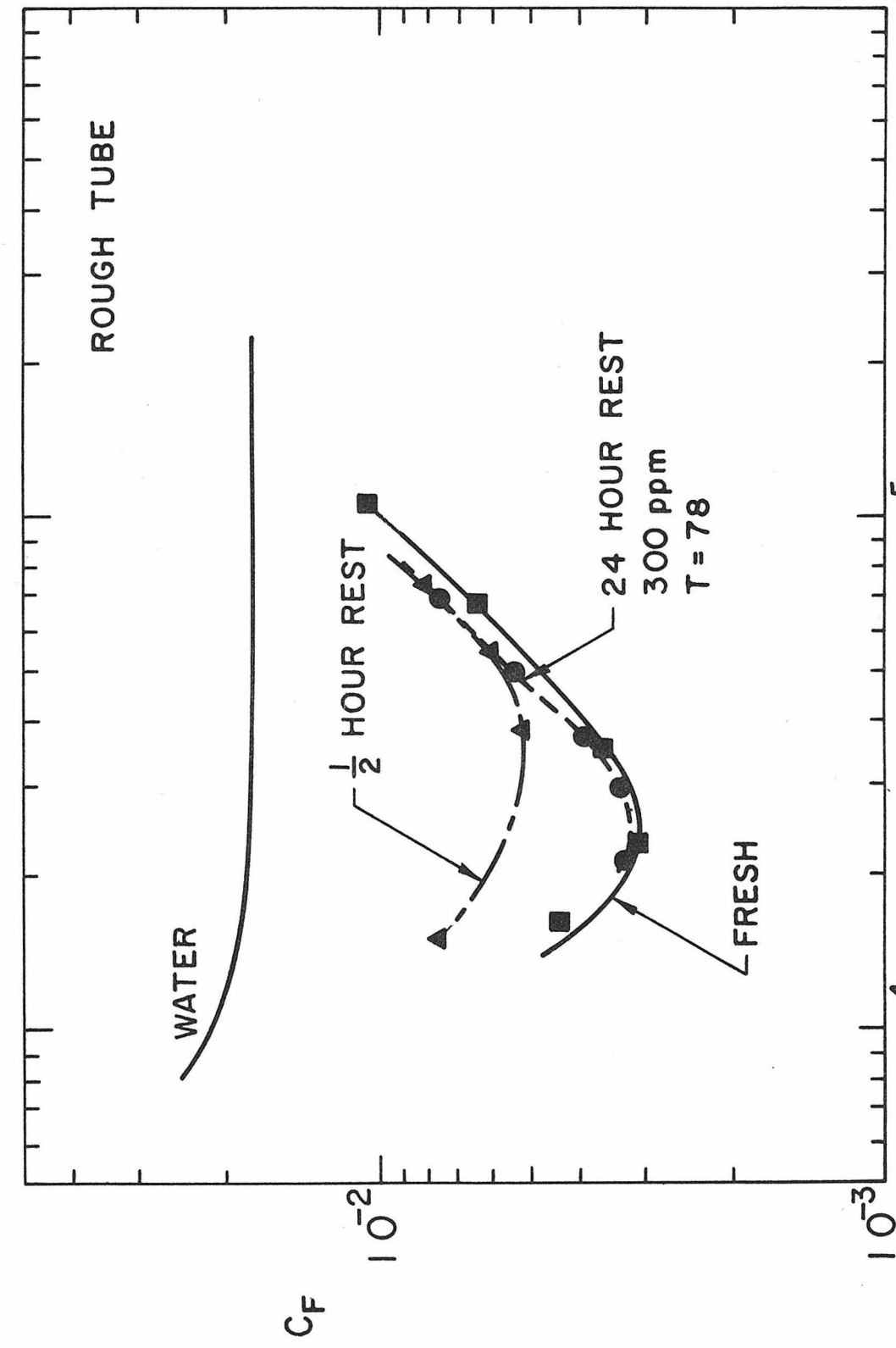

Figure 28. Asbestos 300 ppm, friction coefficient vs. Reynolds number. Results of degradation tests. T = 78°F corresponds to Pr = 6.16.

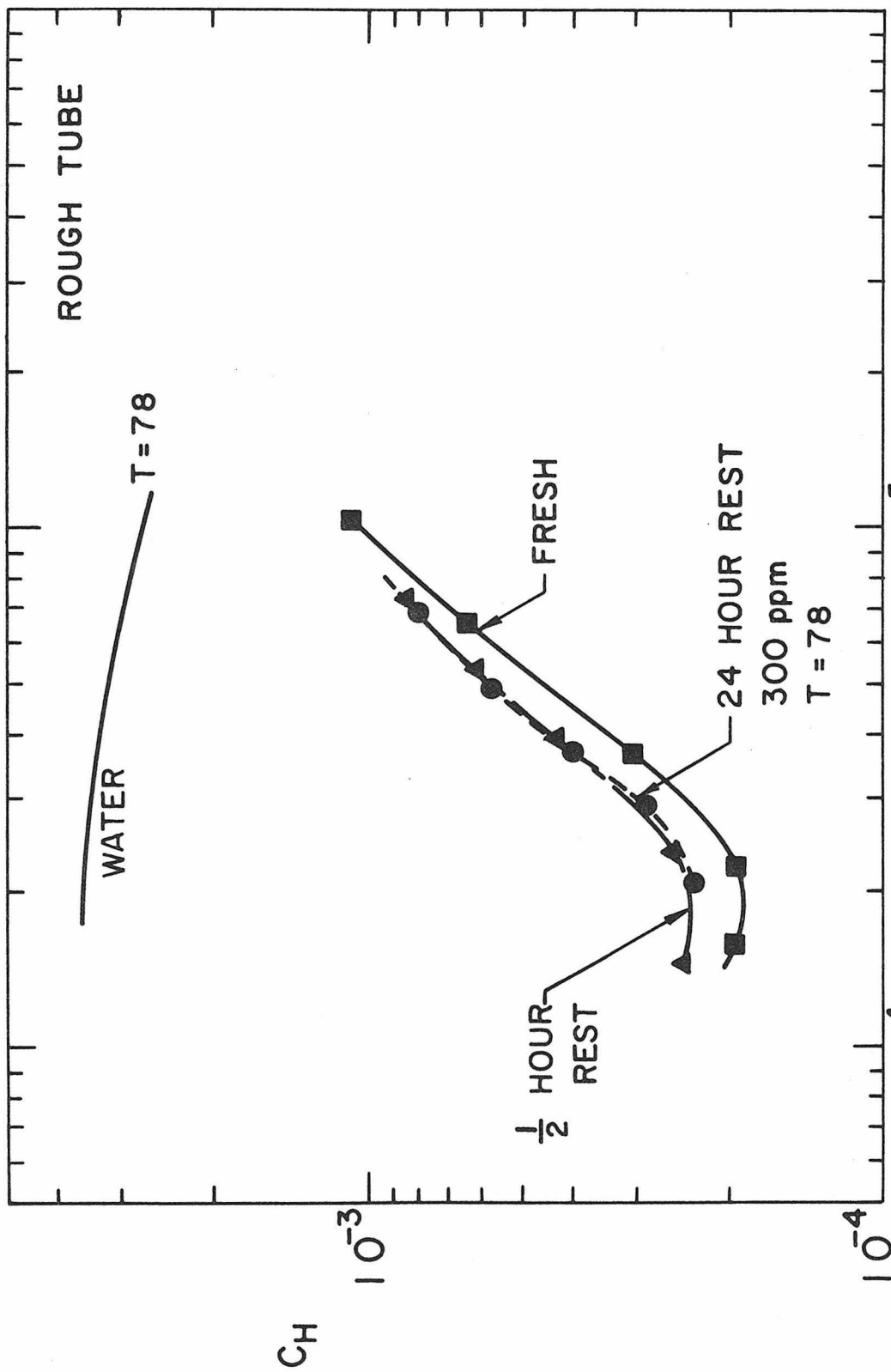

Figure 29. Asbestos 300 ppm heat transfer coefficient vs. Reynolds number. Results of degradation tests. T = 78 °F corresponds to Pr = 6.16.

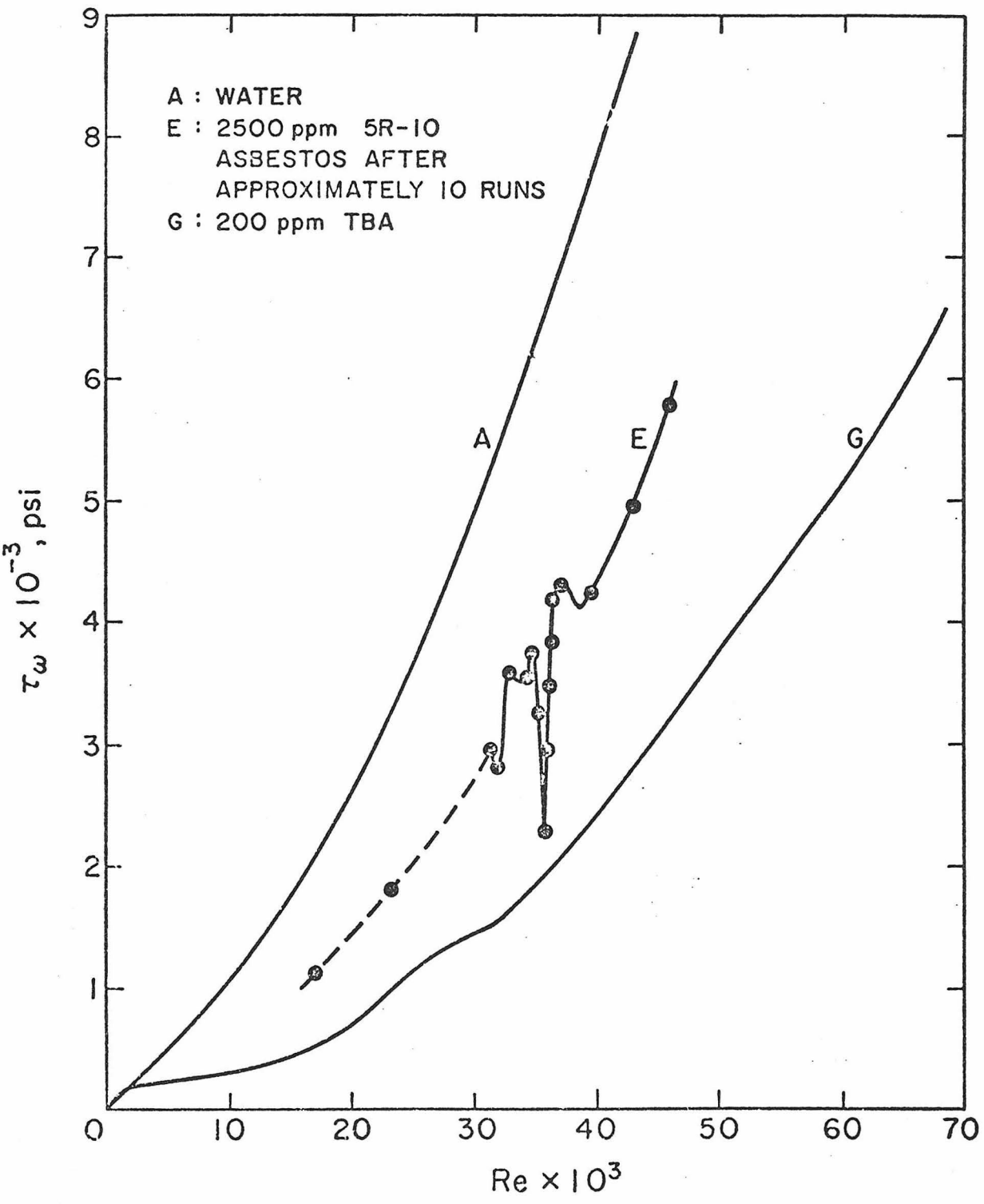

Figure 30 - Wall shear stress vs. Reynolds number in smooth tubes.

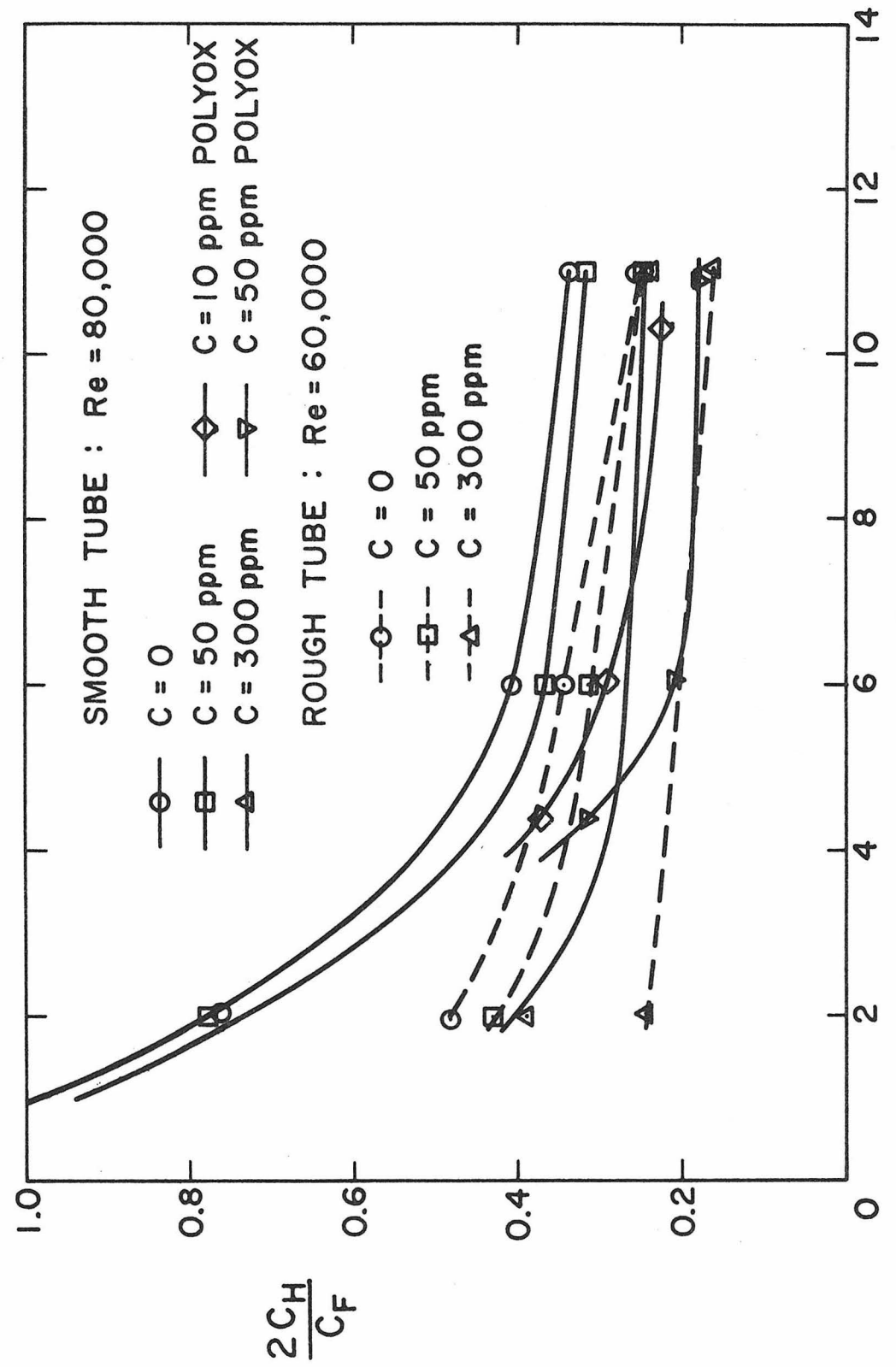

Figure 31. $\frac{2C_F}{CF}$ vs Prandtl number.

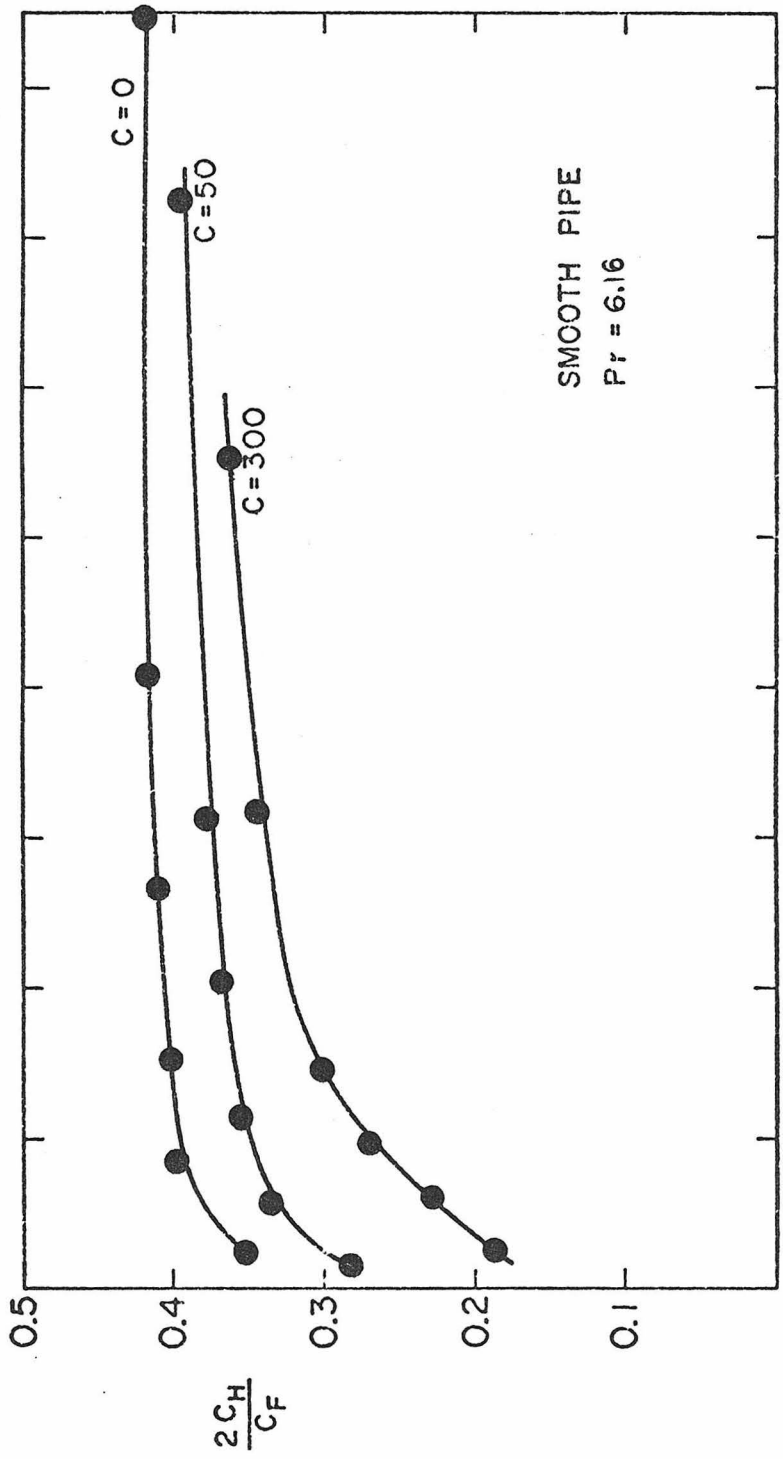

Figure 32 - $\frac{2C_H}{C_F}$ vs. wall shear stress.

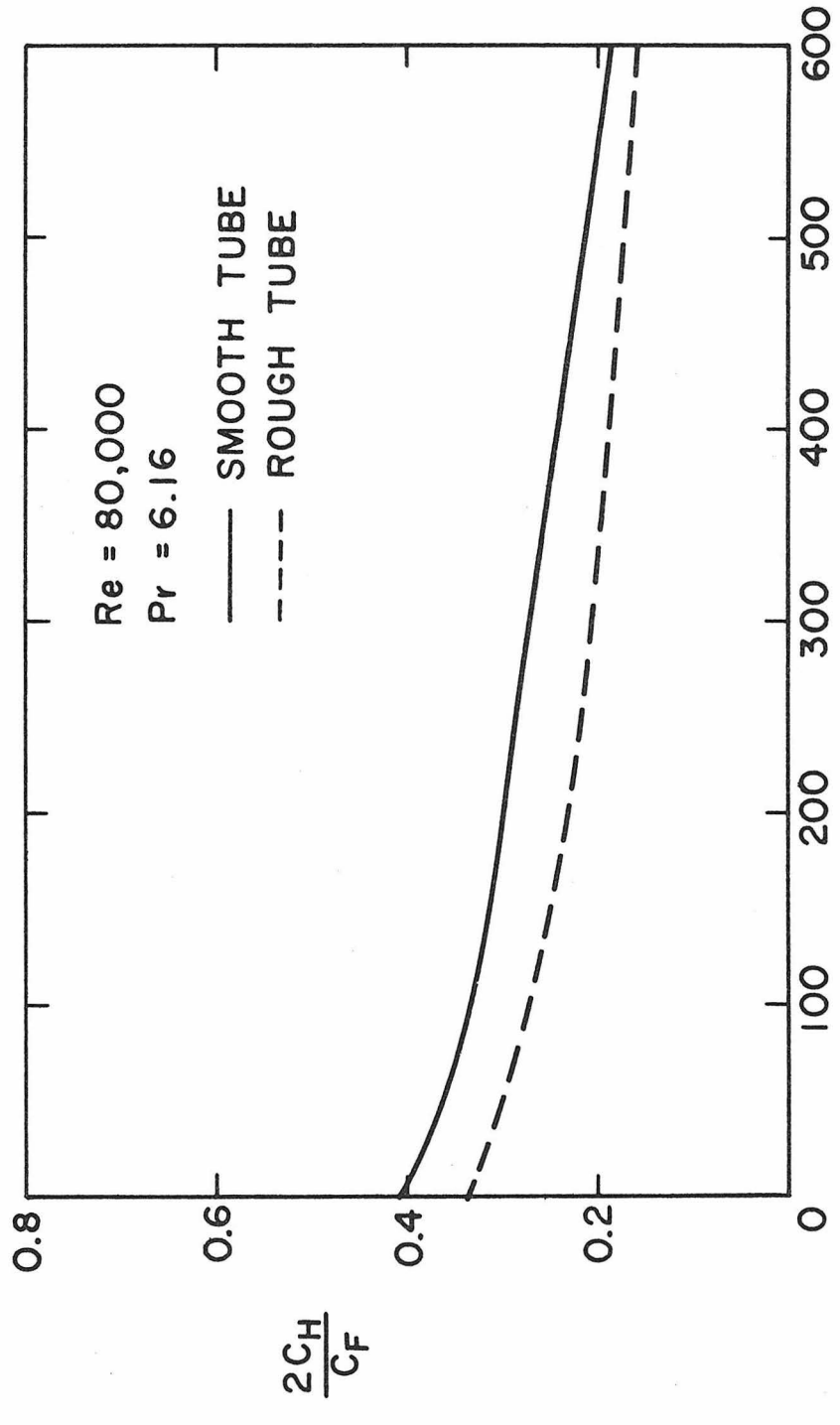

Figure 33. $\frac{2C_H}{CF}$ vs. concentration in smooth and rough tubes, Pr = 6.16, Re = 80,000.

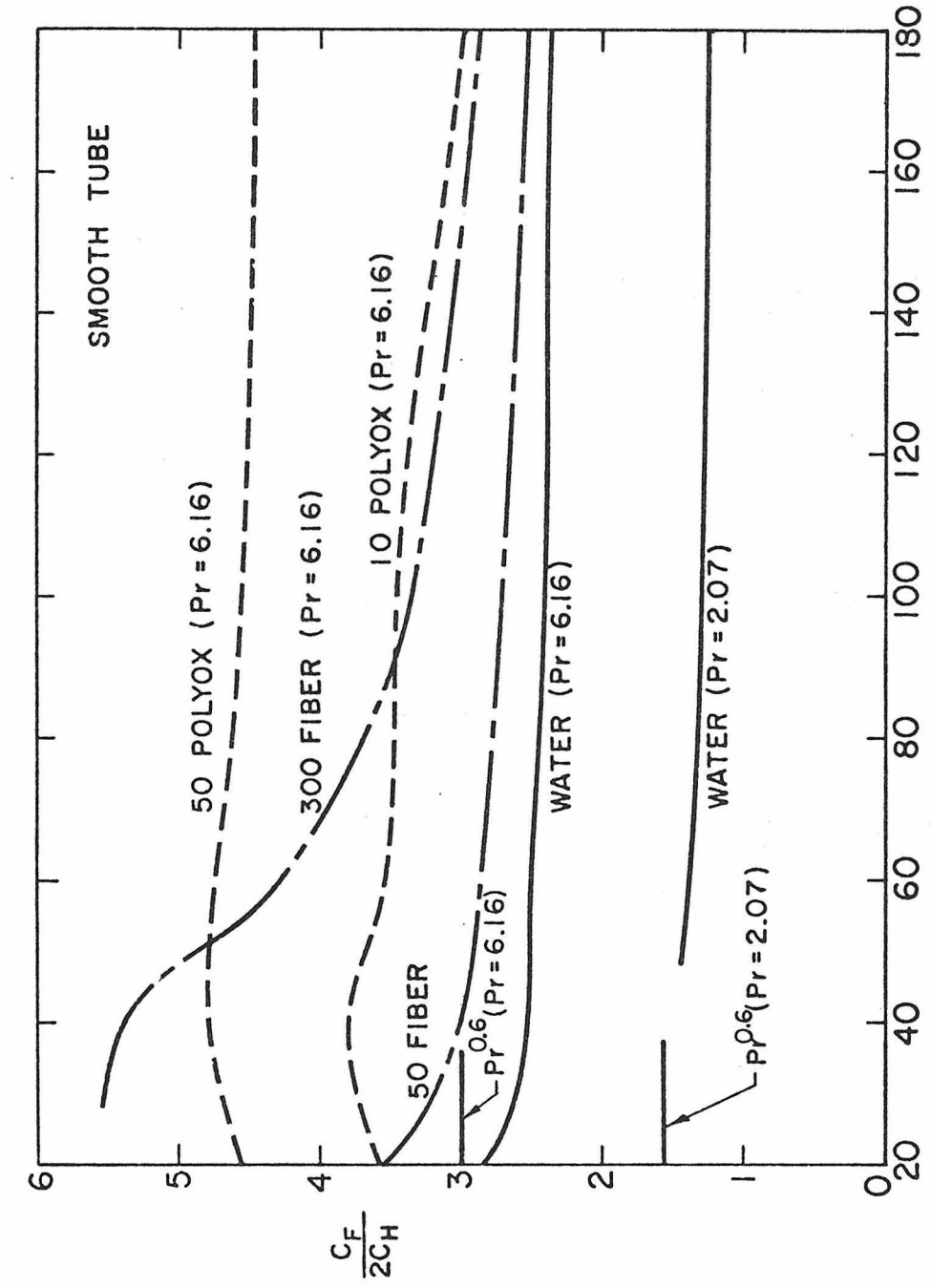

Figure 34. $\frac{2C_F}{CH}$ vs. Reynolds number, all in smooth tube.

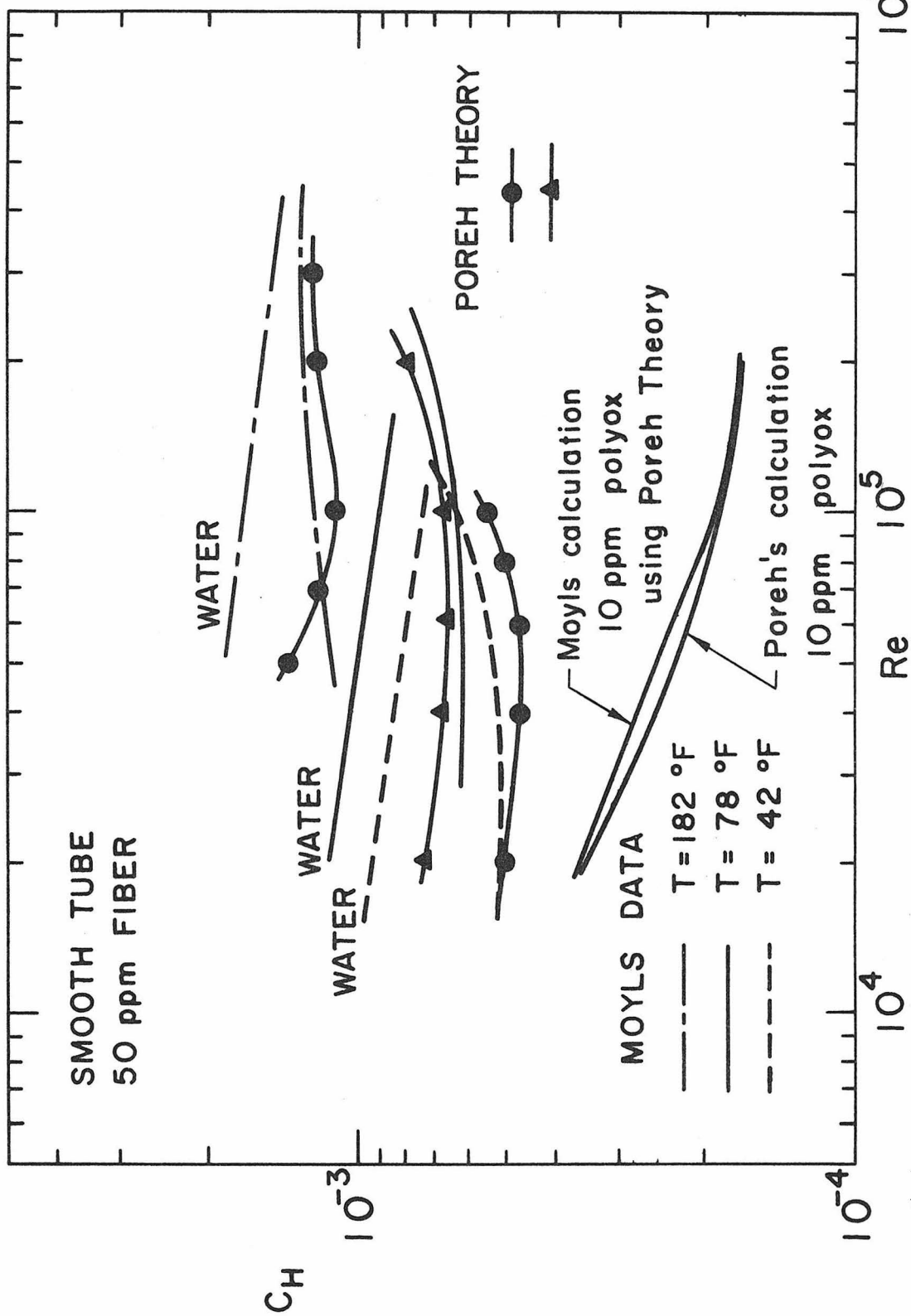

Figure 35. Asbestos 300 ppm, heat transfer coefficient vs. Reynolds number. Points represent computed values.

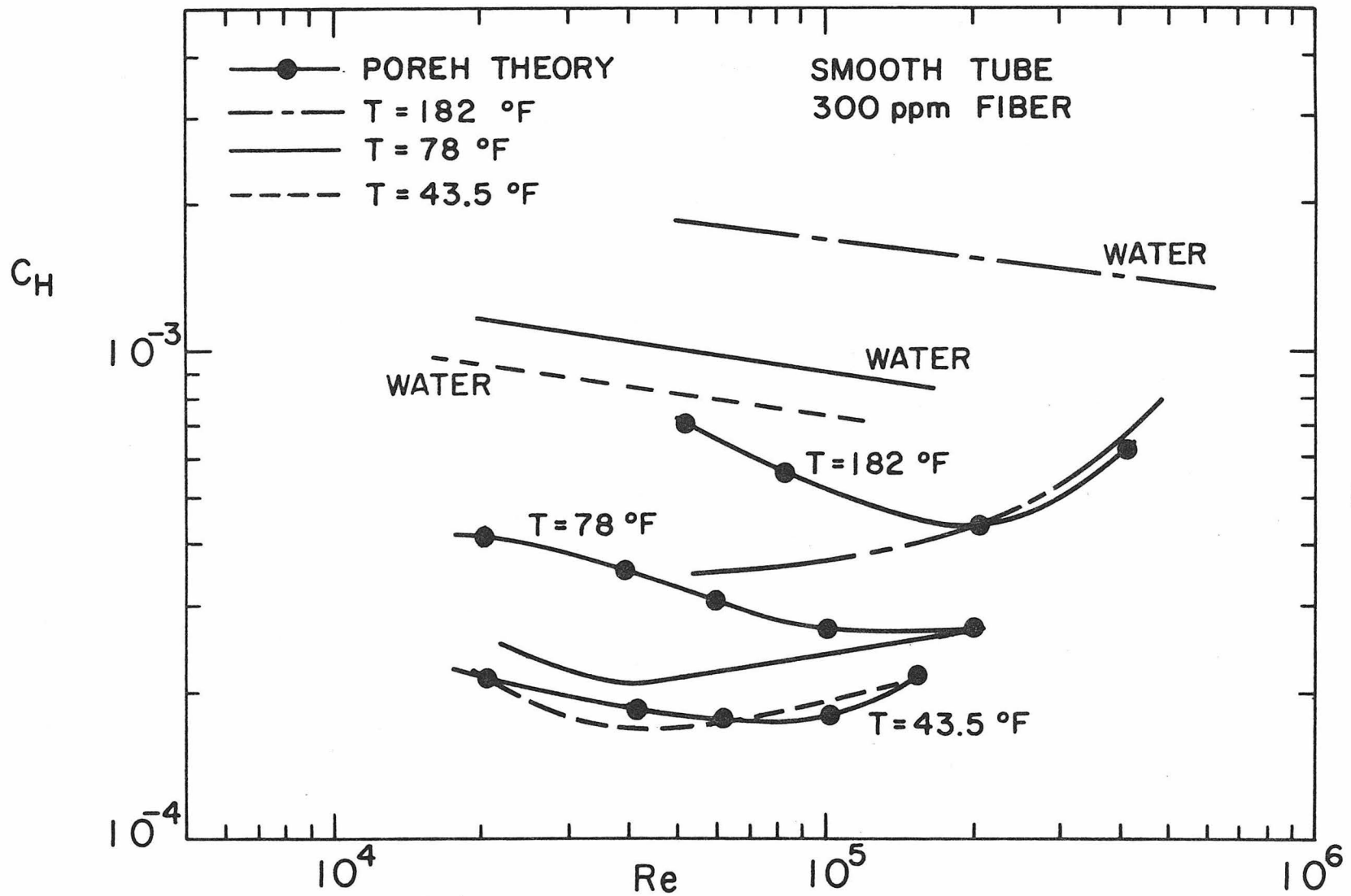

Figure 36. Asbestos 300 ppm, heat transfer coefficient vs. Reynolds number. Points represent computed values.

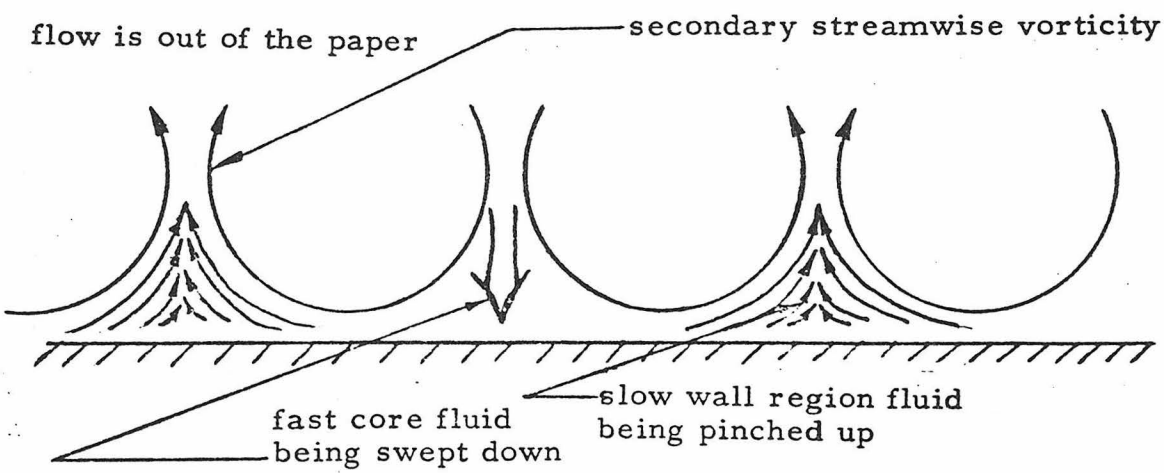

(a) Formation of low speed streaks

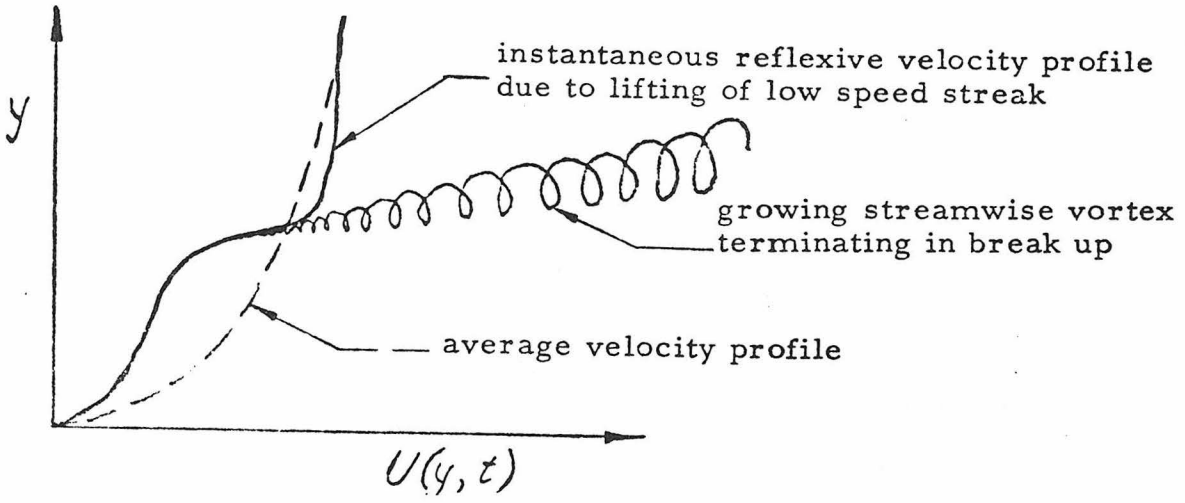

(b) Instantaneous velocity profile and schematic of streamwise vortex

Figure 37. Illustrations of bursting process.

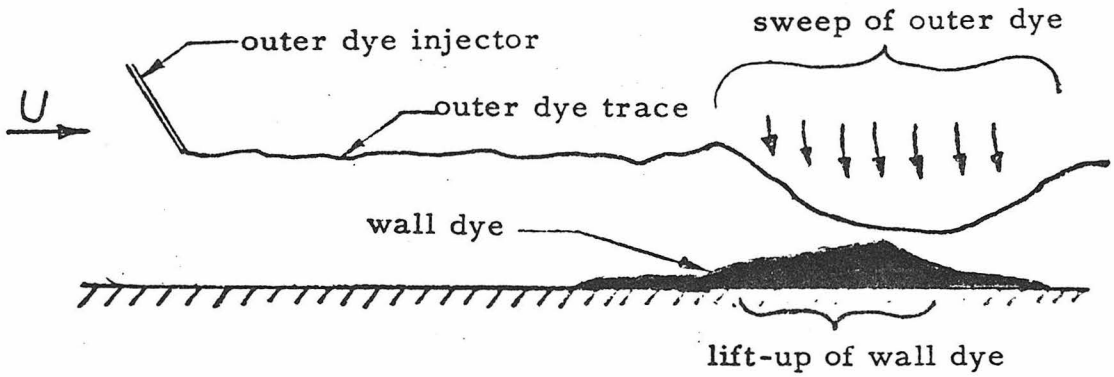

Figure 38 Wall dye lift-up associated with sweep of outer dye.

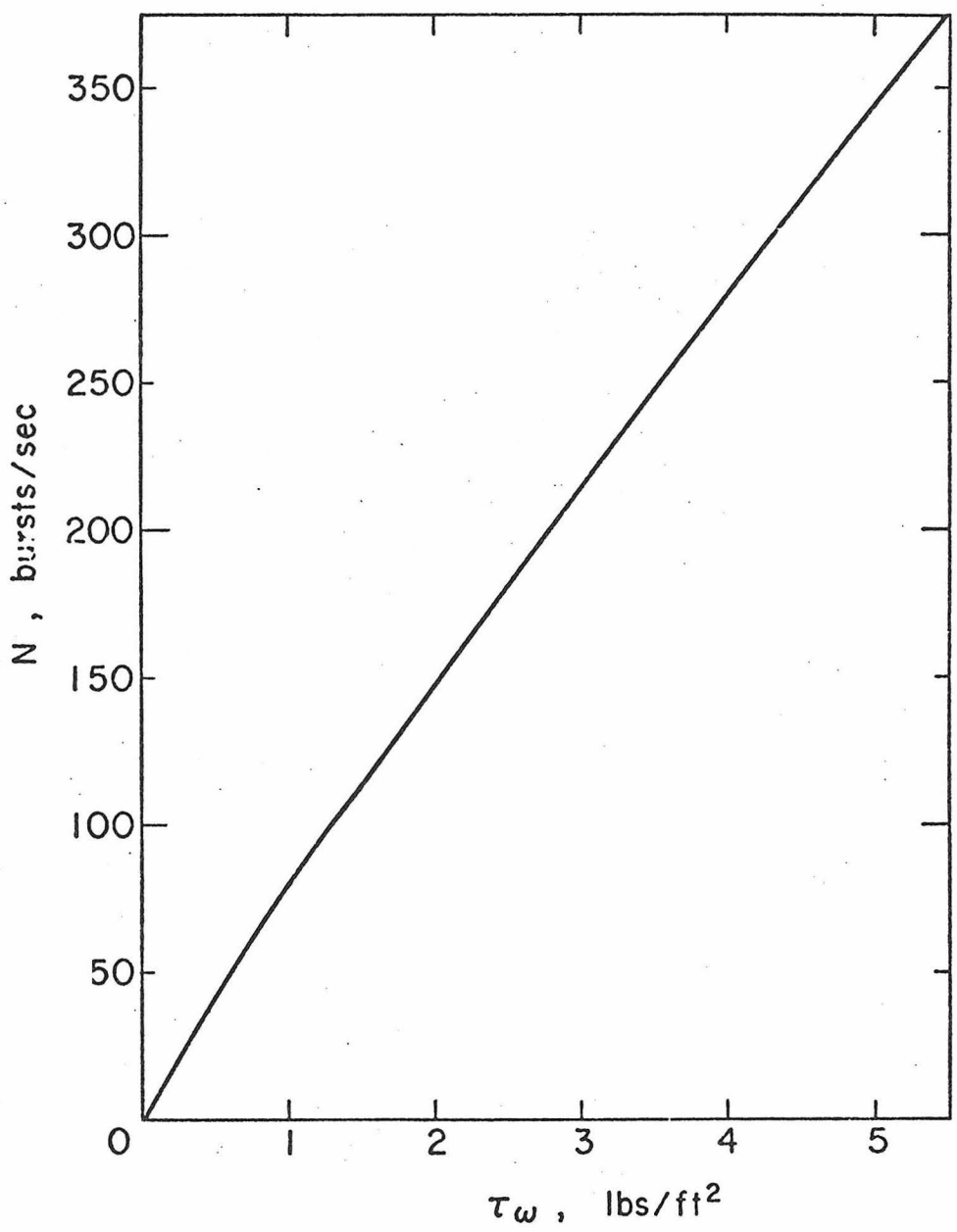

Figure 39. Burst frequency vs. wall shear stress as obtained from work of Corino and Brodkey.